

**THE APPLICATION OF CONTROLLABLE INVERTER-BASED
SERIES COMPENSATION TO POWER OSCILLATION
DAMPING**

by


Nkosinathi Stanford Chonco

BScEng

Submitted as the dissertation component (which accounts for 56% of the degree) in partial fulfillment of the academic requirements for the degree of Master of Science in Engineering, in the School of Electrical Engineering, University of Natal, Durban, South Africa.

September 2000

I hereby declare that all the material incorporated into this thesis is my own original and unaided work except where specific reference is made by name or in the form of a numbered reference. The work contained herein has not been submitted for a degree at any other university.

Signed:  _____
N S Chonco

ABSTRACT

Poorly damped oscillations that occur between the generators in large interconnected power systems often limit the amount of power that can be transmitted through a transmission corridor and are a threat to secure system operation. Coordinated insertion and removal of capacitors in series with a transmission line is one of the approaches that has been known for many years to be capable of enhancing the damping of power system oscillations. Unfortunately however, this approach historically relied on the operation of mechanical circuit breakers which were too slow and unreliable for the high-speed and repetitive operation that such an application demands. Recently-emerged, high-speed power-electronic-based switching devices are finding increasing use in modern power systems in the so-called Flexible AC Transmission Systems (FACTS) concept. One particular FACTS impedance controller, namely the inverter-based series compensator, can rapidly alter the magnitude of capacitive compensating reactance in series with the line to make it practically feasible to enhance the damping of power system oscillations via dynamically-controlled series compensation.

This thesis identifies, in the literature, an insightful approach to the design of an idealised controllable series compensator (CSC) damping scheme; such an approach has been considered in the analyses of the thesis. Three mathematical models of a single-machine infinite bus (SMIB) system are developed and are subsequently used in the initial design and analysis of a CSC damping controller carried out in the thesis. The simple SMIB system case study is used to identify and investigate the factors that have a significant impact on the performance of a CSC damping controller before studying the more complex issue of inter-area mode damping using a CSC.

This thesis successfully confirms the results of a previous analytical study in which an idealised representation of the CSC was used, and extends the scope of that previous study by also considering a detailed representation of one particular type of CSC: the inverter-based series compensator. The two key findings of this extended investigation are that the inverter-based form of controllable series compensator can successfully be used to damp power oscillations and that, where the damping of

oscillations is the particular focus of study, an idealised representation of the inverter-based CSC is suitable for the analyses.

In the case of the inter-area mode damping problem, the selection of an appropriate input signal to the CSC damping controller is a key issue, since the oscillations that are to be damped involve a number of participating generators. This thesis examines the suitability of a few candidate input signals that have been proposed in the literature using the conceptually simpler SMIB system analytical models that have been developed. Finally, the thesis applies the understanding of CSC damping controller design gained from the SMIB study to the problem of inter-area mode damping on a four-generator study system. Time-domain simulation results are presented to demonstrate the impact of the controlled inverter-based series compensator on the damping of the inter-area mode of this system.

ACKNOWLEDGEMENTS

The work presented in this thesis was carried out under the supervision of Dr. Bruce S. Rigby and Professor Ronald G. Harley both of the Department of Electrical Engineering, University of Natal, Durban. I wish to thank Dr. Rigby for his support, guidance, co-operation throughout the course of this thesis, and for his commendable efforts during the correction of this document. I also wish to thank Professor Harley for believing in me and for arranging much needed financial support.

In addition I should like to thank:

my family for their patience especially my mother and aunts for their love;

my friends for their support and encouragement;

the National Research Foundation in South Africa, the University of Natal, and ESKOM TSI for providing financial support;

the staff and postgraduate students of Electrical and Electronic Engineering, unfortunately too many to mention by name, who have together contributed towards a friendly and stimulating work environment over the years.

TABLE OF CONTENTS

Abstract.....	i
Acknowledgements.....	iii
List of Figures and Tables.....	ix
List of Symbols.....	xii

CHAPTER ONE INTRODUCTION

1.1 General.....	1.1
1.2 Thesis Background and Objectives.....	1.3
1.3 Thesis Layout.....	1.4
1.4 Main Achievements and Findings of the Thesis.....	1.6
1.5 Research Publications.....	1.7

CHAPTER TWO REVIEW OF STRATEGIES TO DAMP POWER OSCILLATIONS

2.1 Introduction.....	2.1
2.2 Historical Perspective.....	2.2
2.3 Theory of Power Oscillation Damping via Controllable Series Reactance.....	2.3
2.4 Power Oscillation Damping by Variation of Compensating Reactance in the Literature	
2.4.1 Introduction.....	2.9
2.4.2 Control Approaches.....	2.10
2.4.3 Types of Input Signals for the Controller.....	2.17
2.4.4 Factors Governing the Ability of Variable Impedance Control to Improve Damping.....	2.19
2.4.5 Techniques for the Design and Placement of Variable Impedance Control.....	2.21
2.5 Conclusion.....	2.23

CHAPTER THREE MATHEMATICAL MODELLING

3.1	Introduction.....	3.1
3.2	Different Models of the System and Objectives	
3.2.1	Non-Linear Model of the System Using an Idealised Representation of the Controllable Series Compensator.....	3.2
3.2.2	Linearised (Phillips-Heffron) Model.....	3.2
3.2.3	Detailed Non-Linear Simulation Model.....	3.3
3.3	System Modelling	
3.3.1	Introduction.....	3.5
3.3.2	Simplified Non-Linear System Model.....	3.6
3.3.3	Detailed Non-Linear Mathematical Model.....	3.15
3.3.4	Linearised Phillips-Heffron Mathematical Model.....	3.18
3.4	Results Using Simplified and Detailed System Models	
3.4.1	Introduction.....	3.21
3.4.2	Simulation Results Using the Simplified and Detailed Models.....	3.22
3.4.3	Influence of Various System Parameters on Stability Using the Linearised Model.....	3.24
3.4.4	Influence of Various System Parameters on Stability Using the Simplified Non-Linear Model.....	3.27
3.4.5	Influence of AVR and Exciter Subsystems on System Stability.....	3.30
3.4.6	The Inverter-Based Series Compensator in PSCAD/EMTDC.....	3.34
3.5	Conclusion.....	3.36

CHAPTER FOUR THEORETICAL ANALYSIS OF THE CSC APPLIED TO THE LOCAL MODE DAMPING PROBLEM USING THE PHILLIPS-HEFFRON MODEL

4.1	Introduction.....	4.1
4.2	Theoretical Insights From the Linearised Phillips-Heffron Model	
4.2.1	Introduction.....	4.2
4.2.2	Mechanism of Stabilisation as a Result of Variations in ΔX_{CSC}	4.3
4.2.3	Factors Affecting Stabilisation.....	4.6

4.2.4	Input Signal.....	4.7
4.3	Results and Analysis Using the Idealised CSC Representation	
4.3.1	Confirmation of Swift and Wang's Findings Using Linearised Model...	4.8
4.3.2	Relationship Between Damping and Controller Gain.....	4.13
4.3.3	Non-Linear Simulation Results Using Idealised CSC Model.....	4.16
4.4	Results and Analysis Using the Detailed Model of the Inverter-Based Series Compensator	
4.4.1	Introduction.....	4.21
4.4.2	Simulation Results Using a Fixed Amount of Conventional Series Capacitive Reactance.....	4.23
4.4.3	Simulation Results Using a Fixed Amount of Inverter-Based Series Compensation.....	4.24
4.4.4	Simulation Results Using Controlled Inverter-Based Series Compensation.....	4.25
4.5	Results and Analysis Using Locally-Measured Input Signals	
4.5.1	Introduction.....	4.30
4.5.2	Review of Input Signals.....	4.31
4.5.3	Non-Linear Simulation Results.....	4.33
4.6	Conclusion.....	4.42

CHAPTER FIVE APPLICATION OF THE CSC TO DAMPING INTER-AREA MODE OSCILLATIONS

5.1	Introduction.....	5.1
5.2	System Description	
5.2.1	The Two-Area Power System.....	5.2
5.2.2	Two-Area Power System in PSCAD/EMTDC.....	5.3
5.3	Small-Signal Characteristics of the Study System	
5.3.1	Eigenvalues of the System.....	5.6
5.3.2	Mode Shapes of the System.....	5.7
5.4	Simulation Results	
5.4.1	Introduction.....	5.9
5.4.2	Simulation Results with No Series Compensation.....	5.10
5.4.3	Simulation Results with CSC and Its Damping Controls Inactive.....	5.12

5.4.4 Simulation Results with CSC and Its Damping Controls Active.....	5.14
5.5 Conclusion.....	5.19

CHAPTER SIX CONCLUSION

6.1 Introduction.....	6.1
6.2 Salient Points of the Literature Review.....	6.1
6.3 Mathematical Models for Analysis of a SMIB System.....	6.2
6.4 Findings and Conclusions of the Thesis	
6.4.1 Local Mode Damping Studies Using CSC.....	6.3
6.4.2 Inter-Area Mode Damping Problem Using Inverter-Based CSC.....	6.5
6.5 Suggestions for Further Work.....	6.7

APPENDICES

APPENDIX A PER-UNIT SYSTEM

A.1 Introduction.....	A.1
A.2 Derivation of the Per-Unit System.....	A.2

APPENDIX B LINEARISATION OF THE PHILLIPS-HEFFRON MODEL

B.1 Introduction.....	B.1
B.2 Linearisation of the Simplified Non-Linear Model.....	B.2

APPENDIX C PARAMETERS OF THE SMIB SYSTEM

C.1 Parameters of the SMIB in Per-Unit.....	C.1
---	-----

APPENDIX D PARAMETERS OF THE FOUR-GENERATOR SYSTEM AND ITS PSCAD/EMTDC MODELLING

D.1 Parameters of the Four-Machine System in Per-Unit.....	D.1
D.2 PSCAD/EMTDC System Representation.....	D.2

APPENDIX E SMIB MATLAB CODE

E.1 General.....	E.1
E.2 Non-Linear SMIB System Code.....	E.1

E.3 Linearised SMIB System Code.....	E.4
REFERENCES.....	R.1

LIST OF FIGURES AND TABLES

FIGURES

Fig. 1.1	Simplified two-area power system illustrating the factors which influence power flow.....	1.2
Fig. 2.1	A simplified two-area power system with a dynamically variable series compensating reactance.....	2.3
Fig. 2.2	The improvement in power oscillation damping which can be obtained by dynamically controlled series compensation.....	2.7
Fig. 3.1	A single-machine infinite bus power system with two parallel lines in series with a fixed and a controllable compensating reactance.....	3.4
Fig. 3.2	Two-axis representation of a synchronous machine.....	3.6
Fig. 3.3	A voltage regulator and thyristor-excitation with TGR.....	3.12
Fig. 3.4	A detailed PSCAD/EMTDC representation of a SMIB system with an inverter-based series compensator, including its controls and power electronic switching.....	3.17
Fig. 3.5	Phillips-Heffron linear model of a SMIB system with CSC damping scheme.....	3.19
Fig. 3.6	Time-domain simulation results of the simplified MATLAB non-linear model and a more-detailed PSCAD/EMTDC non-linear model with constant field voltage in each case.....	3.24
Fig. 3.7	Time-domain simulation results showing the influence of various parameters of a SMIB system on system stability using the voltage behind transient reactance model.....	3.30
Fig. 3.8	Time-domain simulation results of a SMIB system including AVR and exciter subsystems at two different values of exciter gain following a temporary disturbance.....	3.33
Fig. 3.9	Simulated response of the inverter-based series compensator to a step increase in the commanded value X_{CSC} in PSCAD/EMTDC.....	3.35

Fig. 4.1	Eigenvalue loci of the SMIB system as the controller gain K_C of the damping controller is increased.....	4.13
Fig. 4.2	Numerical calculation of K_P for the SMIB system at various machine loadings.....	4.15
Fig. 4.3	The relationship between the controller gain and the damping added by the CSC scheme.....	4.15
Fig. 4.4	Time-domain results of the SMIB system using the simplified non-linear model equations.....	4.19
Fig. 4.5	Time-domain simulation results of the SMIB system at two values of the controller gain.....	4.21
Fig. 4.6	Simplified MATLAB and detailed PSCAD/EMTDC non-linear time-domain SMIB models of the same system using a fixed amount of conventional series compensating reactance.....	4.24
Fig. 4.7	Simplified MATLAB and detailed PSCAD/EMTDC non-linear models showing the generator rotor swing following a temporary disturbance.....	4.25
Fig. 4.8	Time-domain simulation results of the SMIB system using an idealised CSC and a detailed inverter-based CSC following a temporary disturbance.....	4.28
Fig. 4.9	Simplified MATLAB and detailed PSCAD/EMTDC non-linear simulation models of the SMIB system showing the predicted responses of the system following a disturbance with a high controller gain in each case.....	4.29
Fig. 4.10	Time-domain simulation results comparing various synthesised signals to the actual speed deviation.....	4.36
Fig. 4.11	Non-linear simulation of the system response in PSCAD/EMTDC following a temporary disturbance using the generator speed deviation and the synthesised rate of change of power flow.....	4.40
Fig. 4.12	Non-linear simulation of the system response in PSCAD/EMTDC following a temporary disturbance using the generator speed deviation and the synthesised speed deviation measurement.....	4.41
Fig. 5.1	An eleven-bus, four-generator, two-area power system.....	5.5

Fig. 5.2	Mode shapes of the oscillatory modes of the system, as presented in [Kundur].....	5.8
Fig. 5.3	Time-domain simulation results of the four-machine system showing various oscillatory modes of the system following a disturbance to the input power of generator G2.....	5.11
Fig. 5.4	Time-domain simulation results with the inverter-based series compensator and its damping controls inactive.....	5.13
Fig. 5.5	Time-domain simulation results showing the damping effect of the inverter-based series compensator using dP_{CSC}/dt as an input to the damping controller for inter-area mode oscillations.....	5.15
Fig. 5.6	Time-domain simulation results showing the damping effect of the inverter-based series compensator using the synthesised speed deviation as an input to the damping controller for inter-area mode oscillations..	5.17
Fig. 5.7	Time-domain simulation results of the four-generator power system at various damping controller gains K_C using the synthesised speed deviation measurement as input to the damping controller in each case	5.19

TABLES

Table 3.1	Eigenvalues of the SMIB system with base-case system parameters
Table 3.2	Eigenvalues of the SMIB system for change in field flux variations
Table 3.3	Eigenvalues of the SMIB system for change in inertia constant
Table 3.4	Eigenvalues of the SMIB system for change in line reactance
Table 3.5	Eigenvalues of the SMIB system for low-gain exciter
Table 3.6	Eigenvalues of the SMIB system for high-gain exciter
Table 4.1	Eigenvalues of the SMIB system with $P_{eo} = 0.2$ p.u, $X_L = 0.8$ p.u, $K_C = 0$
Table 4.2	Eigenvalues of the SMIB system with $P_{eo} = 0.2$ p.u, $X_L = 0.8$ p.u, $K_C = 0.1$
Table 4.3	Eigenvalues of the SMIB system with $P_{eo} = 0.8$ p.u, $X_L = 0.8$ p.u, $K_C = 0.1$
Table 4.4	Eigenvalues of the SMIB system with $P_{eo} = 0.8$ p.u, $X_L = 1.6$ p.u, $K_C = 0.1$
Table 5.1	Eigenvalues of the four-generator system with high-gain exciter and transient gain reduction and AVR, reproduced from [Kundur].

LIST OF SYMBOLS

The commonly used symbols and notations adopted in this thesis are listed below. Other symbols used in the text are explained where they first occur.

Acronyms

AC	Alternating Current
CSC	Controllable Series Compensator
DC	Direct Current
EMTDC	Electro-Magnetic Transient Direct Current
FACTS	Flexible AC Transmission Systems
GTO	Gate-Turn-Off
P-H	Phillips-Heffron
PSCAD	Power System Computer Aided Design
PSS	Power System Stabiliser
SMIB	Single-Machine Infinite Bus
SSSC	Static Synchronous Series Compensator
SVC	Static Var Compensator
TCR	Thyristor Controlled Reactor
TCSC	Thyristor Controlled Series Capacitor
TSC	Thyristor Switched Capacitor

Synchronous generator symbols

B	parameter representing mechanical damping
e_d, e_q	armature voltage, direct and quadrature axis components
E_{fd}	synchronous generator field voltage
E_q'	voltage proportional to the field flux linkages
E_t	synchronous generator terminal voltage
H	inertia constant
i_d, i_q	armature current, direct and quadrature axis components
i_{fd}	synchronous generator field current
i_{kd}, i_{kq}	damper windings current, direct and quadrature axis components
L_d, L_q	direct and quadrature axis stator self-inductances

L_{ad}, L_{aq}	direct and quadrature axis mutual inductances
L_{fd}	field winding self-inductance
L_{kkd}, L_{kkq}	direct and quadrature axis damper winding self-inductances
ψ_d, ψ_q	direct and quadrature axis stator flux linkages
P_e	electrical power output
P_m	mechanical power input
Q_e	reactive power output
R_a	armature winding resistance
R_{fd}	field resistance
R_{kd}, R_{kq}	direct and quadrature axis damper winding resistances
T_{d0}', T_{q0}'	direct and quadrature transient open circuit time constant
T_{d0}'', T_{q0}''	direct and quadrature subtransient open circuit time constant
T_e	electrical torque output
T_m	mechanical torque input
X_d, X_q	direct and quadrature axis stator self-inductive reactances
X_d'	quadrature axis transient reactance
X_{ad}, X_{aq}	direct and quadrature axis mutual reactances
X_{fd}	field winding self-reactance
X_{kdd}, X_{kkq}	direct and quadrature axis damper winding self-inductive reactances
X_ℓ	leakage reactance
δ	rotor angle
$p\delta$	per unit speed deviation from synchronous

System symbols

C	capacitance
L	inductance
E_b	infinite bus voltage
E_t	generator terminal voltage
R_L	transmission line resistance
X_L	transmission line reactance
X_{CSC}	overall CSC reactance
X_{CSC0}	fixed component of CSC reactance

X_{CSCV}	variable component of CSC reactance
ω_d	damped natural frequency
ω_0	system synchronous speed

General

p	derivative operator d/dt
p.u.	per-unit
∂	partial differential operator
Δ	small change operator
o	signifies steady-state value
[Y]	signifies a matrix Y

CHAPTER ONE

INTRODUCTION

1.1 General

A steady growth in load demand coupled with the cost of land required to accommodate new power lines, limited availability of right-of-ways, regulatory policies, and the cost of building new generation plant to meet this increased power demand will inevitably require better utilisation of existing generation and transmission facilities. This situation, in turn, calls for the review of traditional power generation and transmission system theory and practice in order to address the issue of how to operate the existing power system much closer to its stability limits without compromising the security of the system itself. Historically, safe and stable operation of an ac electric power system has been achieved by operating the system far away from its theoretical stability limits. However, it has long been recognised that improved dynamic control of ac power systems would allow better utilisation of these systems [Kimbark1,Smith]. While conventional methods to solve power system dynamic problems have been known for many years [Gyugyi3], these methods have relied on the slow and unreliable operation of mechanical circuit breakers which made them unsuitable for the high-speed use demanded by a dynamic control application. As a result these ideas remained on hold for nearly two decades. Despite these trends, the needs for electric energy have continued to increase.

One response to these pressures, internationally, has been the emergence of the Flexible AC Transmission Systems or FACTS concept: FACTS aims to bring the factors which influence the transfer of power in a transmission system under rapid control by means of modern, power-electronic-based compensating devices in order to allow the system safely to be pushed closer to its limits. The high-speed response of FACTS devices provides fast and efficient control of the power transmitted through transmission lines, and dynamic control applications using these devices have now become practically feasible. As a consequence, a number of FACTS technologies

have emerged with which to improve power system stability, thus allowing the system to be operated closer to its stability limits.

Fig. 1.1 shows a simplified diagram of a two-area power system connected by a transmission corridor. The power P_{tr} transferred down the line is shown by the equation of Fig. 1.1 and reaches a maximum $P_{tr\ max} = |V_S||V_R| / X_L$ when the transmission angle δ reaches 90 degrees, where $|V_S|$ and $|V_R|$ are the transmission system voltage magnitudes and X_L is the series (inductive) reactance of the transmission line. This maximum power transfer $P_{tr\ max}$ is the steady-state power transfer limit of the system. However, the dynamic and transient stability characteristics of the synchronous generators in the system mean that the transmission line must in practice be operated at a power level much lower than this steady state limit in order to allow sufficient margin for the generators to remain in synchronism following disturbances. Flexible AC Transmission Systems devices aim to enhance the control of the electromechanical power oscillations between the generators and the transmission system so as to reduce the need for such large transient or dynamic stability margins inherent with conventional power systems.

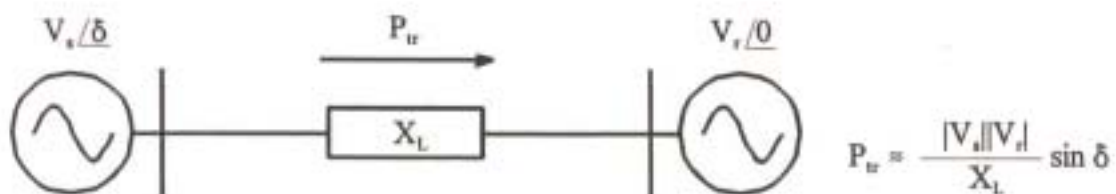


Fig. 1.1: Simplified two-area power system illustrating the factors which influence power flow.

From the system in Fig. 1.1 it is apparent that three possible levers exist for control of power flow: voltage magnitude ($|V_S|$, $|V_R|$), voltage phase (δ), and the transmission line reactance (X_L). Various traditional approaches to control each of these levers using mechanical controllers can now be implemented with modern power-electronic-based devices such as: all-solid state implementation of Static Var Compensator (SVC) for transmission voltage magnitude control; phase-shifters for voltage phase control; controllable series compensators for line reactance control. However, this thesis is concerned with one particular lever, namely the compensation of the series

reactance of the transmission line. In addition the thesis focuses on one application of this lever to system stability, which is to improve the *damping* of the electromechanical oscillations of the generators in the system.

Traditionally, fixed capacitor banks have been used in series with transmission lines to reduce their net inductive reactance and thereby to increase their maximum power transfer capability: with a capacitive compensating reactance X_{CSC} introduced in series with the line of Fig. 1.1 the steady state power transfer limit is increased to $P_{tr\ max} = |V_S||V_R| / (X_L - X_{CSC})$. In this way, the improvement in transient stability margin can be achieved because of the increased power transfer capability at steady-state for a given voltage phase angle and not because of any dynamic control. Modern, FACTS series compensators now allow such series compensating reactance to be controlled dynamically resulting in even further potential improvement in stability margins. Various FACTS series compensators have subsequently emerged, based on the thyristor (for example, the Thyristor Controlled Series Capacitor (TCSC) [Choi,Dolan]) or on Gate-Turn-Off (GTO) inverters (for example, the Static Synchronous Series Compensator (SSSC) [Sen,Mihalic1]). Any of these FACTS series compensators can now, in principle, be used to provide a dynamically varying series compensating reactance for the purpose of enhancing system stability in general and, in particular, the damping of electromechanical oscillations in power systems.

1.2 Thesis Background and Objectives

Power system stability problems can be classified according to whether they involve transient (first-swing) conditions or dynamic (small-signal) conditions. For many modern power systems the amount of power a synchronous generator can be used to deliver is severely limited by small-signal stability concerns [Kundur,Swift1] and for these power systems the problem is one of insufficient damping of the electromechanical system oscillations. As such, adding damping to these oscillations is a prerequisite for a secure system operation. The small-signal stability of a power system manifests itself in two types of electromechanical oscillations namely, local oscillations and inter-area oscillations. In a large power network, oscillations are due to the dynamics of inter-area power transfers between groups of generators interconnected by weak tie-lines, and these oscillations usually exhibit poor damping

when power transfers over a transmission line corridor are high relative to the strength of the transmission lines [Larsen]. On the other hand, local mode oscillations associated with a single generator are well-known and have been studied using a detailed system representation in the neighbourhood of the generator of interest [Klein1].

The aim of this thesis is to investigate the use of a particular type of FACTS series compensator, that is inverter based series compensation, to damp a particular type of dynamic power system instability, the so-called inter-area form of oscillation. The theory of operation of the inverter-based series compensator that is considered in the investigations of this thesis has been presented in [Rigby1]. The studies in [Rigby1] have shown that the inverter-based series compensator is capable of providing dynamically controllable series compensation; these findings have been reconfirmed in a later study in [Chonco3] using a particular power systems simulation software package. In this thesis the inverter-based series compensator in [Rigby1] is now considered for the specific purpose of damping inter-area mode oscillations in power systems.

1.3 Thesis Layout

This thesis consists of five further chapters and appendices. In order to present the analyses of this thesis, the development of various system models, the results and main findings of the thesis, the material has been arranged as follows.

Before an investigation of this kind could be carried out it was necessary to review the technical literature on the subject of controllable series compensation as applied to the damping of electromechanical oscillations. Chapter Two of this thesis, in particular, provides the background to the theory of power oscillation damping using controllable series compensators. This chapter also provides a literature review of the control strategies proposed for varying series compensation to damp electromechanical oscillations in power systems and identifies important design and implementation approaches to be adopted in the subsequent chapters.

A number of design and analysis tools used to represent various subsystems and devices have been developed during the course of the thesis work. Chapter Three presents three mathematical models developed for a single-machine infinite bus power system and explains the purpose of each of the models. These system models are later verified along with a more-detailed simulation model of the system.

Chapter Four presents the results of a case study of a single-machine infinite bus power system in which an inverter-based compensator is used in series with the transmission line. This case study reconfirms and extends the findings of a previous study into local mode damping using controllable series compensation that was carried out by others. An external (damping) controller is used to modulate the compensating reactance provided by the inverter-based series compensator so as to damp out the oscillations of the single generator that occur following system disturbances. However, although in the initial phase of the study an idealised representation of the inverter-based series compensator itself is used, subsequent investigations in the chapter include a detailed representation of the compensator itself (including its internal power electronics and controls). The factors that affect the damping controller performance are investigated and various input signals are synthesised for the damping controller input.

Chapter Five presents a brief case study of a four-generator system in order to investigate the mitigation of the inter-area mode damping problem using an inverter-based series compensator. This chapter uses the concepts developed in Chapter Four to show that the inverter-based series compensator is another useful tool for inter-area mode damping.

Finally, Chapter Six summarises the main results from the studies carried out in the thesis and suggests further research that could be undertaken in future.

1.4 Main Achievements and Findings of the Thesis

The previous section has outlined the contents and arrangement of the thesis. This section now summarises the main findings of the thesis and the achievements made. This thesis has:

- (i) derived and programmed MATLAB [Mathworks] time-domain simulation models and linearised eigenvalue programs for the analysis of a single-machine infinite bus (SMIB) power system containing a controllable series compensator. In addition, a detailed model of the same system, and a model of a four-generator system (including a detailed representation of the inverter-based series compensator itself) have been developed in the power systems simulation package PSCAD/EMTDC [Manitoba];
- (ii) presented a detailed analysis that shows that the generator speed deviation is the logical input signal for a controllable series compensator (CSC) damping controller in a SMIB power system; in addition, the thesis has identified and examined other signals similar to the generator speed deviation that can be measured remotely in the transmission system and that are therefore more suited to the inter-area mode damping problem where the actual generator speed deviation cannot be easily obtained;
- (iii) shown that, for the inverter-based form of series compensation, a simplified representation of the controlled compensator is reasonable for damping studies;
- (iv) demonstrated that an inverter-based CSC can successfully be used to add damping to the inter-area mode of a well-known study system.

1.5 Research Publications

Some of the findings of this thesis have been presented at national conferences [Chonco1,2].

CHAPTER TWO

REVIEW OF STRATEGIES TO DAMP POWER OSCILLATIONS

2.1 Introduction

The previous chapter has described the problems facing power utilities today and explained that Flexible AC Transmission Systems (FACTS) aim to alleviate these problems by allowing power systems to be operated closer to their stability limits without risking the security of the system. The discussions of that chapter showed that since transmission line reactance has a direct influence on transmitted power and can rapidly be controlled with modern FACTS devices, the series line reactance can therefore be used to dynamically control the power flow in a manner that tends to stabilise power swings.

While series compensation using dynamically controllable FACTS series compensators is often regarded as a new technology, the idea itself has been around for some time. Hence this chapter initially provides a historical perspective on the damping of power system oscillations using switched series capacitive compensation. The chapter also describes how a variable series capacitive reactance is able to damp electromechanical system oscillations in power systems using an example of a simplified two-area power system subjected to a large disturbance; from this example, the fundamental operating principle of damping system oscillations using dynamically variable series capacitive compensation is established.

Finally, this chapter reviews various control approaches proposed in the literature for damping power oscillations in power systems. Approaches suited to the inter-area mode-damping problem are identified and the factors with considerable bearing on the variable series impedance controller are discussed.

2.2 Historical Perspective

In 1966, E. W. Kimbark [Kimbark1] proposed the use of a switched series capacitor to change the power flow in a transmission line following a disturbance. Kimbark used the equal area criterion to predict that the transient stability of an electrical power system can be improved by bypassing and inserting a series capacitor. The advantage of switched versus fixed series compensation is that it increases both the steady-state and transient stability limit allowing the system to be operated closer to theoretical stability limits, and it is more economical than fixed compensation [Kimbark1]. It must be noted that the analyses in [Kimbark1] referred to one switching in of a series capacitor after a fault. In 1969, O. J. Smith [Smith] proposed that the electromechanical power oscillations between a generator and a transmission system could be damped by inserting and removing a series capacitor in a transmission line. While reference [Kimbark1] proposed a single switching in of a series capacitor, Smith appears to be the first to propose a coordinated insertion and removal during the transient power swings. Reference [Smith] states that even a small amount of switched series compensation can provide a dramatic increase in the power system stability. In a subsequent paper by Smith and Webster [Webster], the ideas in [Smith] were practically implemented in a laboratory and it was shown that a generator which would otherwise have pole-slipped following a particular system fault was successfully stabilised using coordinated switching of series capacitance.

At the time the ideas in [Kimbark1,Smith,Webster,RamaRao] were proposed, dynamically variable series compensation could only be achieved using capacitor banks switched in and out with mechanical circuit breakers; however such devices were in practice too slow and unreliable for the repeated high-speed use demanded by a dynamic control application and as a result these ideas remained on hold for nearly two decades. Recently however, progress in the field of power electronics has led to the development of high-power electronic switches with which to implement dynamically controllable (FACTS) series compensating devices. The later sections of this chapter review the particular methods which have been proposed for controlling such dynamically variable compensating reactance for the specific purpose of damping electromechanical power oscillations. However, the following section first

explains conceptually how a variable series capacitive compensating reactance is able to actively damp out electromechanical system oscillations.

2.3 Theory of Power Oscillation Damping via Controllable Series Reactance

If the system in Fig. 1.1 is subjected to a disturbance, the generator rotor angle oscillates about a new equilibrium angle provided that, after the disturbance, the system maintains stability. If there is no damping provided to the system the generator rotor angle will oscillate indefinitely. In practice however, there are sources of positive damping such as rotor damper windings and field flux variations. Once again a simplified two-area power system is considered for analysis, but the transmission line is now compensated with a variable series reactance X_{CSC} as shown in Fig. 2.1 below.

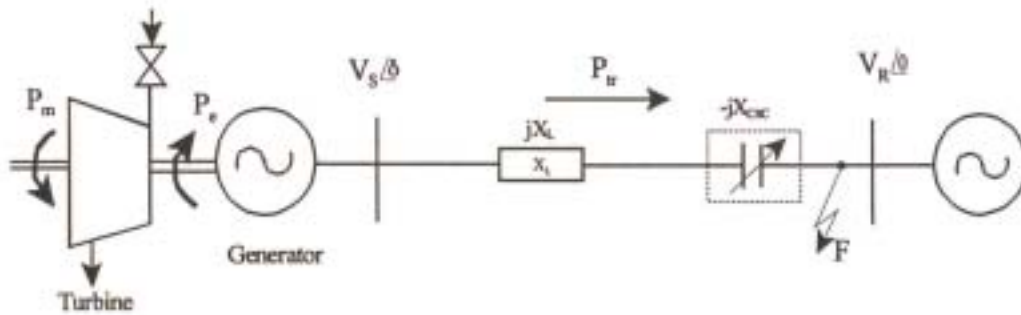


Fig. 2.1: A simplified two-area power system with a dynamically variable series compensating reactance.

If the torques caused by friction, windage and core loss in a machine are ignored, any difference between the mechanical (shaft) torque and electromagnetic torque developed must cause acceleration or deceleration of the generator rotor. If T_m represents mechanical input torque from the turbines, and T_e is electromagnetic torque, the net torque causing acceleration or deceleration is $T_a = T_m - T_e$. A similar equation holds for accelerating or decelerating power $P_a = P_m - P_e$, where P_m is the mechanical power input to the system, and P_e is the electrical power developed for a generator. If the resistance of the transmission line is neglected, then the electrical power developed is the same as power transmitted by the line to the receiving end (that is, $P_e = P_r$). Under steady-state operating conditions the mechanical power input

is equal to the electrical power developed, the accelerating power P_a is zero, the generator speed remains constant at synchronous speed and the generator rotor angle δ remains constant. However, following a disturbance any imbalance between the mechanical input power and the electrical output power results in non-zero accelerating power P_a which accelerates the shaft of the generator changing its rotor angle according to the swing equation:

$$\frac{2H}{\omega_o} \frac{d^2 \delta}{dt^2} = P_m - P_e = P_a \quad (2.1)$$

where,

$$P_e = \frac{|V_s| |V_R|}{X_L - X_{CSC}} \sin \delta \quad (2.2)$$

- and: P_e = electrical power output;
 P_m = mechanical power input to the system;
 P_a = accelerating power;
 H = inertia constant of the machine;
 δ = generator rotor angle;
 ω_o = synchronous speed;
 t = time.

At steady-state when the machine runs at constant speed, $d\delta/dt$ is zero since it is the difference between the generator electrical speed and synchronous speed ($d\delta/dt = \omega - \omega_o = \Delta\omega$), and $d^2\delta/dt^2$ is likewise zero. The mechanical power input to the system is assumed to be constant throughout this analysis. If the system experiences a sudden disturbance, such as a three-phase short circuit fault at the receiving end (as illustrated at point F in Fig. 2.1), the power P_r transmitted to the receiving end in Fig. 2.1 is zero while V_R remains zero. From equation (2.1) it becomes apparent that the speed of the machine must change since there is power imbalance between the input P_m and the output $P_e = P_r = 0$ during the period of the fault. The speed of the machine therefore rises, under the influence of the positive accelerating power, from the initial operating point and the generator rotor angle increases. Once the fault is cleared, V_R is assumed to return to its pre-disturbance value, and from equation (2.2) the electric power

transmitted by the line is now higher than the pre-disturbance value since the rotor angle has advanced. The power imbalance $P_d = P_m - P_e$ is now negative and the machine starts to decelerate. However, although the machine decelerates, its rotor angle continues to increase as long as its rotor speed remains greater than synchronous speed. The machine remains transiently stable provided it can decelerate to synchronous speed before its rotor angle increases beyond the transient stability limit as determined by the equal area criterion.

Consider a case where the generator does remain transiently stable: while its rotor angle increases immediately following the fault clearance, P_e is greater than P_m , and the generator rotor speed continues to decrease (in order to return the energy gained during prefault acceleration back into the transmission system) and the speed at some point drops below ω_s . At that instant, the generator rotor angle begins to decrease such that some time later P_e is again equal to P_m . However, although P_e and P_m are once again equal, the generator speed deviation $\Delta\omega$ is now negative and the generator rotor angle continues to decrease, whereupon the electrical power P_e falls below P_m and the generator rotor begins to accelerate, so returning its speed deviation back towards zero. When the generator speed deviation once again becomes positive under the influence of this positive accelerating power, the generator rotor angle then begins to increase back towards its equilibrium value. Without any source of positive damping the generator rotor angle and speed deviation will each continue to oscillate indefinitely in this manner about their post-fault equilibrium values with constant amplitude. However, if damping is present these oscillations decrease in amplitude with time, and the generator rotor ultimately returns to some post-disturbance steady state value of rotor angle. In this analysis, the value $P_{tr\ max} = |V_1||V_2|/(X_L - X_{CSC})$ has been considered to be constant throughout these generator rotor oscillations; hence from equation (2.2) the power transmitted becomes a function of the generator rotor angle swings, and oscillations in the generator rotor angle δ correspond to oscillations in the transmitted power. The dynamic series compensation aims to provide an additional source of damping, over and above any sources of damping inherent in the system, so as to quickly damp out these system oscillations. It will now be explained how a variable series reactance is able to affect the power transfer in a manner that tends to damp out the power system oscillations.

Again consider a temporary three phase short-circuit fault at the receiving end in point F of Fig. 2.1. While this fault is applied V_R is zero and from eqn. (2.2) $P_e = P_r = 0$. From eqn. (2.2) it is apparent that until such time as the short circuit fault is cleared (that is, whilst V_R remains zero), the impedance of the line has no influence on the accelerating power of the machine. However, once the fault is cleared the controllable capacitive reactance X_{CSC} can be used to influence the transmitted power P_r , and hence the accelerating power imbalances in the generator as explained below.

In simple terms eqn. (2.2) shows what action can be taken in order to influence the power flow (and hence the generator rotor angle) oscillations: when there is insufficient power transferred out of the generator during the post-disturbance transient (that is, when $P_e = P_r$ is less than P_m) then the accelerating power P_a is greater than zero; this transient power imbalance needs to be reduced by increasing the transmitted power P_r such that the magnitude of the positive accelerating power P_a is decreased towards zero. Equation (2.2) shows that the required increase in P_r can be achieved by *increasing* the magnitude of the controlled capacitive compensating reactance X_{CSC} . Likewise, during the post-disturbance transient whenever there is too much power transferred out of the generator (that is, when $P_e = P_r$ is greater than P_m) then the accelerating power P_a is less than zero; hence during this period there is a need to reduce the transmitted power P_r such that the magnitude of the negative accelerating power is decreased back towards zero. Equation (2.2) shows that the required decrease in P_r can be achieved by *decreasing* the magnitude of the controlled capacitive reactance X_{CSC} .

From the above discussion it is apparent what the basic control action should be in order for a controlled compensating reactance to quench a generator's transient rotor oscillations: when the machine accelerates the positive accelerating power must be reduced by an increase in X_{CSC} ; when the machine decelerates, the negative accelerating power must be reduced by a decrease in X_{CSC} . However, at the most basic level an additional amount of compensating reactance X_{CSC} can be inserted whenever the generator speed deviation is positive and removed whenever the speed deviation is negative [Gyugyi3]. Later in this chapter, various other control algorithms that have been proposed for varying X_{CSC} are reviewed.

Fig. 2.2 (a similar figure appears in [Gyugyi3]) now shows an example of this basic technique whereby the improvement in damping is obtained by changing X_{CSC} dynamically according to the generator speed deviation as proposed in [Gyugyi3]. The light curves show an uncontrolled system with no sources of damping after clearing a three-phase short circuit fault; there are sustained oscillations in the generator rotor speed deviation $\Delta\omega$ and the electric power output (hence rotor angle) of the generator. The solid curves show the same system when a small amount of controlled series capacitive reactance X_{CSC} is used. Following the disturbance, whenever the generator rotor speed deviation $\Delta\omega$ becomes positive the controlled capacitive reactance X_{CSC} is switched into the line; whenever the generator rotor speed deviation $\Delta\omega$ is negative the controlled reactance X_{CSC} is switched out of the line. The overall effect is to return the system to its equilibrium state as seen in the solid curves for P_e and $\Delta\omega$.

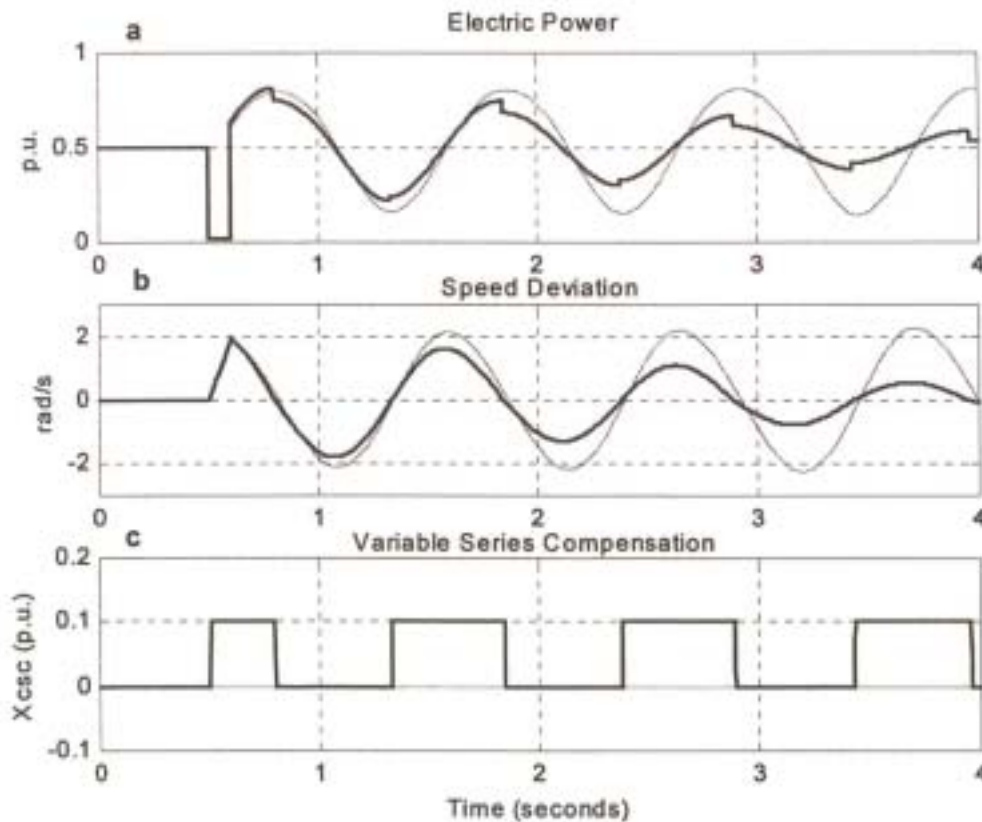


Fig. 2.2: The improvement in power oscillation damping which can be obtained by dynamically controlled series compensation. (a) electric power output (b) generator speed deviation (c) degree of switched capacitive compensation in series with the line.

It should be pointed out that the simple example described here (Fig. 2.2) shows the dynamic series compensation varied in a discrete fashion between maximum and minimum values, the so-called bang-bang type of control. It may however be desirable, as discussed later in this chapter, to vary this controlled series capacitive compensation continuously in sympathy with the power transfer changes, the so-called continuous control approach. The applicability of each of these two types of control strategies will be discussed in more detail in the ensuing sections.

The purpose of this simple example has been to explain the fundamental operating principles of variable series reactance control to damp power oscillations which may be summarised as:

- (i) to decrease the overall line impedance (by increasing the magnitude of the dynamically controlled series capacitive reactance) so as to absorb excess accelerating power; and
- (ii) to increase the overall line impedance (by decreasing the magnitude of the dynamically controlled series capacitive reactance) so as to minimise excess decelerating power.

This fundamental principle has been shown using the example of a bang-bang control where a fixed capacitive reactance is inserted when $\Delta\omega$ is positive and removed when $\Delta\omega$ is negative. In practice, a variety of approaches have been proposed for varying the compensating reactance (for example, bang-bang, continuous) and for synthesising input signals to the controller which contain information about accelerating power. In addition, the problem becomes conceptually more complex when the controlled reactance is to be used to damp the oscillations of one group of machines against another – the inter-area mode oscillation problem. The following section reviews these proposed approaches and discusses their suitability to the particular application of damping inter-area mode oscillations.

2.4 Power Oscillation Damping Strategies by Variation of Compensating Reactance in the Literature

2.4.1 Introduction

This section now presents a review of the various strategies proposed in the technical literature on the broad subject of controllable capacitive reactance X_{CSC} to damp power system oscillations. Since this thesis focuses in particular on the inter-area mode oscillation damping problem, special attention is paid to those control approaches suited to alleviating this problem. The review covers a number of aspects pertinent to the issue of power oscillation damping, namely:

- (i) the types of controls (control laws) which are appropriate to different applications of power oscillation damping;
- (ii) the types of signals that can be used as the input to a variable series capacitive reactance damping controller;
- (iii) the factors that govern the ability of a variable series capacitive reactance to provide additional damping to the system; and
- (iv) possible techniques for the design and correct placement of a controlled capacitive reactance within the transmission network in order to mitigate the power oscillation damping phenomenon.

In addition to a general overview, the review also outlines in more detail some of the more important control and design approaches presented in the literature, where it is deemed necessary. The following subsection reviews the control approaches that have been proposed for the variation of a capacitive reactance X_{CSC} to damp power system oscillations.

2.4.2 Control Approaches

The original idea for damping power system oscillations using variable series compensation was based on switching the series capacitor in a capacitor bank in and out of the transmission line during transient power swings. Control laws, which were bang-bang in nature, were proposed to either insert or bypass the controlled series reactance X_{CSC} at appropriate instants in the transmission line. It is important to note that at the time this idea originated, continuous control was not possible to achieve as circuit breakers had to be used to either insert or remove a series capacitor in a capacitor bank. Nowadays power electronic FACTS devices allow continuous variation of the controlled series reactance X_{CSC} . This means that either bang-bang or continuous control of series reactance can now be used to damp the power system oscillations following a power system disturbance. The decision as to which of these approaches to employ is an important one and depends on the nature of the power oscillation phenomenon under consideration.

As mentioned previously, Smith [Smith] appears to be the first to move from Kimbark's [Kimbark1] earlier idea of a single insertion of a series capacitor to propose multiple and timed insertion and removal of a switched series capacitor to damp the post-disturbance electromechanical oscillations of a synchronous generator. Smith in [Smith] considered a two-generator system, in which the machines were connected by a switched series capacitor (for stabilisation) and a double parallel transmission line and proposed two significant control approaches. Smith proposed an optimal approach to insert the series capacitor (after a disturbance caused by a loss of one of the transmission lines) in an interconnecting transmission line at the beginning of the transient and to remove it when the derivative of the power flow in the line becomes zero; a further insertion was proposed if the kinetic energy due to the generator's speed deviation matched the amount of kinetic energy that could be removed during the rest of the swing. A second control law was also proposed in [Smith] whereby immediate insertion of the capacitor occurs after the disturbance and its first removal occurs when $d\delta/dt < 0$; subsequent re-insertion and removal is based on a decision function.

The stated aim of the control laws proposed in [Smith] is to return the generators to steady state in a dead-beat (non-oscillatory) manner, but these laws require the use of

complicated decision functions which in turn require a knowledge of system angular frequency, shaft angular velocity, moments of inertias of the two machines, target steady-state power flow, reactance of the series capacitor and the voltage behind quadrature axis reactance in each machine. The measurements required for the controller are machine angular velocity ω , transmitted power P_{tr} , a knowledge of which line has been lost as well as pre-transient information. An optimal approach for multi-machine systems was proposed which involves a sequence of insertions and removals of several capacitors used to control different machine swings. Despite the complexity of these control approaches, Smith [Smith] notes that even simple switching based on angle excursions (X_{CSC} switched *in* for increasing angle differences and X_{CSC} switched *out* for decreasing) will greatly improve the transient stability, although it will not yield a dead-beat response.

RamaRao and Reitan in reference [RamaRao] use optimal control theory to propose an approach with two intermittent-duty series capacitors to improve the transient stability of a single-machine infinite bus power system. The proposed optimal control is bang-bang in nature and results from the application of Pontryagin's maximum principle; a switching function is described as the product of an adjoint variable (obtained using the maximum principle) and $\sin(\delta)$. This approach is also aimed at returning the power system transients back to steady-state in a non-oscillatory manner.

The dead-beat control proposed in [Smith] is complicated and is likely to be impractical; indeed the author himself adopts a far simpler and more practical control approach in a subsequent paper [Webster]. Smith and Webster [Webster] describe a practical, laboratory-scale implementation of the ideas in [Smith] using a far simpler control law. The control law adopted is to insert and bypass a series capacitor based on the speed deviation $(\omega - \omega_0)$ between generator shaft speed ω and synchronous speed ω_0 . The proposed bang-bang algorithm is as follows:

$$\begin{aligned} &\text{insert } X_{CSC} \text{ if } \omega - \omega_0 > 0 \\ &\text{bypass } X_{CSC} \text{ if } \omega - \omega_0 < 0. \end{aligned} \tag{2.3}$$

The authors chose the value of X_{CSC} using successive trials, but show, by means of an equation, that a maximum value of X_{CSC} exists above which negative damping can be introduced. A further, and well-known, problem with this bang-bang approach is that of controller chatter: near steady state, small speed deviations can introduce unwanted operation of the control. The authors of [Webster] avoid this problem by including a time-based, exponentially-decreasing override function: this approach enables the full benefit of the bang-bang control when the system is far away from target (steady-state) and gradually phases out the control as the system nears steady-state. These earlier control approaches discussed so far involved the use of a conventional series capacitor with a mechanical circuit breaker used to insert and bypass it.

Essentially, the bang-bang control law proposed in [Webster], shown here in eqn. (2.3), has in one way or another appeared in a number of subsequent studies [Angquist,Gyugyi3,Rigby2] all of which employ modern FACTS series compensators to damp power system oscillations. In reference [Rigby2] the problem of controller chatter was avoided by introducing a small dead-band ε into the basic switching algorithm of eqn. (2.3) such that the series compensating reactance is not altered for small deviations in generator speed. The control algorithm then becomes:

$$\begin{aligned} &\text{insert } X_{CSC} \text{ if } \omega - \omega_0 > \varepsilon \\ &\text{remove } X_{CSC} \text{ if } \omega - \omega_0 < -\varepsilon \end{aligned} \quad (2.4)$$

Again this control algorithm simply senses the speed difference between the machines at either end of the transmission line and changes the power transfer by modulating the line impedance as required in order to damp the system oscillations.

Reference [Noroozian2] also proposes a bang-bang control approach, where the series compensating reactance inserted in the line is varied between a maximum and minimum value; however, [Noroozian2] uses energy functions to derive the following control law:

$$\begin{aligned}
&\text{if } \frac{d}{dt} \cos(\theta) \leq 0 \text{ then switch in } X_{CSC} \\
&\text{if } \frac{d}{dt} \cos(\theta) > 0 \text{ then switch out } X_{CSC}
\end{aligned} \tag{2.5}$$

where θ is the angular difference between the voltage at each end of the compensated line. The control law in eqn. (2.5) is in some respects similar to that proposed in eqn. (2.3) since the term $d/dt(\cos(\theta))$ is expected to contain similar system information to the speed deviation $\Delta\omega$ in eqn. (2.3).

The control strategies reviewed thus far have all concentrated on damping the power swings of one or more generators in cases where the behaviour of each individual generator is of direct concern. However, poorly damped power swings also frequently occur in transmission systems as a result of a large group of generators in one area oscillating against a large group of generators in another, geographically remote, area. Damping such inter-area mode power oscillations using controllable series compensators typically requires a distinct control approach, namely continuous control.

Reference [Noroozian1] examines the control of inter-area mode oscillations using controllable series compensators in a two-area system, with each area represented as an aggregate machine; a continuous control law is proposed as follows:

$$X_{CSC} = K_{CSC}(\Delta\omega_1 - \Delta\omega_2) \tag{2.6}$$

with the control signal selected as the difference between the angular velocity deviations $\Delta\omega_1$ and $\Delta\omega_2$ of the two aggregate machines and K_{CSC} being the variable series compensator controller gain. In practice it would be necessary to synthesise the signals $\Delta\omega_1$ and $\Delta\omega_2$ from measured variables in each area, although this aspect is not considered in [Noroozian1]. The analyses in [Noroozian1] show that in the case of the inter-area mode phenomenon the damping due to the controllable series compensator increases with line loading; this is shown to be advantageous since normally under this condition of increased loading the damping of inter-area modes decreases.

Gronquist [Gronquist] considers the problem of power oscillation damping using a Thyristor Controlled Series Capacitor (TCSC) and exclusively locally measurable variables for its control. The control law derived in [Gronquist] is based on the voltage drop V across the line in which TCSC is placed and its derivative. The voltage V is synthesised by multiplying the measured line current by the known reactance of the line and adding this to the voltage V_{TCSC} across the TCSC itself as follows:

$$V = IX_{LINE} + V_{TCSC} \quad (2.7)$$

The input to the controller is then the product of the synthesised voltage V and its derivative \dot{V} ; based on this input signal a continuous damping-control law is proposed which can be summarised as:

$$\begin{aligned} V * \dot{V} > 0 & : \text{increase TCSC reactance} \\ V * \dot{V} < 0 & : \text{decrease TCSC reactance} \\ V * \dot{V} = 0 & : \text{keep TCSC reactance at nominal.} \end{aligned} \quad (2.8)$$

The control approach proposed in [Gronquist] is worth noting in a number of respects. Firstly, the basic control law is derived using a Lyapunov (energy function) approach without linearising the system equations. Furthermore, the scheme has the advantage of being simple and of relying solely on locally-measured variables, and in this respect it is more desirable than other schemes such as that in [Noroozian1] in which aggregate machine speed signals must be synthesised. Finally, the authors of [Gronquist] show simulation results that indicate that the proposed approach can successfully be used to damp a multi-machine (i.e., three machine) system. For these reasons the control approach proposed in [Gronquist] could be a candidate for consideration for damping the inter-area mode phenomenon. Similarly, de Mello [deMello1] proposes that in the case of controllable series compensation, continuous control using locally-measured variables is the appropriate control approach for inter-area mode damping control; in particular de Mello proposes using the rate of change of the power flowing through the controllable series compensator itself as the most

logical input control signal for power oscillation damping of inter-area modes. The relative performance of the two input signals proposed by Grongquist and deMello is evaluated in a damping control scheme in Chapter Four of this thesis.

The issue of bang-bang versus continuous control of series compensation for power oscillation damping has received a thorough theoretical treatment by Swift et al. [Swift1,2]. In particular, reference [Swift1] investigates the controllable series compensator's (CSC's) damping control by studying a single-machine infinite bus (SMIB) system; the authors integrate a model of the CSC into the well-known Phillips-Heffron model of a synchronous generator infinite bus system. The Phillips-Heffron model of a single machine system has been used for design and analysis of conventional excitation systems and power system stabilisers. The advantage of the Phillips-Heffron model (and its modification to include a controllable series compensator) is that it provides insight into how the CSC and its controller design affect the damping torques of the machines connected to the system, and hence to the damping of system oscillations involving these machines.

In reference [Swift2] a control law is assumed for the CSC of the form:

$$\Delta X_{CSC} = \frac{K_C}{1 + sT_{CSC}} \omega_s \Delta \omega \quad (2.9)$$

where the input to the CSC control is the generator speed deviation $\Delta \omega$, T_{CSC} is the time constant of the signal conditioning on the input signal, the output of the control is the change ΔX_{CSC} in the series compensation and K_C is the controller gain. Closed form linearised equations for the damping torque contributed by the control action are derived in [Swift1] and are used to show the effect of the controller gain K_C on damping as well as the necessary conditions for successful improvement of damping by the scheme. The authors present a detailed analysis to show that the damping provided by the CSC control increases with increasing gain K_C ; the findings of Swift's analysis therefore provide a theoretical justification for the control approach adopted in [Webster] and shown here in eqn. (2.3): for a given magnitude of controllable series capacitive reactance, the best improvement in damping is shown to

occur for infinite controller gain K_C (i.e., bang-bang control). The analysis in [Swift1] also suggests that for robust control performance, the CSC damping control must be designed at conditions of light line loading and weak system connections (the conditions for which the control is least effective). The attraction of the analytical approach of Swift et al. is that it yields insightful design equations for the synchronising and damping torques provided to the system by the CSC's damping control.

In support of the findings of Swift et al, Choi in [Choi] also concludes that bang-bang control of the controllable series compensating element is the most efficient method of increasing the damping of the electromechanical oscillations of the synchronous generators in a power system. Thus, damping power system oscillations by means of a bang-bang control results in the optimum utilisation of the available controllable series compensator. Notwithstanding the theoretical advantages of the bang-bang control shown in [Choi,Swift1], this approach does nevertheless have the significant disadvantage of the chatter problem mentioned previously, which is still relevant today even with the use of modern FACTS devices: bang-bang control can excite unwanted interactions in the system at the later stages of the transient process when the oscillations are no longer severe. Although the analytical techniques of Swift et al. [Swift1,2] are able to identify the synchronising and damping torques obtained using continuous CSC control, no definitive method has been proposed for designing the magnitude of controllable series compensating reactance which should be employed in a bang-bang regimen of control. Further, even the optimisation for the bang-bang controller is mathematically complicated which makes the realisation more difficult than in the case of a linear controller [Lerch].

From the review of the literature presented thus far, it is apparent that the bang-bang method of controlling series compensating reactance is most suited for use in the short time period following a severe system disturbance in order to improve the first swing stability of the generators feeding the transmission system. Furthermore, although continuous control of the series compensating reactance has less impact on power swings, this approach is nevertheless more suited to the requirements of damping inter-area mode oscillations, since these oscillations are in effect a small-signal, dynamic stability problem.

In practice the most effective approach to controlling the reactance of a FACTS series compensator would probably involve combining the bang-bang and continuous control methods in some coordinated manner in order to cater for damping of realistic power system transients under both large and small signal conditions. Indeed some authors such as Choi [Choi] have proposed such an approach using, for example, bang-bang control of a thyristor-switched capacitor to suppress large power swings and continuous control of a thyristor controlled reactor to damp out small oscillations. However, since the focus of this thesis is specifically on the inter-area mode-damping problem the investigations to be carried out in the main part of the work have been concentrated solely on continuous control approaches.

The additional challenge in using controllable series compensation to damp inter-area modes is the selection of a suitable input signal to the controller. However, as the previous discussions have shown, a number of different possible input signals can be obtained in practice. The advantage of the continuous control approach to damping inter-area mode oscillations is that powerful, small-signal linearised analysis methods (eigenvalues, eigenvectors, participation factors, etc.) may be used to great assistance in designing and locating the controlled compensator [Chen1,Choi,Yang]. The following section of the review considers the types of input signals that can be used for the controller and discusses which ones are more suited to the inter-area mode damping problem.

2.4.3 Types of Input Signals for the Controller

This subsection discusses different types of input signals that have been proposed in the literature for damping power system oscillations using variable series capacitive reactance. The control approaches discussed in the previous subsection for the single-machine infinite bus system show that, at the most basic level, the generator speed deviation $\Delta\omega$ is a logical choice of input signal for the controller as evident in the control algorithms of eqns. (2.3), (2.4), and (2.6). The speed deviation signal contains information about the acceleration of the machine and, as explained in section 2.3, the transient imbalances in accelerating power in the generator are what cause the electromechanical power oscillations which are to be damped. In the case of the multi-machine and inter-area mode oscillation damping problem the underlying

mechanism is the same but, as pointed out in [Noroozian1], the oscillations now involve one group of machines oscillating against another group of machines; as explained in the previous subsection, the approach proposed in [Noroozian1] for inter-area mode damping control is also to use speed deviation, but to synthesise the speed deviation between the two aggregate machines involved in the inter-area mode of that study. Such an approach may however present some practical difficulties with geographically remote measurements and may also become more difficult in cases where the inter-area mode oscillations involve more than two groups of machines oscillating against one another as considered in [Noroozian1].

Speed deviation is however not the only input signal which has been proposed for the series impedance controller. In fact, any input signal which contains information about the relative acceleration of machines participating in the inter-area oscillation is a candidate as an input to the power oscillation damping controller. Smith in [Smith] proposed, for a multi-machine system, a frequency deviation controller whereby the series capacitor is inserted and removed based on the sign of the frequency deviation of the group of machines it affects most strongly. The previous section has also discussed the control approaches proposed in [Choi] and [deMello1] whose input signal is based on the instantaneous power imbalances and rate of change of power flow in the system, respectively, each of which are then used to determine switching instants of the variable series capacitive reactance.

However, in a large interconnected power system inter-area mode oscillations are more complex and there are generally many modes, each involving large numbers of generators. When a series connected FACTS impedance controller is placed in the transmission network for damping such inter-area mode oscillations, the speed deviations of the machines of interest are not easily obtainable and hence the need to look at other alternatives. In practice input signals should be synthesised from local measurements whenever possible [Larsen,Grongquist,Yang]. Reference [Grongquist] proposes using only local measurements in the transmission line in which the controlled device is placed to create a synthesised input for the controller (that is, a synthesised voltage V and its derivative as shown in eqn. (2.8)).

Reference [Larsen] discusses a measurement synthesis which has shown promise for damping of inter-area modes: the angular phase difference between synthesised remote voltages on either side of the controllable element is described and is shown to contain information about inter-area modes of interest. Indeed, references [Dolan] and [Larsen] propose a speed deviation controller in which local measurements are used to synthesise an angle difference; this synthesised angle difference is then converted to a speed measurement using a filtered derivative circuit in order to represent the speed at which the ends of the system are moving in relation to each other. References [Choi,deMello,Yang] propose the use of tie-line power flow as an input signal to the controller for damping inter-area oscillations since this signal can be obtained from local measurements only. Thus, for the inter-area mode damping problem, input signals such as the generator speed deviations and the tie-line power flows can be synthesised from local measurements in practice.

As the above discussion of the literature reveals, the proper selection of the input signal for the controllable series compensator damping controller to be used is one of the most important control design decisions to be made. This decision has an important bearing on the performance of the inter-area mode oscillation damping control and this thesis later examines a number of important suggestions in the literature for suitable input signals and compares the effect of these signals on damping. The following section of the review looks at the relative performance of the variable series compensating reactance to provide damping and the factors that govern its ability to improve damping in the power system.

2.4.4 Factors Governing the Ability of Variable Impedance Control to Improve Damping

The opening sections of this chapter have described, in simple physical terms, how the coordinated control of series compensating capacitance can be used to improve the damping of electromechanical power system oscillations. More recently, in the literature, a number of papers have appeared which attempt to qualify more thoroughly the extent to which controlled series capacitance can improve the damping of power system oscillations and the factors which influence this improved damping. As explained in the opening chapter, the electromechanical oscillations in power systems are one of the factors that can limit the amount of power transfer in a

transmission network. Reference [deMello1] states that power system stabilisers are the most efficient means to provide the required additional damping in power systems but that the use of controllable series compensators can also provide important damping benefits in the system in cases where other system considerations dictate this approach.

In contrast to [deMello1], reference [Angquist] states that for low frequency power oscillations power system stabilisers are less effective and suggests the use of controllable reactance to damp out these oscillations. However, the issue of whether power system stabilisers are a more effective solution than controllable series compensators for damping power system oscillations (as debated in [deMello1] and [Angquist]) lies outside the scope of this thesis; for the purposes of this study the important conclusion to be taken from these references is simply that controllable series compensation in itself offers a significant potential benefit to the damping of such oscillations. Reference [Angquist] provides a comparison between the Static Var Compensator (SVC) and the controllable series compensator (CSC), evaluating their relative improvement of system dynamic performance in a two-machine power system. Reference [Angquist] shows that the damping effect obtained with the CSC is higher than that of a SVC per installed MVar and the authors claim that the CSC improves power transfer ten times more than the SVC, per installed MVar. The authors of [Angquist] also show, using the two-machine system, that the location of the CSC damping controller (that is, where CSC could be placed) has no significant influence on its performance whereas in the case of the SVC location plays a very crucial role. However, in multi-machine environments, there is an optimum point in the power system for the location of a CSC damping controller as discussed in the next subsection (section 2.4.5).

In reference [Noroozian1] closed form equations are derived for various types of controllers (CSC, SVC, phase shifter) in order to compare the efficacy of different schemes on line loading and their relative performance is considered. Reference [Noroozian1] also compares the power ratings of controlled series capacitance required for a specified damping factor at different line loadings and concludes that the CSC can have several times more leverage than a SVC or a phase shifter of comparable rating. The important conclusions reached by the authors are, firstly, that

the damping effect due to a CSC increases with line loading, which is very advantageous since damping of system oscillations normally decreases with increased loading of lines and, secondly, that the CSC damping effect is not dependent on load characteristics, as in the case of the SVC.

Reference [Wang2] integrates, in turn, an SVC, a CSC, and a controllable phase shifter into the Phillips-Heffron model of a power system for the single-machine infinite bus case and draws analytical conclusions about the damping effect of each device. The robustness of the damping controllers associated with each of these devices to variations in system operating conditions is compared. The results in [Wang2] also show that at high load conditions more damping is provided by SVC and CSC damping controllers, but that at low load conditions the damping effect of the SVC is negative whilst that of the CSC remains positive over the entire range of system load conditions, which is in accordance with the findings in [Noroozian1]. The following subsection will now review the techniques proposed in the literature for the design and placement of the controlled series compensation for the specific purpose of damping power system oscillations.

2.4.5 Techniques for the Design and Placement of Variable Impedance Control

This subsection of the review presents a summary of the methods proposed in the literature for the design and placement of controlled series capacitive reactance for improved system damping. The previous discussions of section 2.4.2 described Swift and Wang's approach [Swift1] whereby the Phillips-Heffron model of a power system for a single-machine infinite bus system is used to establish a design relationship, using a particular controller input, between the controller gain and damping torque added into the system; an approximately linear relationship was shown to exist between the controller gain and the resulting damping torque component. Further work by Swift and Wang [Swift2] extends the ideas presented in [Swift1] into a multi-machine application and, using the sensitivities of the controllable series compensator (CSC) damping torque to the device location, successfully determines the optimum location of the CSC damping controller in a multi-machine environment. The analysis techniques and concepts of [Swift2] are the same as in [Swift1] but the additional aspect treated, arising out of multi-machine application, is the derivation of indices to determine the best location of a CSC damping controller. Reference [Swift2] proposes

that to optimally utilise the available CSC damping controller in a multi-machine power system, the CSC should be installed close to that generator which is most sensitive to the oscillation mode which is to be damped in the power system.

In reference [Chen1], Chen et al. investigate the design of CSC damping controllers for improving the stability of multi-machine power systems using a numerical pole placement technique, which in turn is used to work out feedback controller gains. Reference [Chen1] states that there are no basic guidelines for best position of the poles to improve damping, and therefore this technique for pole placement primarily relies on sound engineering judgement. The technique used to decide on the location of the CSC controller is based on the magnitude of the residue (controllability) of each natural mode of oscillation in the system, as calculated from the system eigenvalues. Further work by Chen [Chen2] employs sophisticated design techniques such as eigenvalue assignment, sequential design methods, least squares approximation, and linear optimisation in order to design a TCSC controller for a multi-machine, multi-controller system. Mode controllability and mode observability are used to select the Thyristor Controlled Series Capacitor (TCSC) controller sites and effective control signals for a TCSC control scheme.

Reference [Noroozian2] considers the design of TCSC controllers in a two-TCSC, three-generator study example in which the particular TCSC controller inputs used can readily be synthesised from local measurements. Reference [Noroozian2] then considers the effect on performance and robustness of different locations of the FACTS device. In accordance with Swift's [Swift2] findings, simulation results presented in [Noroozian2] show that the effect of the larger TCSC placed on the main system inter-tie is to provide better damping than a smaller size of TCSC placed elsewhere in the system. Reference [Noroozian2] also notes an added advantage of using the particular control approach in eqn. (2.5), which is that controllers situated at different locations do not adversely interact with each other.

Reference [Yang] considers an example of a three-area, six-machine power system and employs the residue method, together with modal sensitivities to determine the best location of the TCSC, and proposes that for a given TCSC and controller design, a larger residue will give a larger change in the damping of the corresponding mode.

References [Chen1] and [Yang] use a similar approach to select the most effective location for a CSC and propose that the best combination of the controller input and output is that which yields the largest residue (that is, sufficient degree of controllability) for the desired mode. Reference [Grongquist] investigates the damping of power swings using energy functions in a three-generator power system with two TCSCs, each rated at 50% of maximum compensation, at different sites of the transmission line system. Grongquist successfully shows the damping effect of these two TCSCs; however, the investigations of [Grongquist] do not compare the amount of damping provided by each TCSC.

2.5 Conclusion

This chapter has presented an overview of the strategies suitable for damping power system oscillations using controllable FACTS series compensators. The review has shown that the choice of control regimen should be guided by the nature of the power oscillation phenomenon to be damped: discontinuous (bang-bang) control of series reactance is suited to maintaining system stability in the first swing following a major disturbance, whilst the various forms of continuous control of series reactance are best suited to damping inter-area mode oscillations.

The review has also identified some promising approaches to the control of series compensation to mitigate inter-area type oscillations, notably those of Grongquist [Grongquist] and de Mello [deMello1] as well as Larsen [Larsen]. Finally, the review has identified in the literature [Swift1,2] an insightful approach to the design of the variable reactance controller itself in order to provide quantifiable increases in system damping.

Chapter Four of this thesis presents the results of an investigation into the methods proposed in [Swift1,2] as applied to the specific case of a single machine infinite bus system, and where the controlled element is an inverter-based FACTS series compensator. These investigations are carried out in order to gain confidence in the techniques proposed in [Swift1,2] in the conceptually simpler single machine case before considering, in Chapter Five of the thesis, the inter-area mode damping problem itself. The investigations in Chapter Four of the thesis also consider and

compare the control approach proposed in [Grongquist] and the ideas in [deMello1,Larsen]. Chapter Five of the thesis investigates the ideas in [Swift1,2] as applied to an inter-area mode damping problem in a particular four-generator study system described in [Kundur]. The next chapter now presents and develops the mathematical models of the SMIB power system used in the analyses and simulation studies of this thesis, including both the detailed and simplified representation of the inverter-based series compensator.

CHAPTER THREE

MATHEMATICAL MODELLING

3.1 Introduction

The analysis and modelling of various system components for power system stability studies has always been a challenge since, for any power system dynamic study, the most appropriate mathematical model must be chosen according to the phenomena being investigated. Whilst the use of an over-simplified system model often leads to erroneous results, an over-represented system model results in an enormous increase in computational costs. Thus, it is essential that the simplifications made be based on a thorough understanding of the phenomena being studied. Since this thesis focuses on the (small-signal) damping of power system oscillations, the usual assumptions associated with such studies [Heffron, Kundur] are applied to the system model and these assumptions are then tested using more-detailed system models.

This chapter develops three mathematical models of a single-machine infinite bus system that are to be used to analyse the behaviour of the system for a range of system operating conditions. In Chapter Four these models are used, in particular, to analyse the influence of the controllable series compensator and its damping controls on the stability of the system. This chapter first derives a simplified non-linear model of the single-machine infinite bus system before describing a detailed non-linear mathematical model of the same system. The simplified model is then linearised to yield the linear Phillips-Heffron model of the system that is used for small-signal eigenvalue analysis. Finally, this chapter presents results where these different models of the system are used to analyse the influence of various important system parameters and subsystems (especially the influence of the exciter and automatic voltage regulator) on system stability.

To date much industry effort in the field of power system stability has been devoted to the issue of transient stability, and high-response exciters are known to enhance the transient stability of the system [Kundur]. Unfortunately however, as a consequence

of the introduction of such exciters, modern power systems have been found to exhibit poorly damped oscillations and hence their introduction has often adversely affected small-signal stability by introducing negative damping. Power system stabilisers have been exclusively designed to provide the desired additional damping to overcome this problem where it exists. This thesis however, addresses the issue of whether a particular FACTS series compensator – an inverter-based series compensator – can be used as another tool to provide additional damping in power systems.

Fig. 3.1 shows a single-machine infinite bus (SMIB) power system considered in the analyses of Chapter Four of the thesis. Before developing various mathematical models of the system, the following section introduces three levels of system modelling and explains the purpose of each level.

3.2 Different Models of the System and Objectives

Fig. 3.1 shows a diagram of the single-machine infinite bus power system, together with an idealised CSC, that is considered in the investigations of Chapter Four of this thesis. This section briefly presents and discusses the various mathematical models of the single-machine infinite bus system in Fig. 3.1 that are used for the simulation and analysis studies presented in the thesis. Three different levels of model of the system in Fig. 3.1 are used in the analyses; these three levels of modelling, and the purpose of each level, can be summarised as follows.

3.2.1 Non-Linear Model of the System Using an Idealised Representation of the Controllable Series Compensator

These non-linear differential equations are used to build up a (simplified) MATLAB model for time-domain simulation studies but the primary purpose of this model is to be linearised so as to provide an analytical model with which to study the effect of damping controller design with an idealised CSC representation.

3.2.2 Linearised (Phillips-Heffron) Model

Linearisation of the model in 3.2.1 yields the linear Phillips-Heffron (P-H) model equations of a single-machine infinite bus power system [Heffron]. The purpose of

this model is to provide a graphical, linearised block diagram model together with analytical equations to show how design of the CSC controller affects damping [Swift1].

3.2.3 Detailed Non-Linear Simulation Model

This model once again represents the system shown in Fig. 3.1 using non-linear differential equations, but with two differences from the non-linear model described in 3.2.1: firstly, the mathematical model of the synchronous machine is slightly more detailed than in the case of the non-linear model in 3.2.1; secondly, the inverter-based CSC itself is now modelled in detail, with both its power-electronic switching, and its internal controls being accurately represented. This more-detailed non-linear model has been developed in the power systems simulation software package PSCAD/EMTDC. The purpose of this non-linear model is twofold: firstly, to serve as a benchmark against which to evaluate the models described in 3.2.1 and 3.2.2 so that the assumptions made in deriving these models can be tested; secondly, to act as the primary time-domain simulation tool for these and later (multi-machine) studies in the thesis.

For the time-domain studies carried out in the thesis the PSCAD/EMTDC simulation environment was chosen over MATLAB environment, because the former is a dedicated power systems simulation tool. The advantage of PSCAD/EMTDC is that the extension of the study to a multi-machine power system and the investigation of various input signals to the controller is made easier; the disadvantage is that the powerful control analysis and design features of MATLAB (linearisation and eigenvalue calculation to name two) are no longer available. The following section develops various mathematical models of a single-machine infinite bus system in Fig. 3.1 that are used in the analyses of the thesis.

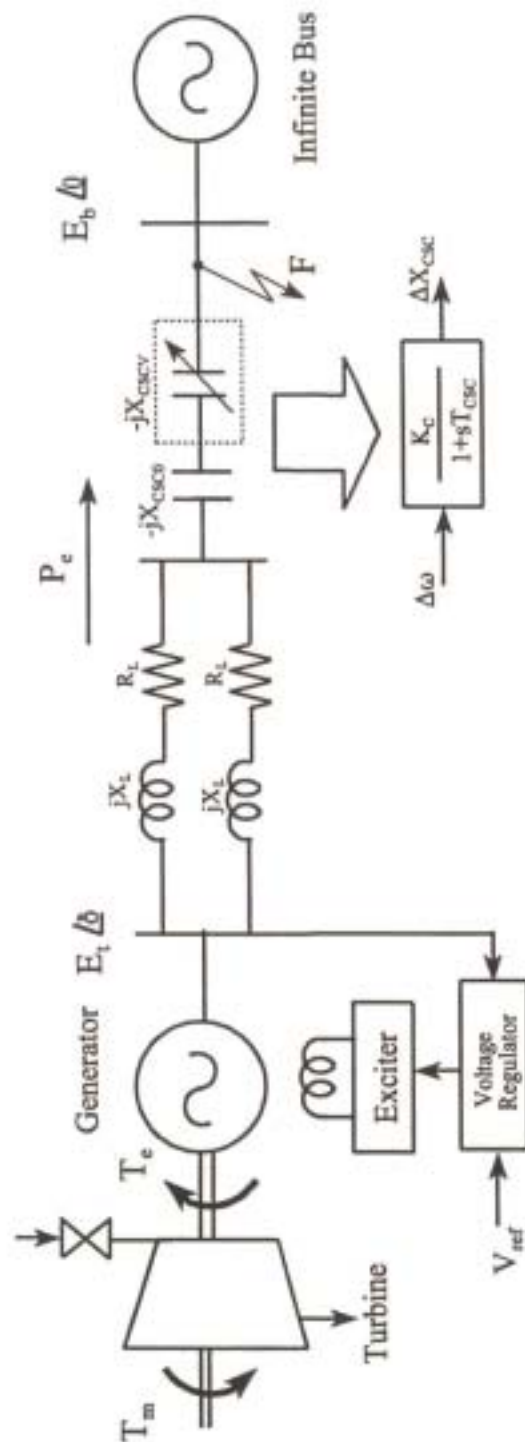


Fig. 3.1: A single-machine infinite bus power system with two parallel lines in series with a fixed and a controllable compensating reactance.

3.3 System Modelling

3.3.1 Introduction

In the single-machine infinite bus power system under consideration in this study (Fig. 3.1), the transmission line consists of two parallel lines of lumped impedance $R_L + jX_L$. At the receiving end of the power system (infinite bus) the controllable series compensator is inserted in a single line; the compensation provided by the CSC is made up of a fixed component of compensating reactance $-jX_{CSC0}$ and a dynamically variable component $-jX_{CSCV}$. In the analyses of Chapter Four, the generator feeding the line is considered to have an automatic voltage regulator (AVR) and a high-gain, thyristor-type exciter with transient gain reduction (lead-lag network). The purpose of including a high-gain thyristor exciter with transient gain reduction and AVR in the generator model is twofold: firstly, whilst realistic, this particular combination of conditions is also known [Kundur] to adversely affect the inherent damping torque in the system and it therefore constitutes an example of a poorly damped system with which to test the ability of the CSC controller to restore this component of torque; secondly, since the exciter and AVR characteristics are known to have a significant impact on damping torques in a power system it is important to represent these devices in the system model in order to ensure a realistic representation of the problem being studied.

The effect of the turbine-governor dynamics in these studies is ignored such that the mechanical input torque T_m to the turbine is assumed to be constant over the time frame of the investigation. Finally, the power oscillation damping controller is considered to have, as its input, the generator speed deviation $\Delta\omega$; the controller itself comprises a simple proportional gain K_C and first order lag term. In the idealised representation of the CSC the change in compensation X_{CSCV} demanded at the output of the controller is assumed to occur instantaneously in the transmission line. The system in Fig. 3.1, and the derivation of the Phillips-Heffron (P-H) model that follows, is based on the work of Swift and Wang [Swift1,2] as well as Phillips and Heffron [Heffron]. The Phillips-Heffron equations are obtained by linearising a set of non-linear differential equations for the system in Fig. 3.1 consisting of the generator equipped with an automatic voltage regulator (AVR) and thyristor-type excitation

system; the extension of the Phillips-Heffron model to include an idealised representation of the CSC is the work of Swift and Wang.

3.3.2 Simplified Non-Linear System Model

Synchronous generator electrical system

The two-axis model of a synchronous generator is shown in Fig. 3.2. Amortisseur effects are represented by one damper winding on the d-axis and one damper winding on the q-axis; these windings are short circuited. The following assumptions for the system in Fig. 3.1 are made:

- (i) the synchronous generator is ideal with a sinusoidal air gap mmf and a linear magnetic circuit;
- (ii) iron and stray losses are negligible; and
- (iii) the generator and network to which it is connected are balanced.

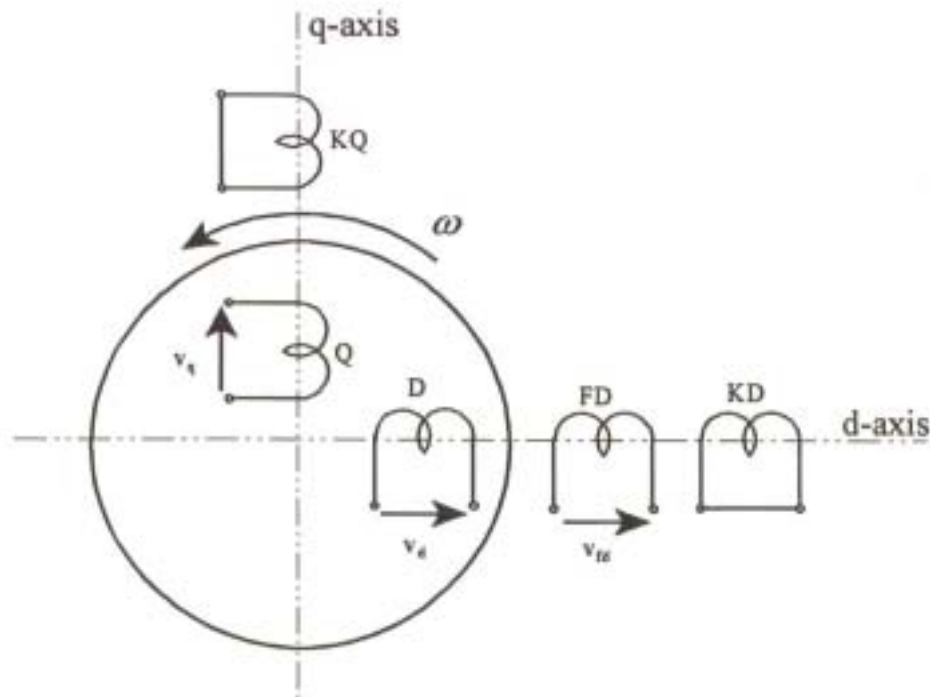


Fig. 3.2: Two-axis representation of a synchronous machine.

To write the equations for this machine, a generator convention has been adopted for the stator windings and a motor (load) convention has been adopted for the rotor (field and damper) windings; the convention is that used in [Kundur]. The per-unit system has been described in Appendix A. With these conventions the voltage equations of the five coils of Fig. 3.2 in the rotor reference frame are as follows:

$$v_d = p\psi_d - R_a i_d - \psi_q \omega \quad (3.1)$$

$$v_q = p\psi_q - R_a i_q + \psi_d \omega \quad (3.2)$$

$$v_{fd} = p\psi_{fd} + R_{fd} i_{fd} \quad (3.3)$$

$$v_{kd} = p\psi_{kd} + R_{kd} i_{kd} \quad (3.4)$$

$$v_{kq} = p\psi_{kq} + R_{kq} i_{kq} \quad (3.5)$$

where the terms $\psi\omega$ and $p\psi$ are speed and transformer voltages, respectively.

The stator and rotor flux linkages are:

$$\begin{bmatrix} \psi_d \\ \psi_{fd} \\ \psi_{kd} \\ \psi_q \\ \psi_{kq} \end{bmatrix} = \begin{bmatrix} -L_d & L_{ad} & L_{ad} & 0 & 0 \\ -L_{ad} & L_{fd} & L_{ad} & 0 & 0 \\ -L_{ad} & L_{ad} & L_{kdd} & 0 & 0 \\ 0 & 0 & 0 & -L_q & L_{aq} \\ 0 & 0 & 0 & -L_{aq} & L_{kq} \end{bmatrix} \begin{bmatrix} i_d \\ i_{fd} \\ i_{kd} \\ i_q \\ i_{kq} \end{bmatrix} \quad (3.6)$$

where all inductances are constant and saturation effects are ignored.

The electromagnetic torque is given by:

$$T_e = \frac{\omega_o}{2} (\psi_d i_q - \psi_q i_d) \quad (3.7)$$

The above equations (3.1) to (3.7) describe the generator electrical behaviour and together with two differential equations which describe its mechanical behaviour in the next subsection form a seventh-order model. This seventh-order model represents the stator and rotor electrical transients and mechanical transients. For the purposes of this study, the following assumptions are applied to the fifth-order electrical model of the generator in Fig. 3.2:

- (i) the effects of the generator stator transients ($p\psi$ terms in eqns. (3.1-2)) are neglected, and a further simplification is added by neglecting the effect of generator speed variations; however, this does not mean that the generator speed is considered to be constant – rather, the generator speed changes are assumed to be too small to have a significant effect on the generator stator voltages;
- (ii) damper (amortisseur) windings are neglected.

With these assumptions, the stator flux linkages from eqn. (3.6) are:

$$\psi_d = -L_d i_d + L_{ad} i_{fd} \quad (3.8)$$

$$\psi_q = -L_q i_q \quad (3.9)$$

and the rotor flux linkage equation is:

$$\psi_{fd} = -L_{ad} i_d + L_{fd} i_{fd} \quad (3.10)$$

or in terms of reactances equations (3.8-10) become,

$$\omega_o \psi_d = -X_d i_d + X_{ad} i_{fd} \quad (3.11)$$

$$\omega_o \psi_q = -X_q i_q \quad (3.12)$$

$$\omega_o \psi_{fd} = -X_{ad} i_d + X_{fd} i_{fd} \quad (3.13)$$

where ω_o is the system synchronous speed.

The rotor voltage equation remains the same as in eqn. (3.3) and is now the only differential equation associated with the electrical characteristics of the generator. In order to write these equations in an alternative form [Kundur] consider the following variables:

$$E_{fd} = X_{ad} i_{fd} \quad \text{voltage proportional to } i_{fd}$$

$$E_q' = \omega_o \frac{X_{ad}}{X_{fd}} \psi_{fd} \quad \text{voltage proportional to } \psi_{fd}$$

$$E_{fd} = \frac{X_{ad}}{R_{fd}} v_{fd} \quad \text{voltage proportional to } v_{fd}$$

and with the reactances defined as:

$$X_d = X_l + X_{ad} = \text{direct-axis reactance of the generator};$$

$$X_q = X_l + X_{aq} = \text{quadrature-axis reactance of the generator};$$

$$X_{ffd} = X_{ad} + X_{fd} = \text{self-inductive reactance of the generator field circuit};$$

$$X_d' = X_l + X_{ad} X_{fd} / (X_{ad} + X_{fd}) = \text{direct-axis transient reactance of the generator};$$

and

$T_{do}' = X_{fd}/(\omega_o R_f) =$ direct-axis open circuit transient time constant of the generator.

Using the above variables eqn. (3.11) now becomes,

$$\omega_o \psi_d = -X_d i_d + E_{fd} \quad (3.14)$$

Multiplying eqn. (3.13) through by X_{ad}/X_{fd} and using the above variables yields

$$E_q' = E_{fd} - (X_d - X_d') i_d \quad (3.15)$$

Finally, multiplying eqn. (3.3) through by X_{ad}/X_{fd} and using the definition of the direct-axis open circuit transient time constant of the generator yields

$$pE_q' = \frac{1}{T_{do}'} [E_{fd} - E_{fd}] \quad (3.16)$$

The state variable representing the dynamic changes in rotor flux linkage is now E_q' , the q-axis component of the voltage behind transient reactance X_d' ; hence this model is sometimes called the voltage behind transient reactance model of the synchronous generator [Kundur]. Equation (3.16) is the only differential equation representing the electrical characteristics of the synchronous machine, in particular the dynamic variations in the field circuit of the machine. Field flux variations within the machine make an important contribution to the small-signal stability (damping) of the swing dynamics, and their effect (and hence that of the AVR and exciter) should therefore be represented in the system model; however, although the electrical model of the synchronous machine derived in this section neglects the contribution to system stability of the generator stator transients, this transient model contributes to computational simplicity [Kundur] and is shown in a later section of this chapter to be reasonable for those stability analyses for which it is used in the thesis.

Synchronous generator mechanical system

Eqn. (2.1) in Chapter Two of this thesis describes the power balance of a generator in an electric power system, and a similar equation holds for torque balance of the generator in terms of the angular position δ of its rotor. The second order equation (eqn. 2.1) may further be written as two first-order differential equations to describe the mechanical motion with an additional damping term as follows:

$$p\Delta\omega = \frac{\omega_s}{2H} (T_m - T_e - B\Delta\omega) \quad (3.17)$$

$$p\delta = \omega_s \Delta\omega \quad (3.18)$$

The differential equations (3.17) and (3.18) together form the so-called swing equation of the machine; this is the fundamental equation which governs the electromechanical oscillations of the synchronous machine in stability studies. For the purposes of the analyses of this thesis, the mechanical input torque to the machine T_m is considered to be constant at any given operating condition; the electrical torque T_e in eqn. (3.17) corresponds to the net air-gap power in the machine and accounts for the total output power of the generator plus losses in the armature winding. The parameter B in eqn. (3.17) represents the damping of the synchronous generator as a result of dissipative forces acting on its mechanical shaft system.

AVR and exciter model equations

The automatic voltage regulator and the excitation system are subsystems that impact significantly on both transient (first-swing) and dynamic (small-signal) stability [Kundur,deMello2]: a high-gain thyristor exciter and AVR have a beneficial effect on the synchronising component of torque produced by the generator but can have a detrimental effect on the damping component of torque produced by the generator. It is therefore essential for the study of inter-area mode damping that the AVR and excitation systems are accurately represented [Klein]. In this study, a voltage regulator and a thyristor-type excitation system with transient gain reduction are represented as shown schematically in Fig. 3.3.

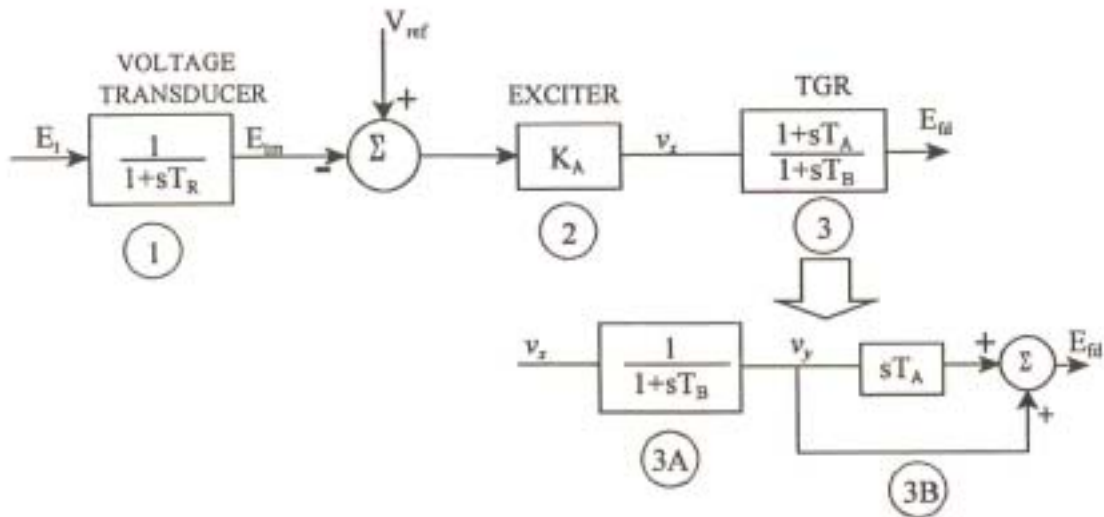


Fig.3.3: A voltage regulator and thyristor-excitation system with Transient Gain Reduction (TGR).

The differential equations describing the AVR and exciter model may be written by inspection of Fig. 3.3 as follows. From the block labelled (1) in Fig. 3.3, the following expression may be written:

$$E_t = (1 + pT_R)E_m \quad (3.19)$$

where E_t is the machine terminal voltage and T_R is the voltage transducer time constant. Re-arranging eqn. (3.19) yields the first order differential equation associated with the voltage regulator:

$$pE_m = \frac{1}{T_R}(E_t - E_m) \quad (3.20)$$

Similarly, from block (3A) in Fig. 3.3 the following differential equation is obtained:

$$pv_y = \frac{1}{T_B}(v_x - v_y) \quad (3.21)$$

From block (3B), the expression for the voltage E_{fd} applied to the generator field winding in the synchronous machine model is

$$E_{fd} = T_A p v_y + v_y$$

this expression in conjunction with eqn. (3.21) yields:

$$E_{fd} = \frac{T_A}{T_B} v_x - \left(1 - \frac{T_A}{T_B}\right) v_y \quad (3.22)$$

where T_A and T_B are the lead and lag time constants, respectively, in the transient gain reduction stage.

From Fig. 3.3 it is seen that $v_x = K_A (V_{ref} - E_{tm})$; eqns. (3.21) and (3.22) then become:

$$p v_y = \frac{1}{T_B} [K_A (V_{ref} - E_{tm}) - v_y] \quad (3.23)$$

$$E_{fd} = \frac{T_A}{T_B} K_A (V_{ref} - E_{tm}) + \left(1 - \frac{T_A}{T_B}\right) v_y \quad (3.24)$$

The mathematical model that describes the AVR and exciter under consideration is therefore given by eqns. (3.20), (3.23) and (3.24).

Controllable series compensator model equation

Eqn. (2.9) in Chapter Two describes a CSC damping controller where the generator speed deviation $\Delta\omega$ is assumed as the controller input, filtered by a first-order lag term $1 / (1+sT_{CSC})$ as proposed by Swift and Wang in [Swift1,2]; the output of the damping controller is the change $\Delta X_{CSC} = X_{CSCV}$ in the capacitive reactance required from the CSC, and the controller gain is K_C . The differential equation describing this controllable series compensator and power oscillation damping controller is obtained by re-arranging eqn. (2.9) as follows:

$$p X_{CSCV} = \frac{1}{T_{CSC}} (K_C \omega_o \Delta\omega - X_{CSCV}) \quad (3.25)$$

In this model the CSC itself is assumed to be ideal; that is, it is assumed that the CSC is able to ensure that whatever variable compensating reactance X_{CSCV} is demanded at the output of the damping controller appears instantaneously in the transmission line. The total series compensation provided by the CSC at any instant is then given by

$$X_{CSC} = X_{CSC0} + X_{CSCV} \quad (3.26)$$

Summary of non-linear equations

Non-linear differential equations for the system in Fig. 3.1 have been derived in this section and are now summarised below.

$$p\Delta\omega = \frac{\omega_o}{2H}(T_m - T_e - B\Delta\omega) \quad (3.27)$$

$$p\delta = \omega_o\Delta\omega \quad (3.28)$$

$$pE_q' = \frac{1}{T_{do}}[E_{fd} - (E_q' + (X_d - X_d')i_d)] \quad (3.29)$$

$$pE_m = \frac{1}{T_R}(E_i - E_m) \quad (3.30)$$

$$pv_y = \frac{1}{T_B}[K_A(V_{ref} - E_m) - v_y] \quad (3.31)$$

$$E_{fd} = \frac{T_A}{T_B}K_A(V_{ref} - E_m) + \left(1 - \frac{T_A}{T_B}\right)v_y \quad (3.32)$$

$$pX_{CSCV} = \frac{1}{T_{CSC}}(K_C\omega_o\Delta\omega - X_{CSCV}) \quad (3.33)$$

where eqns. (3.27) and (3.28) represent mechanical dynamics of the machine while eqn. (3.29) represents electrical dynamics of the synchronous machine. Eqns. (3.30-3.32) represent the AVR and exciter subsystems and eqn. (3.33) represents the controllable series compensator and its damping controls.

3.3.3 Detailed Non-Linear Mathematical Model of the System

The previous subsection discussed a simplified non-linear model of a single-generator infinite bus system with an idealised controllable series compensator. This subsection now briefly describes a detailed non-linear simulation model of the same system, developed in the simulation package PSCAD/EMTDC, that is used to establish the validity of the simplified model of the previous subsection.

The PSCAD (Power System Computer Aided Design) program has been designed to help simulate power systems; a graphical diagram of the system is built in PSCAD using pre-coded building blocks. The EMTDC (Electro-Magnetic Transient Direct Current) program, provided with PSCAD, contains a library of power system component models and is the software which performs the electromagnetic transients analysis on a user-defined power system; these two software packages are normally referred to as PSCAD/EMTDC. For the purposes of this study, a detailed simulation model of the system in Fig. 3.1 was developed in the PSCAD/EMTDC program; the graphical block diagram for this PSCAD/EMTDC model is shown in Fig. 3.4. The different segments of the detailed system in Fig. 3.4 may be explained as follows.

The PSCAD/EMTDC graphical representation of the system once again comprises, at the sending end, a synchronous generator, with AVR and exciter in a single block, synchronised through a transmission line to an infinite bus (ideal three-phase voltage source) at the receiving end. The synchronous machine in this model is a full two-axis model; the amortisseur windings are once again neglected but the stator transients in the machine model are now represented. The transmission line consists of a single line, with all three phases shown, and is once again represented by lumped impedances (with resistances in ohms units and inductances in henries units). However, the dynamic behaviour of the transmission line is now represented: that is, transmission line components are no longer represented simply as fundamental frequency (50Hz) impedances in this PSCAD/EMTDC simulation model.

Finally, the controllable series compensator used in the non-linear model in Fig.3.4 is a detailed representation of an inverter-based series compensator. This compensator comprises a voltage-source inverter based on gate-turn-off (GTO) thyristors; the compensator's internal control circuits ensure that the inverter inserts a voltage in

series with the transmission line in lagging quadrature with the transmission line current via series injection transformers. In this way, the device replicates in the transmission line the voltage drop across a series capacitive reactance whose magnitude can rapidly be controlled. The voltage-source inverter is switched using sinusoidal pulse width modulation (SPWM) at 1 KHz as in [Rigby1]; the SPWM switching frequency affects the achievable bandwidth of the inverter controller, although 1 KHz is typical of inverters used in high power FACTS applications [Rigby1]. The theory of the operation of this inverter-based compensator scheme to ensure that the inserted voltages always maintain the correct phase relationship relative to the transmission line currents at different system operating conditions has been described in [Rigby1]. In this PSCAD/EMTDC model of the study system in Fig. 3.1, the inverter-based compensator is modelled in detail: the opening and closing of each power-electronic device in the inverter and the snubber circuit across each power-electronic device is represented, as well as the charging dynamics of the inverter's dc capacitor, and the internal controls that ensure the device behaves as a capacitive reactance of the desired magnitude X_{CSC} commanded at its input.

The power oscillation damping controller external to the compensator in Fig. 3.4 is identical to that in the simplified system model of the previous section: the input $\Delta\omega$ (labelled deltaW in Fig. 3.4) is fed through a first order filter and proportional gain to yield the value of the variable component of compensating reactance X_{CSCV} . This variable component X_{CSCV} is added to the magnitude of the fixed component of compensating reactance X_{CSC0} to yield the overall commanded value X_{CSC} that is fed to the inverter controls. Thus, whereas in the simplified model of the previous subsection the compensator was assumed to be ideal (that is, the commanded value of X_{CSCV} appeared instantaneously in the transmission line) in the detailed model of Fig. 3.4, the internal dynamics and response of the compensator itself are now represented in the system model.

This subsection has described the development of the detailed time-domain simulation model of the SMIB system that is to be used in the analyses of this thesis. The following subsection now derives a linearised Phillips-Heffron model of the system in Fig. 3.1.

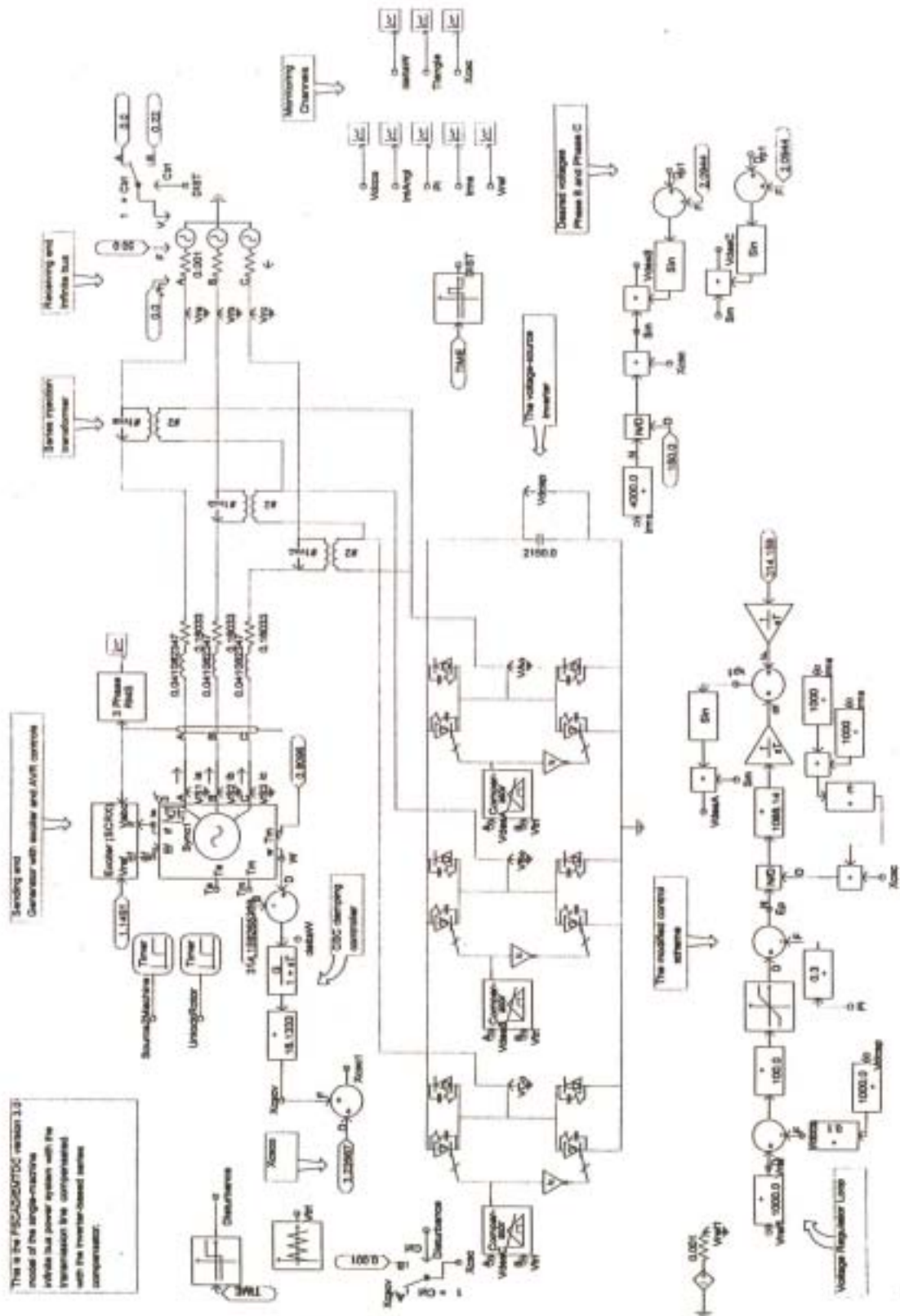


Fig. 3.4: A detailed PSCAD/EMTDC representation of a SMIB system with an inverter-based series compensator, including its controls and power electronic switching.

3.3.4 Linearised Phillips-Heffron Mathematical Model

In order to consider the small-signal stability of a single-machine infinite bus power system, the non-linear differential equations in eqns. (3.27) to (3.33) may be linearised about a particular operating point and the relations shown in Fig. 3.5 are obtained; these relations, sometimes called Phillips-Heffron model equations, have been treated previously in [Swift1,Heffron]. The linearised system equations from which the block diagram in Fig. 3.5 is obtained have been derived in Appendix B and are presented below. The extension of the P-H model to include the CSC and its damping controls is due to Swift and Wang [Swift1,2].

$$(2Hs^2 + Bs)\Delta\delta = \Delta T_m - \Delta T_e \quad (3.34)$$

$$\Delta T_e = K_1\Delta\delta + K_2\Delta E_q' + K_P\Delta X_{CSC} \quad (3.35)$$

$$\Delta E_q' = \frac{K_3}{1+sT_3}(\Delta E_M - K_4\Delta\delta - K_q\Delta X_{CSC}) \quad (3.36)$$

$$\Delta E_t = K_5\Delta\delta + K_6\Delta E_q' + K_V\Delta X_{CSC} \quad (3.37)$$

$$\Delta E_M = \left[\left(\frac{1+sT_A}{1+sT_B} \right) K_A \right] \left[V_{ref} - \left(\frac{1}{1+sT_R} \right) \Delta E_t \right] \quad (3.38)$$

$$\Delta X_{CSC} = \frac{K_C}{1+sT_{CSC}} \omega_o \Delta \omega \quad (3.39)$$

The terms K_1 to K_6 , K_q , K_V , and K_P in these equations are coefficients that depend on the operating point of the system; the detailed expressions for these coefficients (except K_q and K_V) can be found in Appendix B. The coefficients K_q , K_V and K_P in the linearised model are of particular interest since they describe the influence of changes in the controlled element (the CSC reactance ΔX_{CSC}) on key system variables associated with the electromechanical swing mode of the generator. These latter coefficients are derived from the linearisation of the system model as follows:

$K_V = \partial E_t / \partial \Delta X_{CSC}$ represents the sensitivity of the generator terminal voltage to changes in the CSC reactance at a given operating point;

$K_q = \partial E_q' / \partial \Delta X_{CSC}$ represents the sensitivity of the generator field flux linkages to changes in the CSC reactance at a given operating point;

$K_p = \partial P_e / \partial \Delta X_{CSC}$ represents the sensitivity of the electrical power output of the generator to changes in the CSC reactance at a given operating point.

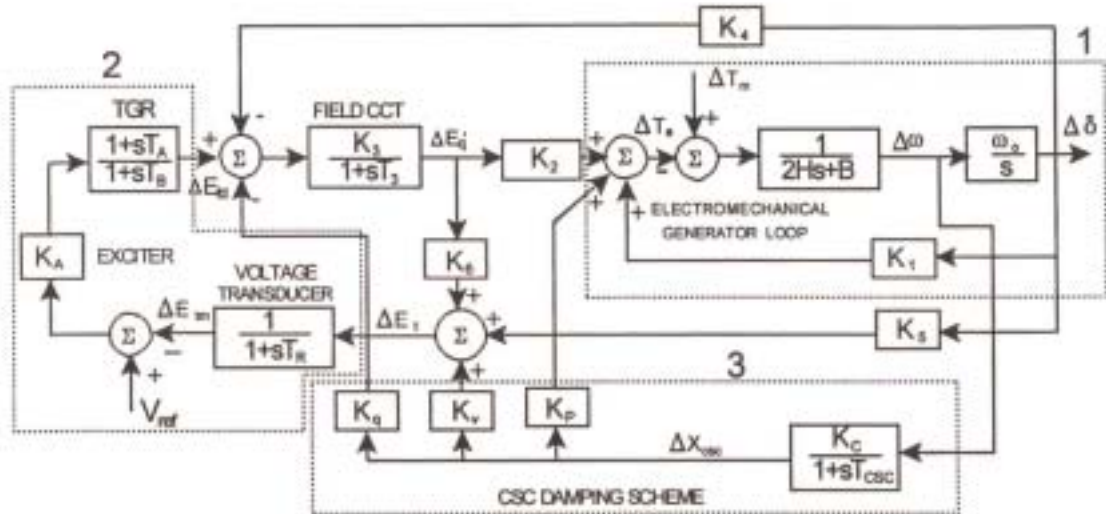


Fig. 3.5: Phillips-Heffron linear model of a single-machine infinite bus power system with CSC damping scheme.

The following subsections describe and explain each of the subsystems of the linearised system model shown in the block diagram of Fig. 3.5.

The electromechanical generator loop

The dotted box (1) in Fig. 3.5 represents the electromechanical loop of the generator which relates the mechanical dynamics of the generator rotor angle to changes ΔT_e in the electrical output torque of the machine. The small-signal stability of the system requires that, under dynamic conditions following a system disturbance, sufficient synchronising and damping torque components are present in the electrical torque signal ΔT_e . Synchronising torque is defined as the component of the electrical torque variation ΔT_e that is in phase with the generator's rotor angle deviations $\Delta \delta$, whilst damping torque is defined as the component of ΔT_e in phase with the generator's speed deviations $\Delta \omega$. Thus when examining the performance of a power oscillation damping scheme, one is interested in determining from Fig. 3.5 how the controller

affects the electromagnetic torque ΔT_e at the input to the electromechanical loop and, in particular, how it affects the component of ΔT_e in phase with $\Delta\omega$ (damping torque).

The diagram in Fig. 3.5 illustrates that, with no external damping controls in place (that is, with dotted box (3) removed), stabilising torques are applied via two distinct loops containing the gain terms K_1 and K_2 . Of these, the output of the block K_1 is purely a synchronising torque since it is fed from the rotor angle deviation $\Delta\delta$ directly through the algebraic gain term K_1 ; the output of the block K_2 however represents a torque that results from dynamic variations in the field flux linkages which in turn result from variations in generator rotor angle $\Delta\delta$; thus, the output of block K_2 contains both synchronising and damping components of torque whose relative magnitudes depend on the operating conditions of the system.

AVR and exciter loop

The dotted box labelled (2) represents the small-signal dynamics of the AVR and exciter system; the deviation ΔE_t in the terminal voltage of the machine is the input to this subsystem and its output is the deviation ΔE_{fd} in the field voltage. The terminal voltage deviations ΔE_t are themselves determined by the changes $\Delta\delta$ in the generator rotor angle (through coefficient K_3) and by the changes $\Delta E_q'$ in the rotor flux linkages (through coefficient K_6).

The CSC damping control scheme

The dotted box (3) shows the CSC damping scheme where the output of the damping controller is the change in the series capacitive reactance ΔX_{CSC} provided by the controllable series compensator. Chapter Two of this thesis reviewed a number of possible input signals that have been proposed for power oscillation damping; in the initial analyses presented in Chapter Four of this thesis the input signal to the controller has been chosen as the generator speed deviation $\Delta\omega$ as suggested in references [Webster,Rigby2,Noroozian1]. Alternative input signals, synthesised from locally-measured variables, are also considered for analysis in Chapter Four. In the linearised system model of Fig. 3.5 the controller block comprises the numerator term K_C (simple proportional controller gain) and the denominator term $1 + sT_{CSC}$ (first order input filter on the controller input signal).

This section has presented the non-linear models and linearised Phillips-Heffron model of the SMIB system in Fig. 3.1 that are used in Chapter Four to analyse the effects of the CSC damping controller and its contribution to synchronising and damping torques in this system. The following section presents the results of a case study to establish the validity of the models presented thus far.

3.4 Results Using the Simplified and Detailed System Models

3.4.1 Introduction

The previous section has developed three mathematical models of the SMIB system in Fig. 3.1. This section presents the results of a case study of the system in Fig. 3.1 using these different levels of models before considering the key issue of the damping of electromechanical system oscillations of this system in Chapter Four. The purpose of simulations carried out in this section using various system models is explained for each study presented below.

- (i) Non-linear time-domain simulation results using the simplified MATLAB model are compared to the simulated responses of the same system obtained using the more-detailed model of the generator in PSCAD/EMTDC; this study is carried out in order to examine the extent to which the level of detail in the generator model affects the predicted response of the system.
- (ii) The simplified MATLAB non-linear model, together with the linearised model, is then used to investigate the impact of system parameters and operating point on system stability using both the linearised eigenvalue analysis and non-linear time-domain simulation. The mathematical models of the generator used in these initial studies of parts (i) and (ii) above (both simplified and detailed) correspond to those described in sections 3.3 but *without* the AVR and exciter subsystems included in each case.

- (iii) The simplified MATLAB models (both non-linear and linearised) are then extended to include the effects of the generator exciter and automatic voltage regulator subsystems in order to examine how these subsystems affect the stability of this system.
- (iv) Finally, simulated results of the inverter-based series compensator model that has been developed in PSCAD/EMTDC are presented to confirm the correctness of this model and to show that the device replicates a series capacitive reactance whose magnitude can rapidly be controlled.

Appendix C shows the parameters of the system considered in the investigations to be carried out in this section. In the analyses of this section, the total transmission line impedance between the sending and receiving end (excluding the compensator) is $(0.01 + j0.6)$ p.u. The initial steady-state operating conditions at the infinite bus are in each case $P_b = 0.5$ p.u., $Q_b = 0.03$ p.u., and $E_b = 1.0$ p.u. The disturbance considered in each case is a temporary three-phase short circuit fault at point F in Fig. 3.1 lasting 100 milliseconds.

3.4.2 Simulation Results Using the Simplified and Detailed Models

In this study, the generator model used for the simplified non-linear time-domain simulation studies is the voltage behind transient reactance model of the synchronous generator; the non-linear differential equations that describe this generator model reduce to eqns. (3.27) to (3.29) (when the AVR and exciter subsystems are ignored). Since the purpose of this study is to examine the level of detail in the generator model, the characteristics of the system dynamics with this simplified model are compared to the characteristics of the system dynamics with the more-detailed two-axis model in PSCAD/EMTDC. In both models of the system, the effects of the exciter and AVR, and CSC with its damping controls are ignored in order to concentrate on the suitability of the simplified generator model equations (eqns. (3.27) to (3.29)) for small-signal analyses.

Fig. 3.6 now shows the predicted responses of the single-machine infinite bus power system under consideration following the temporary fault at F: the bold curves show the response predicted using the voltage behind transient reactance model equations

(3.27) to (3.29), and the light curves show the response predicted using the more-detailed two-axis equation model in PSCAD/EMTDC. The comparison of the predicted results using the two simulation models shows that although both models predict the generator rotor angle to be stable (light damping), the predicted amplitude of the rotor angle oscillations in each swing is slightly smaller in the case of the more-detailed two-axis model of the generator. This phenomenon can be explained briefly as follows.

As explained before, the more-detailed two-axis generator model (in PSCAD/EMTDC) represents the generator stator transient ($p\psi$) terms; these stator transients can have a significant impact in the generator particularly for symmetrical (three-phase) faults close to the generator terminals. The stator transient terms contribute a dc braking component of torque and an oscillatory component of torque whose combined effect is to reduce the amplitude of the rotor swings following a disturbance [Kundur]. As such, the amplitude of the generator rotor angle oscillation is expected to be smaller in each swing where the more-detailed two-axis model is used than in the case of the voltage behind transient reactance model where the effects of the generator stator transients are not represented.

However, the simulation results shown in Fig. 3.6 demonstrate that the damping characteristics of the system predicted using the two models agrees very closely (that is, both models show the generator rotor angle oscillations decreasing at the same rate). Thus, while the effects of the generator stator transients could be important in cases where the first-swing stability is of primary concern, the damping of system oscillations is the primary focus of the studies to be conducted in the main part of this thesis; therefore, it is reasonable to neglect the generator stator transients in the system model of Fig. 3.1.

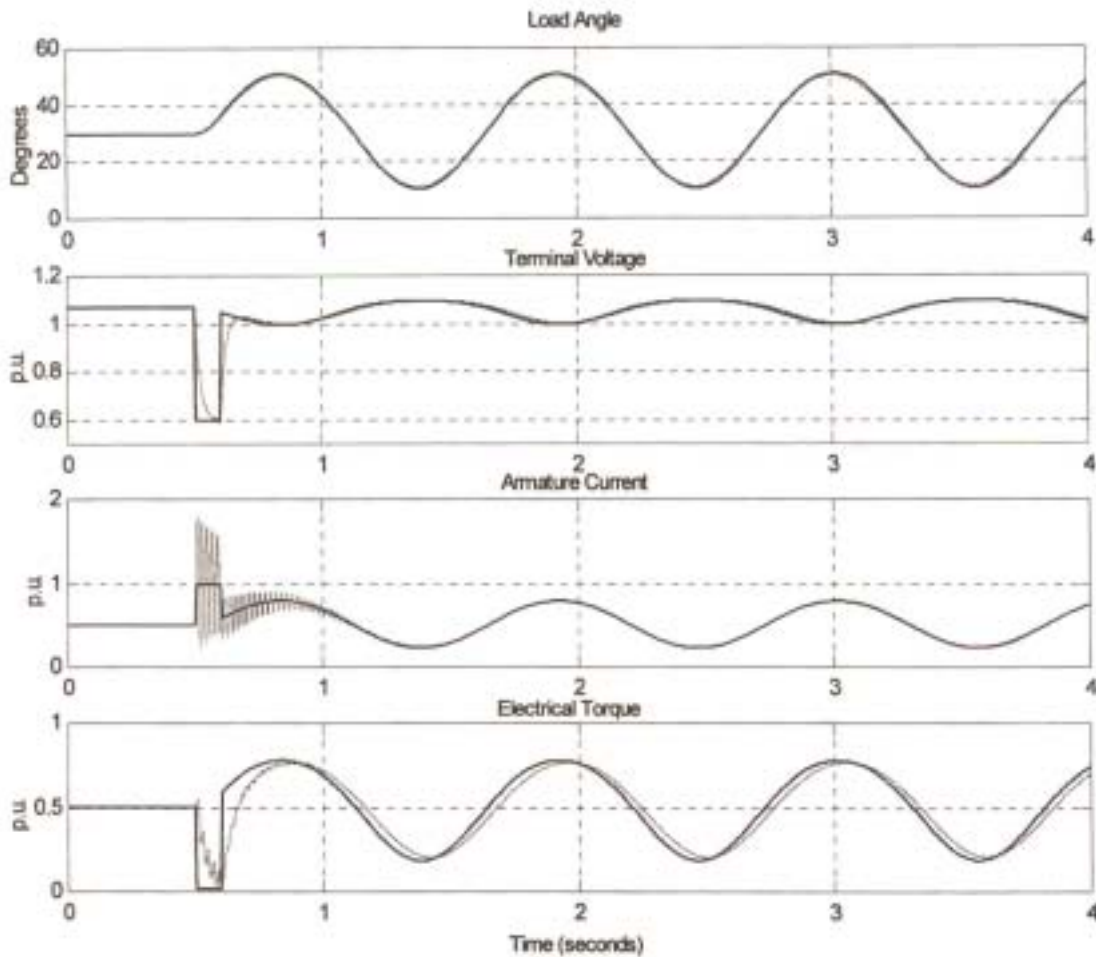


Fig. 3.6: Time-domain simulation results of the simplified MATLAB non-linear model (dark curves) and a more-detailed PSCAD/EMTDC non-linear model (light curves) of a SMIB system, with constant field voltage in each case.

3.4.3 Influence of Various System Parameters on Stability Using the Linearised Model

The previous subsection has briefly illustrated, via a time-domain simulation result, that the assumptions made in the simplified (MATLAB) non-linear model are reasonable if the objective is to analyse the small-signal stability (damping) of the system. In this subsection, the linearised model is now used to calculate the eigenvalues of the system for a range of system parameters. The small-signal stability characteristics of the system predicted by these eigenvalues are then confirmed using the simplified non-linear time-domain simulation model. In this study, the generator model is once again considered to have a constant field voltage with the exciter and AVR subsystems neglected; the linearised system model of this section has been

obtained by linearising a set of non-linear differential equations (3.27) to (3.29). In order to analyse the dynamic behaviour of the system using the eigenvalue technique, it is necessary to review a few basic concepts. The small-signal stability characteristics of a power system may be determined from the eigenvalues of its linearised model as follows.

- (i) A real eigenvalue corresponds to a non-oscillatory mode; a positive real eigenvalue represents an increasing (unstable) mode and a negative real eigenvalue represents a decaying (stable) mode.
- (ii) Complex eigenvalues occur in conjugate pairs of the form $\lambda = \sigma \pm j\omega_d$; each pair corresponds to an oscillatory mode. The real component σ of the eigenvalue pair gives the damping and the imaginary component ω_d gives the frequency of oscillation of the mode. An eigenvalue with a negative real part represents a damped (stable) oscillation whilst an eigenvalue with a positive real part represents an oscillation of increasing amplitude (unstable). The damping ratio ζ determines the rate of decay of the amplitude of the oscillation.

The operating point of the single-machine infinite bus system considered in this study is the same as in the previous subsection. The eigenvalues of the system are now presented for various combinations of system parameters in Tables 3.1 to 3.4 below. The changes in parameters in these studies are of arbitrary magnitude and are intended simply to show the broad relationships between system parameters and system characteristics.

Table 3.1 Base-case: $T_{do}' = 9.2065$ s, $X_L = 0.6$ p.u., $H = 4.0$ s.

Eigenvalue	Real part	Imaginary part	ω_d and ζ
FLD	-0.1348	0	
SM	-0.0041	$\pm j5.855$	$\omega_d = 0.93$ Hz, $\zeta = 0.0007$

Table 3.2 Change in field flux variations: $T_{do}' = 0.2$ s, $X_L = 0.6$ p.u., $H = 4.0$ s.

Eigenvalue	Real part	Imaginary part	ω_d and ζ
FLD	-6.4096	0	
SM	-0.0854	$\pm j5.7602$	$\omega_d = 0.92$ Hz, $\zeta = 0.0148$

Table 3.3 Change in inertia constant : $T_{do}' = 9.2065$ s, $X_L = 0.6$ p.u., $H = 2.0$ s.

Eigenvalue	Real part	Imaginary part	ω_d and ζ
FLD	-0.1348	0	
SM	-0.0041	$\pm j8.2803$	$\omega_d = 1.32$ Hz, $\zeta = 0.0005$

Table 3.4 Change in line reactance: $T_{do}' = 9.2065$ s, $X_L = 0.4$ p.u., $H = 4.0$ s.

Eigenvalue	Real part	Imaginary part	ω_d and ζ
FLD	-0.1472	0	
SM	-0.0037	$\pm j6.3961$	$\omega_d = 1.02$ Hz, $\zeta = 0.0006$

The small-signal characteristics of the SMIB power system for these combinations of system parameters may be explained as follows.

Base-case

The linearised eigenvalue results in Table 3.1 show that the system has two eigenvalues associated with different modes of the system: the real eigenvalue FLD is associated with the field circuit dynamics which constitute a non-oscillatory mode; the complex conjugate eigenvalue SM is associated with the electromechanical swing mode of the generator which constitutes an oscillatory mode. The real eigenvalue FLD is negative, thus representing the stability of the non-oscillatory mode; the component of system's response associated with this eigenvalue is stable. The complex eigenvalue SM has a small but positive damping ratio ($\zeta = 0.0007$), hence this eigenvalue predicts the electromechanical swing mode oscillations to be lightly damped with a frequency of 0.93 Hz. Field flux linkage variations and stator resistance are the sources of positive damping in the system under study (mechanical damping is here assumed to be zero).

Change in field flux variations

Table 3.2 now shows the eigenvalues of the system with the same operating conditions and system parameters as in Table 3.1 but with the direct-axis open circuit transient time constant of the generator reduced from a value of $T_{do}' = 9.2065$ s to a value of $T_{do}' = 0.2$ s. In the case of a reduced T_{do}' , the eigenvalue associated with field circuit dynamics FLD lies further into the left-hand plane; thus the component of the system's response associated with this eigenvalue is more stable at this operating point. The eigenvalue SM has an improved damping ratio ($\zeta = 0.0148$) as a result of

the increased contribution of field flux linkage variations to damping with the reduced time constant of the field circuit.

Change in inertia constant

Table 3.3 now shows the eigenvalues of the system with the same operating conditions and system parameters as in Table 3.1 but with the generator inertia constant reduced from a value of $H = 4.0$ s to a value of $H = 2.0$ s. Despite this change in inertia constant, the eigenvalue FLD predicts that the component of system's response associated with the field flux linkage variations has the same effect as in Table 3.1; the eigenvalue SM predicts that the electromechanical swing mode oscillations are once again lightly damped with a small positive damping ratio ($\zeta = 0.0005$) but with a higher oscillation frequency of 1.32 Hz than is the case in Table 3.1. These results illustrate that, as expected, the generator inertia primarily affects the frequency of oscillation of the generator swing dynamics.

Change in transmission line reactance

Table 3.4 now shows the eigenvalues of the system with the same system operating conditions and parameters as in Table 3.1 but with the transmission line reactance reduced from a value of $X_L = 0.6$ p.u. to a value of $X_L = 0.4$ p.u. At this operating point, the eigenvalue FLD once again predicts this non-oscillatory mode to be stable and the eigenvalue SM predicts the electromechanical swing mode oscillations to be lightly damped with a positive damping ratio ($\zeta = 0.0006$) and an oscillation frequency of 1.02 Hz. The increased value of ω_d of the swing mode oscillation from Table 3.1 illustrates that, as expected, a strengthening of the transmission line (reduction in X_L) increases the synchronising torque and natural frequency of the system.

3.4.4 Influence of Various System Parameters on Stability Using the Simplified Non-Linear Model

The previous subsection has presented the linearised system eigenvalues used to examine the small-signal behaviour of the SMIB power system under consideration for various system parameter combinations. This subsection now presents time-domain simulation results of the SMIB system using the voltage behind transient reactance model (eqns. (3.27) to (3.29)) for the same operating conditions and system parameters considered in Tables 3.1 to 3.4 in order to confirm the predictions of the

linearised model. Three plot windows in Fig. 3.7 show the predicted response of the system when subjected to a temporary three-phase fault at point F lasting 100 milliseconds for each of these combinations of system parameters.

Base-case simulation

The linearised eigenvalues of the system for the base-case in Table 3.1 predicted that, at that operating point and combination of system parameters, the electromechanical swing mode oscillations are lightly damped. The time-domain simulation response corresponding to the same combination of factors is shown in the dark curves of Fig. 3.7, repeated in each plot window (a), (b) and (c). The base-case time-domain simulation therefore confirms that, as predicted in Table 3.1, the generator rotor angle response is lightly damped with an oscillation frequency of about 0.93 Hz.

Change in field flux linkage variations

The linearised eigenvalues of the system in Table 3.2 predicted, with the direct-axis transient open circuit time constant of the generator reduced from a value of $T_{do}' = 9.2065$ s (as in Table 3.1) to a value of $T_{do}' = 0.2$ s, the electromechanical swing mode oscillations to have an improved damping factor. The simulation results in Fig. 3.7 (a) now compare the time-domain response of the system with the parameters as in Table 3.1 (bold curve) to the time-domain response of the same system with the parameters as in Table 3.2 (light curve); in each case the operating point of the system is the same. The significance of the time-domain results in Fig. 3.7 (a) is two-fold: firstly, the results confirm that the damping of the swing mode oscillations is improved when T_{do}' is reduced as predicted by the linearised model; secondly, the results show that the amplitude of the generator's first swing is increased (that is, that the synchronising torque has been reduced) as a result of the ability of the field flux linkages to vary more rapidly.

Change in inertia constant

The linearised eigenvalue results of the system in Table 3.3 predicted, with the generator inertia constant reduced from a value of $H = 4.0$ s (as in Table 3.1) to a value of $H = 2.0$ s, the electromechanical swing mode oscillations to be lightly damped with a higher oscillation frequency of 1.32 Hz. The simulation results in Fig. 3.7 (b) now compare the time-domain response of the system with the base-case

parameters (bold curve) to the time-domain response of the system with a low generator inertia constant (light curve). As predicted in the linearised analysis, the time-domain response in each case is lightly damped but the oscillation frequency is higher (at 1.32 Hz) with the reduced inertia constant. The time-domain response of the system also shows that, as would be expected, the amplitude of the rotor oscillations is larger when the generator inertia has been reduced.

Change in transmission line reactance

The linearised eigenvalue results of the base-case and those of Table 3.4 predicted that reducing the transmission line reactance from a value of $X_L = 0.6$ p.u. to a value of $X_L = 0.4$ p.u increases the frequency of the electromechanical swing mode oscillations from 0.93 Hz to 1.02 Hz, with the oscillations lightly damped in each case. To confirm this effect, the simulation results in Fig. 3.7 (c) now compare the time-domain response of the system in the base-case (bold curve) to that of the system with the reduced transmission line reactance (light curve). This result confirms that, while the generator rotor angle response in each case remains lightly damped, in the case of a reduced line reactance the generator rotor angle has a higher oscillation frequency. The simulation results in Fig. 3.7 (c) also show that by reducing the transmission line reactance, a lower value of steady-state rotor angle is required for the same active power transfer to the infinite bus as would be expected.

The results presented thus far (both non-linear and linearised) have shown the impact of system parameters on the SMIB system stability while at the same time providing confirmation of the validity of the linearised system model to be used later in the thesis. The following subsection now presents the results of a case-study of the SMIB system when the AVR and exciter are represented in the system model.

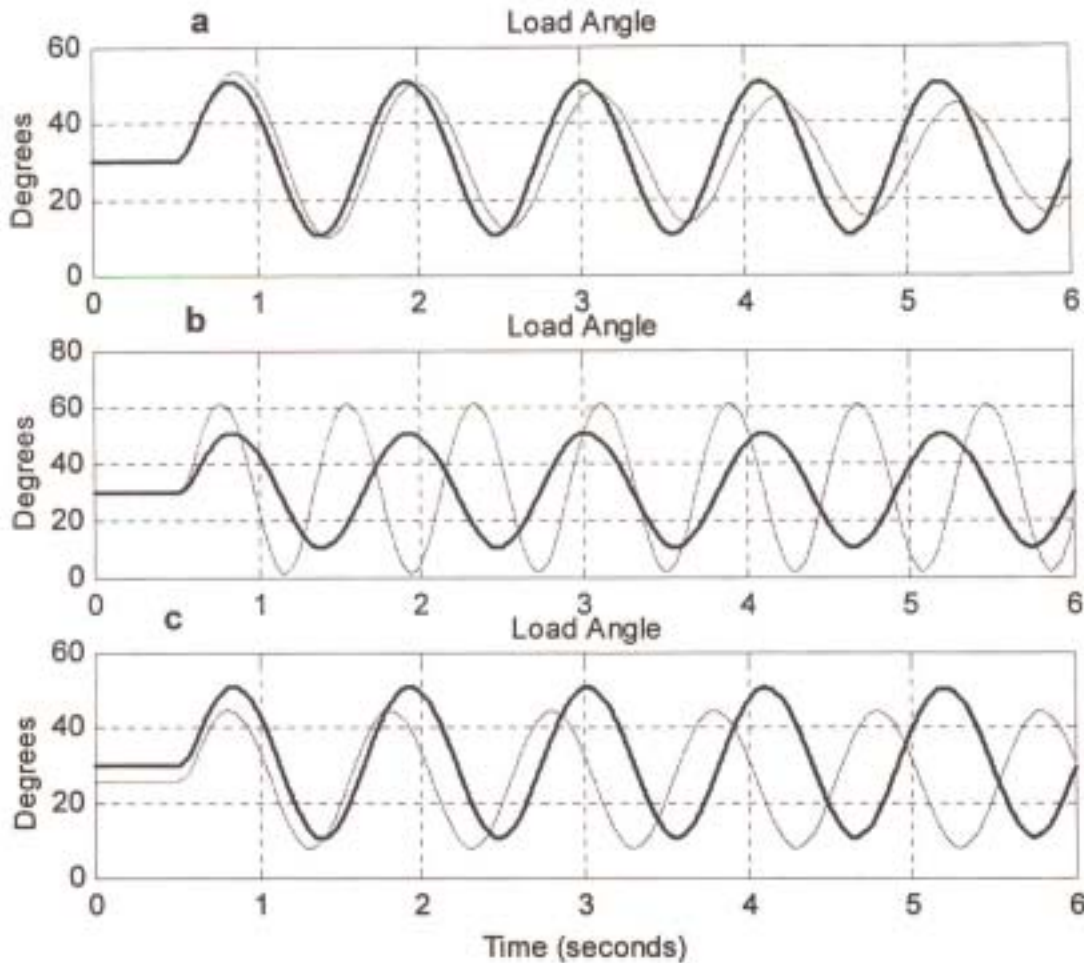


Fig. 3.7: Time-domain simulation results showing the influence of various parameters of a single-machine infinite bus system on system stability using the voltage behind transient reactance model.

3.4.5 Influence of AVR and Exciter Subsystems on System Stability

Results using linearised model

The analyses of the previous subsections have been carried out using both non-linear and linearised models where the influence of the AVR and exciter subsystems have been neglected in the system; this subsection now extends the analyses to include the effect of these subsystems on the system characteristics. The linearised model of this subsection has been obtained by linearising a set of non-linear differential equations (3.27) to (3.32) which include the thyristor-type exciter (with lead-lag network) and AVR in the system model. The purpose of this subsection is to examine the extent to which the exciter and AVR subsystems influence the small-signal stability of a SMIB

power system, in particular its small-signal (damping) characteristics, and to verify the models of the system themselves. The system operating conditions and parameters for this study are once again those of the base-case study in the previous subsection, and the exciter and AVR parameters are shown in Appendix C. The eigenvalues of the system in Tables 3.5 and 3.6 below have been calculated at two different values of exciter gain K_A .

Table 3.5 Low-gain exciter: $K_A = 1.0$

Eigenvalue	Real part	Imaginary part	ω_d and ζ
AVR	-99.99		
SM	-0.0041	$\pm j5.827$	$\omega_d = 0.93$ Hz, $\zeta = 0.0007$
EXC	-0.120	$\pm j0.070$	$\omega_d = 0.01$ Hz, $\zeta = 0.864$

Table 3.6 High-gain exciter: $K_A = 200.0$

Eigenvalue	Real part	Imaginary part	ω_d and ζ
AVR	-98.955		
SM	+0.075	$\pm j5.828$	$\omega_d = 0.93$ Hz, $\zeta = -0.0129$
EXC	-0.719	$\pm j0.839$	$\omega_d = 0.13$ Hz, $\zeta = 0.651$

The small-signal characteristics of the SMIB power system shown in Tables 3.5 and 3.6 at these two values of exciter gain may be explained as follows.

Low-gain exciter

Table 3.5 shows that there are now three eigenvalues associated with different modes of the system: the real eigenvalue AVR is associated with the automatic voltage regulator with its value (-99.99) determined by the voltage transducer time constant T_R ; the complex conjugate eigenvalue SM is associated with the electromechanical swing mode of the generator; the complex conjugate eigenvalue EXC is associated with the dynamics of the field and excitation system. The eigenvalues of the system for this set of conditions show that the component of the system response associated with the eigenvalue AVR decays rapidly as it lies far into the left-hand plane. The complex eigenvalue EXC, although it lies close to the imaginary axis, is stable and has a very high damping ratio ($\zeta = 0.864$); therefore the component of system's response associated with this eigenvalue decays rapidly. Finally, the complex eigenvalue SM lies close to the imaginary axis; however, this eigenvalue also has a

very low damping ratio ($\zeta = 0.0007$) and therefore the electromechanical swing mode is the dominant component of system's response with an oscillation frequency of 0.93 Hz.

High-gain exciter

Table 3.6 now shows the eigenvalues of the system at the same operating conditions as in Table 3.5 but with the exciter gain increased from a value of $K_A = 1.0$ to a value of $K_A = 200$. For this set of conditions, once again, the component of system's response associated with each of the eigenvalues AVR and EXC decays rapidly; however, the eigenvalue SM now has a negative damping ratio ($\zeta = -0.0129$). Thus, the component of system's response associated with electromechanical swing mode oscillations is unstable and these oscillations increase with time. This result therefore indicates that with an AVR and a high-gain thyristor exciter the electromechanical swing mode oscillations in this system have become negatively damped.

Simplified non-linear model with AVR and exciter

The linearised eigenvalue results in Tables 3.5 to 3.6 have been used to examine the small-signal characteristics of the SMIB power system with a thyristor-type exciter with lead-lag network and AVR in the system model. In order to confirm the findings of the linearised model, this subsection now presents time-domain simulation results of this system using the set of non-linear differential equations (3.27) to (3.32).

Fig. 3.8 now shows the predicted response of the system (including AVR and exciter) following a temporary three-phase fault at point F in Fig 3.1 lasting 100 milliseconds with the initial operating conditions and system parameters corresponding to those of Tables 3.5 and 3.6. However, the bold curve in Fig 3.8 shows the time-domain response with the low-gain exciter ($K_A = 1.0$ as in Table 3.5) while the light curve shows the time-domain response with the high-gain exciter ($K_A = 200$ as in Table 3.6). The significance of the time-domain simulation results Fig. 3.8 is two-fold: firstly, with a low-gain exciter the generator rotor angle swings are lightly damped and therefore stable at this operating point, whereas in the case of a high-gain exciter the generator rotor angle swings increase with time and are therefore unstable at this operating point; secondly, the amplitude of the first rotor swing (and hence the

synchronising torque) of the system in the case of an AVR and high-gain exciter is noticeably improved as would be expected [Kundur].

The studies conducted in this chapter have presented linearised eigenvalue results and non-linear time-domain simulation results of the SMIB system both with and without the exciter and AVR in the system models. In these studies the CSC and its damping controls have not been included in the system models since the impact of the CSC is the subject of later chapters in the thesis. The following subsection briefly presents time-domain simulation results of the inverter-based series compensator in order to confirm the correctness of the model of this system component before it is used in the investigations of Chapter Four.

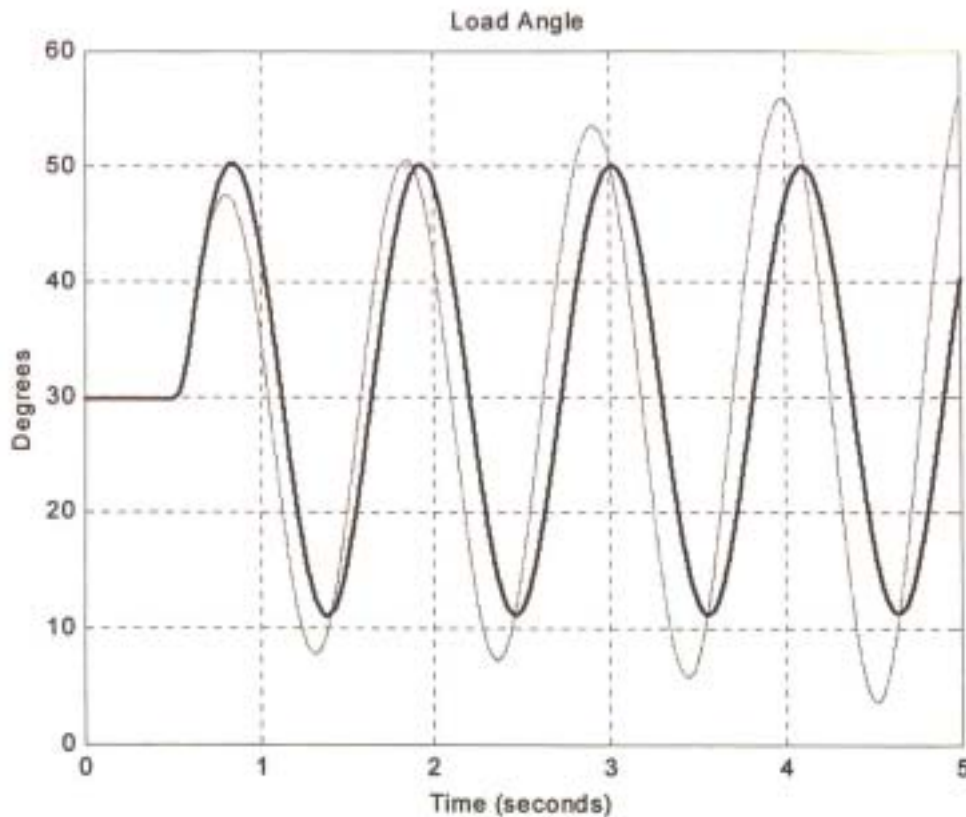


Fig. 3.8: Time-domain simulation results of a SMIB system including AVR and exciter subsystems at two different values of exciter gain K_A following a temporary disturbance.

$K_A = 1.0$ (bold curve), $K_A = 200.0$ (light curve).

3.4.6 The Inverter-Based Series Compensator in PSCAD/EMTDC

This subsection briefly presents simulation results of the inverter-based compensator scheme that demonstrate that the device replicates a variable series compensating reactance. This scheme, which was proposed in [Rigby1], has been modelled in detail in PSCAD/EMTDC for the investigations of this thesis. In the results shown here, the inverter-based series compensator has been inserted into a three-phase transmission system fed from ideal ac voltage sources at each end, just as it was considered in [Rigby1]. The studies of Chapter Four and Five examine the performance of this compensator in a more realistic transmission system connected to a synchronous machine (or multiple synchronous machines).

As explained previously, the inverter-based series compensator provides a series compensating reactance whose magnitude can rapidly be controlled. While various time-domain simulation results of the inverter-based series compensator scheme in PSCAD/EMTDC were presented in [Chonco3], and were shown to be in accordance with those in [Rigby3], the time-domain simulation results presented in this subsection are intended to show that while the inverter-based series compensator in PSCAD/EMTDC does replicate the behaviour of a 50 Hz compensating reactance, the magnitude of its series compensating reactance can rapidly be controlled.

In this study, the parameters of the inverter-based series compensator and its controls were deliberately chosen to correspond to those of reference [Rigby1] for ease in comparing the results. The simulated performance of the inverter-based series compensator in PSCAD/EMTDC is shown in Fig. 3.9: the results show the simulated response of the inverter-based series compensator scheme to a step increase in the commanded value of X_{CSC} from a value of 5Ω to a value 9Ω and back to 5Ω . The transmission line current has been scaled by a factor of 5 so that with a value of $X_{CSC} = 5\Omega$ the transmission line current i_a and the compensating voltage v_{xa} have the same amplitude on the graph. The time-domain response in Fig 3.9 shows that at all values of X_{CSC} the compensating voltage lags the line current by 90 degrees so that the device appears as a capacitive reactance. Also, Fig. 3.9 shows that when the commanded value of X_{CSC} is changed the effective magnitude of this compensating reactance (the ratio of the amplitude of v_{xa} to i_a) responds very rapidly (within one ac cycle). The

results in Fig. 3.9 and the response of the compensator are in accordance with those shown in [Rigby1].

A detailed explanation of how the inverter-based series compensator is able to maintain the correct phase relationship between the injected voltages and the transmission line currents, and to control rapidly the magnitude of reactance in a transmission line it is connected to, can be found in [Rigby1]. For the purposes of this study, it can be seen that the inverter-based series compensator modelled in PSCAD/EMTDC provides a rapidly controllable compensating reactance of known magnitude. In the chapters that follow in the thesis, this feature of the inverter-based series compensator is made use of to damp the electromechanical oscillations in power systems.

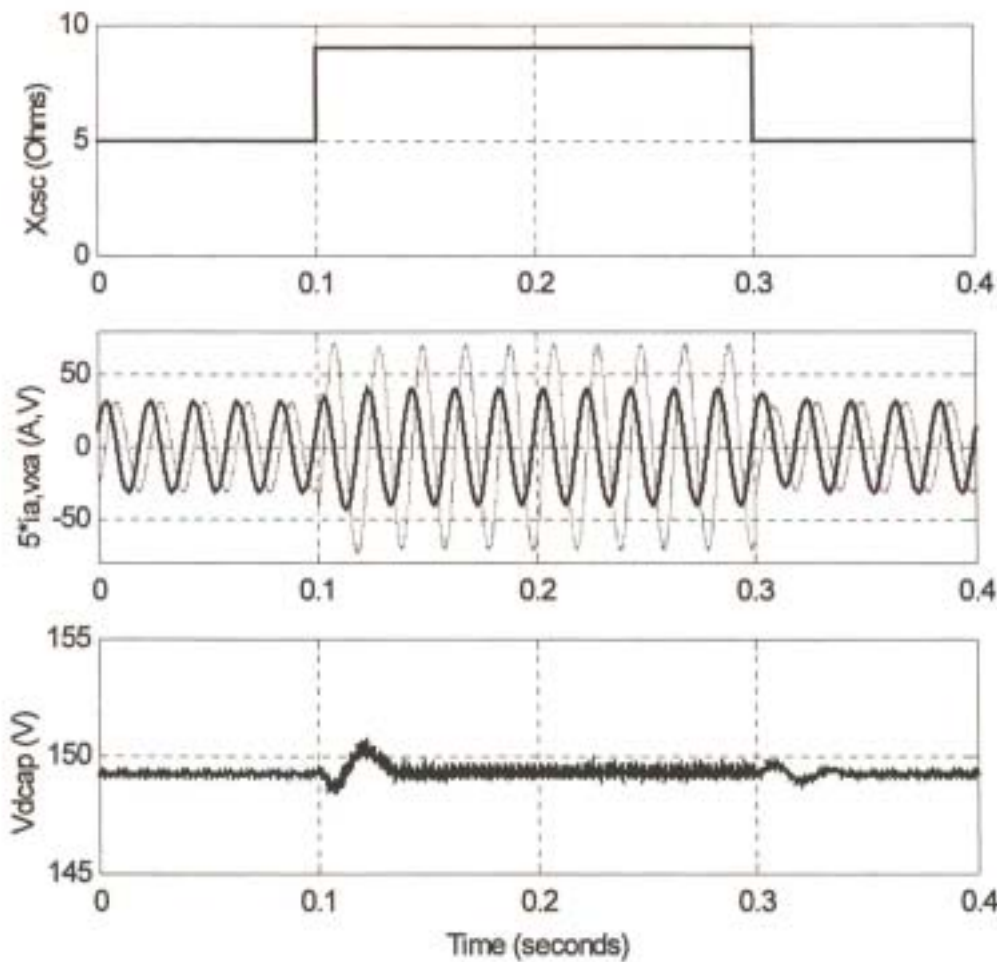


Fig. 3.9: Simulated response of the inverter-based series compensator to a step increase in the commanded value X_{CSC} from 5Ω to 9Ω in PSCAD/EMTDC with two voltage sources at either end of the transmission line system.

3.5 Conclusion

This chapter has developed three mathematical models of the single-machine infinite bus system to be considered in the studies of Chapter Four, and has explained the significance of each model. The development of the simplified system models has been described, and a more-detailed model of the system has been used to assess the validity of the simplified models. The studies have been conducted in the chapter in order to examine the influence of various important system parameters and the influence of the AVR and exciter subsystems on system stability using the various system models.

The results presented have shown that the assumptions made in deriving the simplified models of the system are reasonable since the chief-objective of this thesis is to analyse the small-signal behaviour of the power systems considered in the thesis. The simplified system models have been used to investigate the influence of various system parameters on system stability. The subsequent investigations involving the use of the AVR and exciter models have shown the effect of these subsystems on system stability: a high-gain exciter can have a beneficial effect on the generator synchronising torque while destroying the generator damping torque which is small in itself.

A particular inverter-based series compensator has been described in this chapter, and it is intended to use this compensator, together with an external damping controller, to provide a dynamically variable series compensating reactance in a manner that yields additional damping torque in the generators of the system; both an idealised and a detailed representation of the inverter-based series compensator have been described. Simulated results using the detailed model of the inverter-based series compensator have shown that this scheme is capable of providing a series capacitive reactance whose magnitude can rapidly be controlled. In the chapter that follows, detailed theoretical analyses using the different models of the SMIB system in Fig. 3.1 are carried out to examine the influence of the CSC and its damping controls on the stability of the system, using both the idealised and the detailed representation of the inverter-based series compensator.

CHAPTER FOUR

THEORETICAL ANALYSIS OF THE CSC APPLIED TO THE LOCAL MODE DAMPING PROBLEM USING THE PHILLIPS-HEFFRON MODEL

4.1 Introduction

Chapter One of this thesis explained that since the transmission line impedance has a direct influence on transmitted power, a controllable series compensating reactance can be used to control accelerating power in the generators connected to the system in order to bring them back to steady state more rapidly. Chapter Two of the thesis then discussed the basic theory of dynamic variation of transmission line impedance to control the electromechanical oscillations of generators in power systems; in that chapter, the basic control action for the variable series compensating reactance to improve the damping of generator power swings was explained using a specific two-area power system.

Chapter Two of the thesis also provided a review of what possible control signals can be used as inputs to a CSC-based power oscillation damping scheme. The review highlighted that, particularly for the inter-area mode damping phenomenon, it would be desirable to use an input signal to the damping scheme that is synthesised from measurements that can be made at the location of the CSC within the network, since generator variables would not, in practice, be easily obtainable. Chapter Two also reviewed possible control strategies for damping electromechanical system oscillations (either bang-bang control or some form of continuous control of series compensating reactance) and showed that the decision as to which approach to use depends on the power oscillation phenomenon to be damped. Finally, the review considered the work of Swift and Wang [Swift1,2] who proposed a simplified modelling and analysis method for CSC-based power oscillation damping schemes; the major attraction of the analytical approach of Swift and Wang is that it provides insightful design equations for the synchronising and damping torques provided to the system by the CSC's damping control scheme, and this approach was considered in

the mathematical modelling of the system in Chapter Three.

This chapter now presents the results of a study in which a controllable inverter-based series compensator is used to damp the electromechanical system oscillations of a single-machine infinite bus (SMIB) system. The study initially confirms Swift and Wang's findings [Swift1,2] using a SMIB system that is compensated with an idealised CSC and damping control scheme; their findings are then reconfirmed using a more accurate SMIB system representation in which the inverter-based series compensator used as the controllable element is modelled in detail. Finally, the study compares the performance of the power oscillation damping scheme using the generator speed deviation as the controller input with the performance of the same scheme but using a controller input signal synthesised from variables measured locally to the CSC.

The objective of the studies conducted in this chapter has been to investigate the effects of issues such as controller design and signal selection on the performance of a CSC power oscillation damping scheme in a conceptually simple case (SMIB) before considering (in Chapter Five) the issue of using the CSC to damp the more complex, inter-area oscillations of a multi-generator system. Different models of a SMIB power system were developed in Chapter Three of the thesis. The following section now reviews the work of Swift and Wang, where detailed theoretical analyses using the linearised Phillips-Heffron model were used to examine the influence of an idealised CSC and damping controller on the stability of the system.

4.2 Theoretical Insights From the Linearised Phillips-Heffron Model

4.2.1 Introduction

Chapter Three of the thesis has described the single-machine infinite bus power system (Fig. 3.1) to be considered in the studies of this chapter and has presented the various mathematical models to be used and explained the purpose of each model. In the simplified non-linear model, the non-linear equations of the system with an idealised CSC representation were presented and it was pointed out that although these equations can be used for time-domain simulation of the system, the primary purpose of the model is to be linearised about a chosen operating point so as to yield

the linearised Phillips-Heffron (P-H) model. Chapter Three subsequently presented the linearised P-H model of the system and, in this chapter, this model is used to analyse the stabilising torques contributed to the system by the CSC controller. The aim of this section is to review the work of Swift and Wang [Swift1,2] where a detailed treatment of the linearised P-H model is used to show the effect of the CSC on the stability of a single-generator infinite bus power system. The issues to be discussed may be summarised as follows:

- (i) the manner in which dynamic variations in series compensating reactance ΔX_{CSC} influence the synchronising and damping torques of the generator;
- (ii) those factors that have a considerable bearing on synchronising and damping torques contributed to the system by variations in series compensating reactance ΔX_{CSC} ; and
- (iii) what type of input signal should be considered in the analysis in order to ensure that variations in series compensating reactance ΔX_{CSC} yield the desired component of torque.

This section therefore summarises the theoretical insights that can be gained from the analyses of Swift and Wang using the linearised Phillips-Heffron model of Fig. 3.5 before reconfirming their results in the later sections of this chapter.

4.2.2 Mechanism of Stabilisation as a Result of Variations in ΔX_{CSC}

In order to achieve stable operation of a power system, sufficient damping and synchronising torques are required to successfully bring the system to the post-disturbance steady-state condition following a disturbance. Hence, to be able to analyse the influence of the CSC damping control scheme in Fig. 3.5 on the stability of the system, it is necessary that the torque contributed to the electromechanical generator loop due to variations in ΔX_{CSC} be resolved into its components: one in phase with the generator rotor angle deviation $\Delta\delta$ (synchronising torque component); the other in phase with the generator speed deviation $\Delta\omega$ (damping torque component). In the analysis of Swift and Wang [Swift1,2], the control input signal to

the CSC damping scheme is assumed to be generalised, that is, it is assumed to have a component partially in phase with both $\Delta\omega$ and $\Delta\delta$. However, in the Phillips-Heffron model shown in Chapter Three of this thesis (Fig. 3.5) the input to the CSC controller is the generator speed deviation $\Delta\omega$. In order to understand the reason for this specific choice of controller input signal for this study, consider first the generalised case of Swift and Wang, where the input signal $\Delta\varphi$ to the CSC controller is some function $f(\Delta\delta, \Delta\omega)$.

In this general case, the *output* of the controller (variation in series compensating reactance ΔX_{CSC}) will likewise have a component in phase with $\Delta\omega$ and a component in phase with $\Delta\delta$, thus contributing to both the synchronising and damping torques in the system. With this generalised CSC controller input $\Delta\varphi$, the resulting controller output ΔX_{CSC} can be expressed in the $\Delta\delta - j\Delta\omega$ plane as follows.

$$\Delta X_{CSC} = K_C C(s) \Delta\varphi = K_C K_{SCSC} \Delta\delta + K_C K_{DCSC} \omega_e \Delta\omega \quad (4.1)$$

where,

- ΔX_{CSC} = the variation in series compensating reactance (CSC output);
- K_C = controller gain;
- $\Delta\varphi$ = $f(\Delta\delta, \Delta\omega)$ = generalised control input signal;
- $C(s)$ = $1 / (1 + sT_{CSC})$ = signal conditioning of the CSC controller;
- K_{SCSC} = synchronising torque coefficient due to ΔX_{CSC} ;
- K_{DCSC} = damping torque coefficient due to ΔX_{CSC} .

From the linearised system model in Fig. 3.5 it can be seen that the influence of the controller output ΔX_{CSC} on the electromechanical generator loop is through blocks K_q , K_F , and K_P . However, the output from the blocks K_q and K_F is attenuated by first-order lag loops before contributing, via a single block K_2 , to the electromechanical generator loop. The torque output from the channels K_q and K_F (via K_2) as a result of variations in ΔX_{CSC} is therefore referred to [Swift1,2] as the indirect torque contribution of the CSC damping controller. By contrast, variations in the controller output ΔX_{CSC} have a direct effect on the torque in the electromechanical generator loop via the algebraic gain block K_P in Fig. 3.5. The torque at the output of this

channel K_P as a result of variations in the CSC output ΔX_{CSC} is therefore referred to [Swift1,2] as the direct torque contribution due to the CSC damping controller.

The analyses carried out by Swift and Wang [Swift1,2] have shown that the amplitude of the indirect torque contribution due to variations in ΔX_{CSC} is significantly smaller than the amplitude of the direct torque contribution due to variations in ΔX_{CSC} . Thus, in order to study the effect of variations in CSC output on system stability it is reasonable to neglect the indirect torque contribution and consider only those variations in torque ΔT_e that result from variations in CSC reactance ΔX_{CSC} through the algebraic channel K_P .

Therefore, considering only this direct torque contribution via channel K_P (now referred to as ΔT_{direct}), by inspection of Fig. 3.5 the following expression is obtained:

$$\Delta T_{direct} = K_P \Delta X_{CSC} \quad (4.2)$$

which from eqn. (4.1) is

$$\Delta T_{stabilize} \approx \Delta T_{direct} = K_P K_C K_{SCSC} \Delta \delta + K_P K_C K_{DCSC} \omega_o \Delta \omega \quad (4.3)$$

Eqn. (4.3) shows that with a generalised input signal containing components in phase with both $\Delta \omega$ and $\Delta \delta$ the CSC controller contributes to both the synchronising and damping torques of the system; the magnitude and sign of each of these torque components (that is, whether they are stabilising or destabilising) depends on the controller gain K_C and the operating point of the system (through the operating-point-dependent term K_P). However, in the particular study being conducted in this thesis, the specific focus of the investigation is the use of the controllable series compensation to provide system *damping*. Equation (4.3) shows that if, as in this case, the objective is only to provide additional damping torque, then not only is it unnecessary to have any component of the input signal in phase with $\Delta \delta$, in fact the input signal should ideally be the speed deviation of the generator $\Delta \omega$. Thus, since the objective of this study is in fact to provide damping, all further linearised analysis

assumes that the input to the CSC damping controller is simply the generator speed deviation $\Delta\omega$ as shown in Fig. 3.5.

4.2.3 Factors Affecting Stabilisation

The previous subsection discussed the impact of the CSC controller output ΔX_{CSC} on the small-signal stability of the electromechanical generator loop via the three channels K_q , K_r , and K_p by considering a generalised input signal as in [Swift1,2]. The analysis showed that there are direct and indirect torque contributions due to variations in ΔX_{CSC} ; of these torques, the indirect component can be neglected and only the direct component is considered to make a significant contribution to the electromechanical loop of the generator via the K_p channel. Whilst this direct torque component could be made to contribute both synchronising and damping torques, the investigations to be carried out in this chapter are focused on the provision of damping torque and, as a consequence, the input signal to the CSC has been chosen as the generator speed deviation $\Delta\omega$. This section now analyses the direct torque contribution resulting from variations in ΔX_{CSC} for this particular input signal $\Delta\omega$ and considers the factors with a considerable bearing on the ability of ΔX_{CSC} variations to provide additional damping torque to the system.

With the assumptions made in the previous subsection (that is, neglecting the indirect damping torque, and input signal only comprising $\Delta\omega$) then the expression for the stabilising torque contributed by CSC controller in eqn. (4.3) reduces to

$$\Delta T_{stabilise} \approx \Delta T_{direct} = K_p K_C K_{DCSC} \omega_0 \Delta\omega \quad (4.4)$$

Furthermore, provided the signal conditioning $C(s)$ does not introduce a significant phase shift between $\Delta\omega$ and ΔX_{CSC} within the CSC controller itself, the stabilising torque in eqn. (4.4) is purely a damping torque. Hence the linearised expression for the direct damping torque ΔT_D contributed to the system from the CSC controller, with the generator speed deviation as input, may be written as

$$\Delta T_D \approx K_p \Delta X_{CSC}(\Delta\omega) = K_p K_C K_{DCSC} \omega_0 \Delta\omega \quad (4.5)$$

This subsection now uses eqn. (4.5) to examine, for the particular controller input $\Delta\omega$, the factors that affect the amount of damping torque contributed by the CSC controller in the system.

Appendix B shows the full expression for the term K_P in eqn. (4.5), and from this expression it is evident that K_P is a function of both the system operating point as well as the system parameters. Firstly, the expression for K_P predicts that as the machine loading P_{eo} increases, the value of K_P also increases and hence from eqn. (4.5) the damping torque produced as a result of variations in series compensating reactance ΔX_{CSC} increases; thus, the expression for K_P in conjunction with eqn. (4.5) shows that the CSC damping scheme becomes more effective at high values of machine (and hence transmission line) loading. Secondly, the expression for K_P shows that as the transmission line reactance X_L increases (a condition corresponding to a weakening of the system connection), the value of K_P decreases and hence from eqn. (4.5) the damping torque produced as a result of variations in controller output ΔX_{CSC} decreases; thus, the CSC damping scheme's effectiveness deteriorates as the line reactance increases. These two findings taken together therefore suggest that, in order to ensure robust control performance of the CSC damping scheme, the design of its controller should be carried out for worst case conditions of light loading and a weak system connection.

Finally, eqn. (4.5) predicts that for a given value of K_P the damping torque increases approximately linearly with the controller gain K_C . Therefore at a high value of the controller gain the CSC damping scheme is most effective (large controller action); however, there is a maximum value of reactance beyond which series capacitive compensation may yield negative damping [Webster,Chen1] and hence in practice, since the compensator has finite capacity, limits are placed on the allowable series compensation and the controller output ΔX_{CSC} becomes bang-bang with a very high controller gain. At low values of the controller gain, K_C , the output of the CSC damping scheme is continuous; the review of literature in Chapter Two showed that this latter form of control approach is more suited to the damping of inter-area mode oscillations.

4.2.4 Input Signal

The discussions of this section have shown that in order to maximise the benefits of the CSC damping controller, the ideal input signal is the generator speed deviation $\Delta\omega$ since, with this particular input signal, all of the torque added to the electromechanical loop via the K_P channel is in phase with $\Delta\omega$ provided that the time constant T_{CSC} of the signal conditioning is sufficiently small so as not to introduce any phase lag between this input and the output ΔX_{CSC} in the frequency range of interest.

However, although the generator speed deviation $\Delta\omega$ is the logical signal to use for the input to the CSC damping controller in this single-machine case, in a large interconnected power system obtaining such a signal may present some practical difficulties, with geographically remote measurements making the speed deviations of the machines of interest difficult to obtain [Larsen,Noroozian2]. The later studies of this chapter therefore examine whether it is possible to synthesise a signal using only variables that are measured locally to the CSC in the transmission line, but which nevertheless contains similar information to the generator speed deviation signal $\Delta\omega$.

The following section now presents the results of a study of the SMIB system in Fig. 3.1 assuming the generator speed deviation $\Delta\omega$ as an input to the CSC controller; first the linearised Phillips-Heffron model is used to verify the theoretical predictions of this section (and hence those of Swift and Wang [Swift1,2]), and then these predictions are further reconfirmed by means of non-linear time-domain simulation results.

4.3 Results and Analysis Using the Idealised CSC Representation

4.3.1 Confirmation of Swift and Wang's Findings Using Linearised Model

This section presents and discusses the results of a linearised analysis of the sample single-machine infinite (SMIB) bus power system shown in Fig. 3.1; the findings from these linearised results are later confirmed using non-linear time-domain simulation studies. The reasons for the linearised eigenvalue studies of this section are twofold: firstly, to get a thorough understanding of how linearisation and eigenvalue methods could be used to design a controllable series compensator (CSC) damping

control for the SMIB case; secondly, to demonstrate the general analytical findings of Swift and Wang (outlined in the previous section) using numerical analysis techniques for the particular study system being considered. The results will show how the performance of the CSC damping scheme is affected by changes in the controller gain, system connection, and the machine loading.

Eigenvalue analysis has already been used in the previous chapter to demonstrate the small-signal dynamic behaviour of the SMIB system with no CSC in place. This section now presents the eigenvalues of the SMIB system in Fig. 3.1 with AVR and exciter in place as well as with the idealised controllable series compensator of Swift and Wang [Swift1,2]. In the studies of this section a double parallel transmission line is considered, as shown in Fig. 3.1, in series with a fixed component of series compensating reactance ($X_{CSC0} = 0.1$ p.u.) and a variable component of series compensating reactance. The parameters of the system, unless stated otherwise, are as shown in Appendix C. The eigenvalues of this system, calculated using the linearised Phillips-Heffron model of Fig. 3.5, are now examined for a number of different operating conditions in order to establish the impact of the CSC damping scheme on the system stability.

Table 4.1: Eigenvalues of the system with $P_{eo} = 0.2$ p.u., $X_L = 0.8$ p.u., $K_C = 0$.

Eigenvalue	Real part	Imaginary part	ω_d and ζ
AVR	-99.648	0	
IPF	-100	0	
SM	0.003	$\pm j6.698$	$\omega_d = 1.07$ Hz, $\zeta = -0.00045$
EXC	-0.306	$\pm j0.530$	$\omega_d = 0.084$ Hz, $\zeta = 0.50$

Table 4.2: Eigenvalues of the system with $P_{eo} = 0.2$ p.u., $X_L = 0.8$ p.u., $K_C = 0.1$.

Eigenvalue	Real part	Imaginary part	ω_d and ζ
AVR	-99.598	0	
IPF	-99.1727	0	
SM	-0.4354	$\pm j6.715$	$\omega_d = 1.07$ Hz, $\zeta = 0.065$
EXC	-0.306	$\pm j0.530$	$\omega_d = 0.084$ Hz, $\zeta = 0.50$

Table 4.3: Eigenvalues of the system with $P_{eo} = 0.8$ p.u., $X_L = 0.8$ p.u., $K_C = 0.1$.

Eigenvalue	Real part	Imaginary part	ω_d and ζ
AVR	-99.5403	0	
IPF	-96.5265	0	
SM	-1.7604	$\pm j6.5922$	$\omega_d = 1.05$ Hz, $\zeta = 0.258$
EXC	-0.330	$\pm j0.575$	$\omega_d = 0.0915$ Hz, $\zeta = 0.50$

Table 4.4: Eigenvalues of the system with $P_{eo} = 0.8$ p.u., $X_L = 1.6$ p.u., $K_C = 0.1$.

Eigenvalue	Real part	Imaginary part	ω_d and ζ
AVR	-99.1612	0	
IPF	-97.82	0	
SM	-1.1537	$\pm j5.556$	$\omega_d = 0.88$ Hz, $\zeta = 0.203$
EXC	-0.476	$\pm j0.717$	$\omega_d = 0.11$ Hz, $\zeta = 0.55$

The small-signal stability of the single-machine infinite bus power system under consideration may be understood from the eigenvalues of Tables 4.1 to 4.4 as follows.

No CSC damping control

Firstly, Table 4.1 shows the eigenvalues of the system with the CSC damping scheme inactive (damping scheme controller gain K_C set to zero). Table 4.1 shows that there are four eigenvalues associated with different modes of the system: the real eigenvalue AVR is associated with the voltage regulator of the generator and its value (-99.648) is determined by the voltage transducer time constant T_R ; the real eigenvalue IPF is associated with the input filter in the CSC damping controller and its value (-100) is determined by the time constant of this filter T_{CSC} ; the complex eigenvalue SM is associated with the electromechanical swing mode of the generator; the complex eigenvalue EXC is associated with the dynamics of the field and excitation system.

The real eigenvalues AVR and IPF lie far into the left-hand complex plane and hence the components of the system's response associated with each of these eigenvalues will decay rapidly. The complex eigenvalue EXC lies close to the imaginary axis but has a high damping factor ($\zeta = 0.50$); hence the generator field flux variations that are associated with this eigenvalue are well damped but do not decay rapidly. This eigenvalue EXC indicates that although well damped, the field flux variations are (as

expected) an important component of the system's dynamic response. Finally, the complex eigenvalue SM is also close to the imaginary axis but, for this set of operating conditions, it has a negative damping factor ($\zeta = -0.00045$). Thus, for the steady-state operating conditions in Table 4.1 (and with no CSC damping control active) the electromechanical swing mode of the system is unstable. As suggested in [Kundur] and subsequently shown in the analyses of Chapter Three, for a generator with a high-gain thyristor exciter, transient gain reduction and AVR, and with the damper windings neglected, the system damping is expected to be adversely affected; this combination of factors has been chosen deliberately to provide a poorly damped base-case system on which to study the influence of the CSC damping controller on the damping of the swing mode oscillations.

CSC damping control

Table 4.2 now shows the eigenvalues of the system at the same operating point as considered in Table 4.1, but with the CSC damping control now in operation with a controller gain $K_C = 0.1$. Comparison of Tables 4.1 and 4.2 shows that with the addition of the CSC damping control the damping factor of the swing mode eigenvalue becomes positive ($\zeta = 0.065$). The eigenvalues in Table 4.2 therefore indicate that the CSC damping control is able to stabilise the swing mode oscillations of the system at this operating point, but that these oscillations nevertheless remain poorly damped. This situation can be worsened or improved depending on the system operating conditions and hence the following subsections now consider the factors with significant influence on the performance of the damping scheme.

CSC damping control with increased line loading

Table 4.3 now shows the eigenvalues of the system with the CSC damping control in operation as in the previous case (Table 4.2) but with the real power delivered by the generator increased from 0.2 p.u. to a value of 0.8 p.u. Although there is no change in the gain of the CSC damping controller from Table 4.2 to Table 4.3 ($K_C = 0.1$) the swing mode eigenvalue in Table 4.3 now has a higher damping factor ($\zeta = 0.258$). Comparison of Tables 4.2 and 4.3 shows that the effectiveness of the CSC damping control scheme is increased at high line loadings.

CSC damping control with increased line reactance

Table 4.4 now shows the eigenvalues of the system with the CSC damping control in operation and at the same line loading of Table 4.3 but with an increase in the line reactance from 0.8 p.u. to a value of 1.6 p.u. Once again there is no change in the damping controller gain ($K_C = 0.1$) but the electromechanical swing mode eigenvalue SM in Table 4.4 now has a lower damping factor ($\zeta = 0.203$) than is the case in Table 4.3 ($\zeta = 0.258$). Comparison of Tables 4.3 and 4.4 shows that the effectiveness of the CSC damping control scheme is reduced when the system interconnection is weakened.

The eigenvalues of Tables 4.1 to 4.4, therefore, have shown that the CSC damping control is able to stabilise the electromechanical swing mode of the system in Fig. 3.1. Furthermore, the results show how the operating conditions and parameters of the system affect the performance of the CSC damping control for a given controller design. The following subsection examines how, for a given operating point, the design of the CSC controller itself influences the damping of the swing mode oscillations.

Effect of CSC controller gain K_C

Fig. 4.1 shows the loci of the eigenvalues of the system in Fig. 3.1 as the CSC damping controller gain K_C is increased from $K_C = 0$ to $K_C = 1.4$. In this study the transmission line once again has an inductive reactance $X_L = 0.8$ p.u. and transmits a steady state electrical power of $P_{eo} = 0.2$ p.u. but the controller gain K_C is increased from 0 to 1.4. It can be observed that as K_C increases, the eigenvalue associated with the machine rotor angle dynamics (SM) moves further into the left-hand plane, corresponding to an improvement in the damping of the swing mode oscillations. As the controller gain K_C increases, the damped natural frequency ω_d of the eigenvalue associated with swing mode oscillations SM is decreasing and therefore the swing mode frequency is reduced whilst its damping factor is increasing. The eigenvalues associated with the voltage regulator (AVR), and exciter (EXC) are relatively unchanged and those associated with the input filter of the damping controller (IPF) make a slight but insignificant shift to the right. Fig. 4.1 (b) is an enlarged section of

Fig. 4.1 (a) showing the rotor angle oscillatory mode eigenvalue as the value of K_C increases.

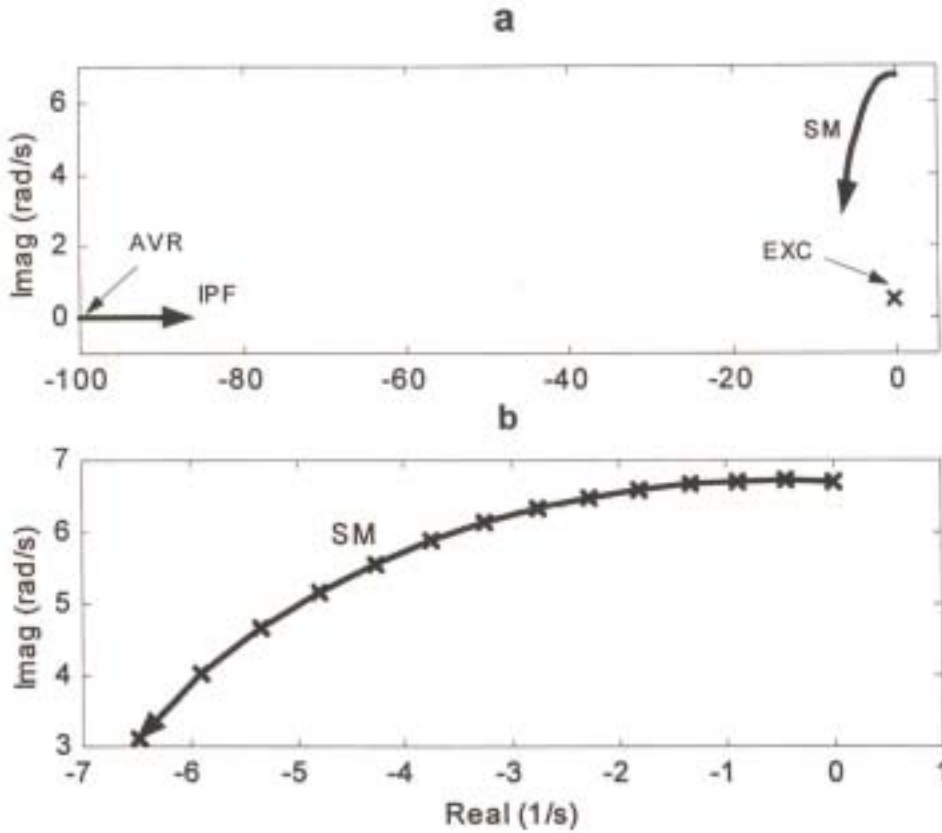


Fig. 4.1: Eigenvalue loci of the SMIB system as the controller gain K_C of the damping controller is increased.

4.3.2 Relationship Between Damping and Controller Gain

The analytical discussions of section 4.2 have explained, using the linearised Phillips-Heffron model, that the damping torque added to the system by the CSC controller is expected to increase almost linearly with the controller gain K_C , and it has been further shown that this component of torque is dependent on the value of the system coefficient K_P which in turn depends on the system operating conditions and system parameters. The aim of this subsection therefore is twofold: firstly, to reconfirm by means of numerical calculations using the linearised model that the damping torque contributed to the system by the CSC damping scheme is a linear function of the controller gain K_C ; secondly, to determine for the system under consideration (Fig. 3.1) whether the value of the coefficient K_P is always positive for various system

operating conditions in order to ensure positive damping of the swing mode oscillations.

Consider again the full expression for the term K_P in Appendix B which is shown to depend on the system parameters as well as machine loading. Firstly, for a synchronous generator the quadrature-axis reactance (X_q) is larger than the direct-axis transient reactance (X_d') [Kundur] and consequently in the expression for K_P in Appendix B, X_{qT} is greater than $X_{dT'}$. Secondly, for any given system operating condition, the steady state electrical power term P_{eo} in the expression for K_P is greater than the steady state electrical power term corresponding to the reluctance torque P_{eo2} , and therefore the difference between P_{eo} and P_{eo2} is always positive. These two observations mean, firstly, that the value of K_P is always positive so that for a positive controller gain K_C the damping torque contributed by the CSC is a *stabilising* torque; in addition, at higher values of the transmitted electrical power the difference between P_{eo} and P_{eo2} increases, and hence so does the positive value of K_P .

Fig. 4.2 now shows the numerical calculation of K_P at different generator loadings for two conditions of the system in Fig. 3.1: only one of the two parallel transmission lines in service (representing a weak system connection) and both of the parallel transmission lines in service (representing a strong system connection). The numerical result shown in Fig. 4.2 confirms that at the various operating conditions of the system the value of K_P is always positive. Fig. 4.2 further confirms that, for a given transmission system connection, as the generator loading increases, the value of K_P also increases. Finally Fig. 4.2 confirms that, for a given generator loading, the value of K_P is lower for a weak system connection when compared to that of a strong system connection.

The analytical discussions in the previous section of this chapter have predicted that the damping torque contributed to the system by the CSC damping scheme increases with the controller gain K_C . Indeed, the eigenvalue loci shown in the previous subsection (Fig. 4.1) have shown that as the CSC controller gain increases the damping factor of the SM eigenvalue, and hence the performance of the CSC, increases. Fig. 4.3 now shows the results of numerical calculation of the damping

contribution of the CSC at different values of the controller gain K_C ; these results show not only that the damping factor increases as the controller gain is increased, but that the increase in damping is, as expected, approximately a linear function of the controller gain.

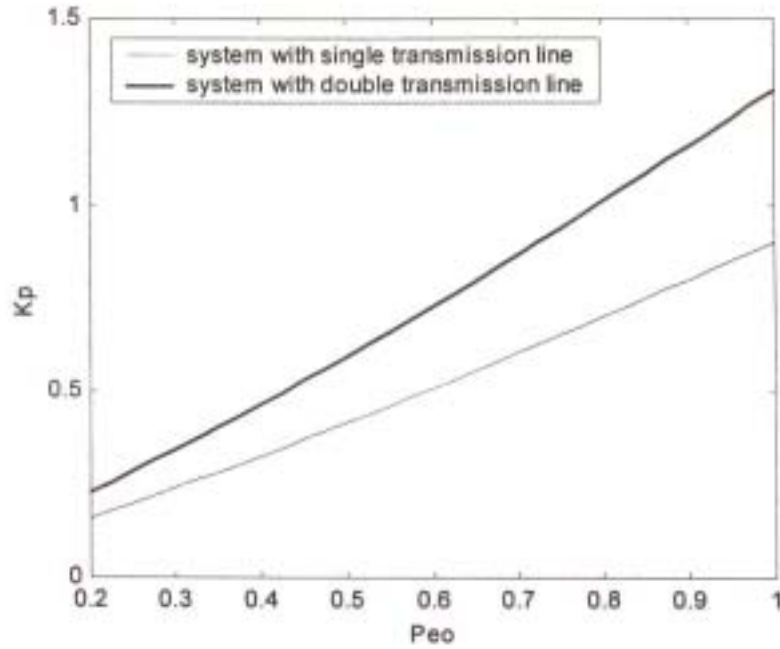


Fig. 4.2: Numerical calculation of K_p for the SMIB system at various machine loadings.

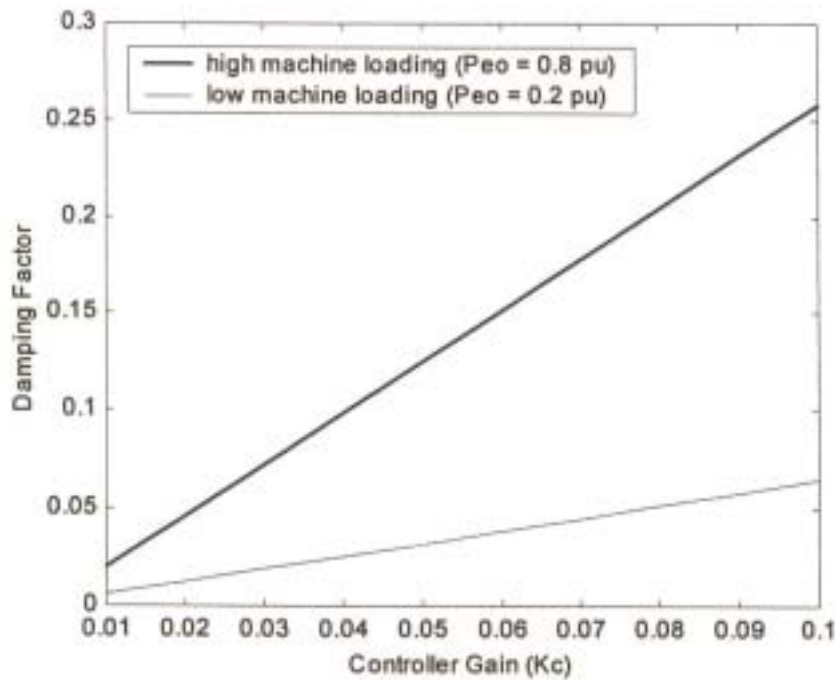


Fig. 4.3: The relationship between the controller gain and the damping added by the CSC scheme.

In summary, this subsection has reconfirmed that the value of K_p in the expression for the damping torque (eqn. (4.5)) added to the system by the CSC damping controller, at various system operating conditions, is always positive, and has subsequently shown that the damping torque contribution by the CSC controller is a linear function of the controller gain K_C . This subsection further reconfirmed the influence of various factors that contribute to the performance of the CSC damping controller namely, the generator loading, system parameters and controller gain. The following subsection reconfirms the predictions of the linearised P-H model using an idealised representation of the CSC by means of non-linear time domain simulation studies.

4.3.3 Non-Linear Simulation Results Using Idealised CSC Model

The previous subsection considered the linearised Phillips-Heffron (P-H) model of the single-generator infinite bus power system of Fig. 3.1. The influence of the CSC controller on the damping of the system oscillations, and the factors affecting its performance, were studied using both the P-H graphical model (Fig. 3.5) and via eigenvalue analysis techniques. In this subsection the predictions of the linearised model of the system are now examined further by means of time-domain simulation studies using the simplified non-linear differential equation model (eqns. (3.27) to (3.33)) in which the CSC response is assumed to be ideal. In a later section of this chapter these predictions are re-confirmed using the detailed model of the system in which the internal dynamics of the CSC element are accurately represented. In each of the studies that follow, the time-domain simulation model is used to predict the response of the system when it is subjected to a temporary three-phase short circuit at the terminals of the infinite bus (point F in Fig. 3.1), lasting 100 milliseconds. The three plot windows in Fig. 4.4 compare the time response of the system in Fig. 3.1 to this disturbance for the same combination of operating conditions which were considered in the eigenvalue predictions of Tables 4.1 to 4.4 in section 4.3.1 of this chapter.

Time-domain response with and without CSC damping control

The light curve in Fig. 4.4 (a) shows the response of the system in Fig. 3.1 to the disturbance at the infinite bus with no CSC damping control action (controller gain $K_C = 0$), with the steady state value of power P_{e0} equal to 0.2 p.u. and with the line

reactance $X_L = 0.8$ p.u.; the system eigenvalues corresponding to this combination of operating conditions were shown in Table 4.1 of section 4.3.1. The linearised results in Table 4.1 predicted that, under these conditions, the swing mode oscillation is unstable with the CSC damping control inactive; the time-domain simulation shown by the light curve in Fig. 4.4 (a) now confirms that the generator rotor angle response in this base-case study is, as predicted, negatively damped such that the rotor angle oscillations grow with time (oscillatory instability) when the CSC damping control is inactive.

The dark curve in Fig. 4.4 (a) shows the response of the system in Fig. 3.1 with the values of power $P_{eo} = 0.2$ p.u. and $X_L = 0.8$ p.u. unchanged from the base-case study, but with the CSC damping controller now active (controller gain $K_C = 0.1$); the system eigenvalues corresponding to this combination of operating conditions was shown in Table 4.2 of section 4.3.1. The linearised results in Table 4.2 predicted that with the CSC damping controls operative and with this value of controller gain K_C , the swing mode of the system becomes stable but remains lightly damped; the dark curve shown in Fig. 4.4 (a) now confirms this prediction via time-domain simulation.

Taken together, the two curves in Fig. 4.4 (a) visually demonstrate the change in the damping of the generator rotor oscillations of the system in Fig. 3.1 for a given system connection ($X_L = 0.8$ p.u.) and steady state power transfer ($P_{eo} = 0.2$ p.u.) when the CSC damping controls are activated.

Effect of line loading on the CSC damping controller performance

Comparison of Tables 4.2 and 4.3 in section 4.3.1 predicted that, for a given CSC damping controller gain and transmission line reactance, a higher value of the transmitted electrical power yields a higher damping ratio, hence more damping torque is contributed by the CSC controller in the system. The time-domain simulation results in Fig. 4.4 (b) are now intended to demonstrate this effect of transmission line loading on the performance of the CSC damping controls at a particular value of controller gain K_C . The light curve in Fig. 4.4 (b) once again shows the time-domain response of the generator rotor angle with the CSC damping controls active ($K_C = 0.1$) and with the values of $P_{eo} = 0.2$ p.u. and $X_L = 0.8$ p.u. from the base-case study (the same response that is shown as the dark curve in the previous plot

window of Fig 4.4 (a)); the dark curve in Fig. 4.4 (b) now shows the response of the generator rotor angle when the line loading has been increased to $P_{eo} = 0.8$ p.u. but with $K_C = 0.1$ and $X_L = 0.8$ p.u. unchanged. A comparison of the light and dark curves in Fig. 4.4 (b) clearly shows that at the higher line loading the generator swing mode is noticeably more damped, despite the fact that the CSC damping controls are the same in each case.

Effect of line reactance on the CSC damping controller performance.

Comparison of Tables 4.3 and 4.4 in section 4.3.1 predicted that, for a given controller gain and machine loading, an increase in the transmission line reactance reduces the damping ratio of the eigenvalue associated with the swing mode oscillations and hence deteriorates the CSC damping scheme's effectiveness. The time domain simulation results in Fig. 4.4 (c) are now intended to demonstrate this effect of the strength of system interconnection on the performance of the CSC damping controls at a particular value of controller gain K_C . The light curve in Fig. 4.4 (c) once again shows the time-domain response of the generator rotor angle with the CSC damping controls active ($K_C = 0.1$) and with the values of $P_{eo} = 0.8$ p.u. and $X_L = 0.8$ p.u. from the eigenvalue study of Table 4.3 (the same response that is shown as the dark curve in the previous plot window of Fig 4.4 (b)); the dark curve in Fig. 4.4 (c) now shows the response of the generator rotor angle when the line reactance has been increased to $X_L = 1.6$ p.u. but with $K_C = 0.1$ and $P_{eo} = 0.8$ p.u. unchanged. A comparison of the light and dark curves in Fig. 4.4 (c) confirms that with the increased line reactance (weaker system interconnection) the generator swing mode is less damped for the same real power transfer and CSC controller gain, as predicted in the eigenvalues of Tables 4.3 and 4.4.

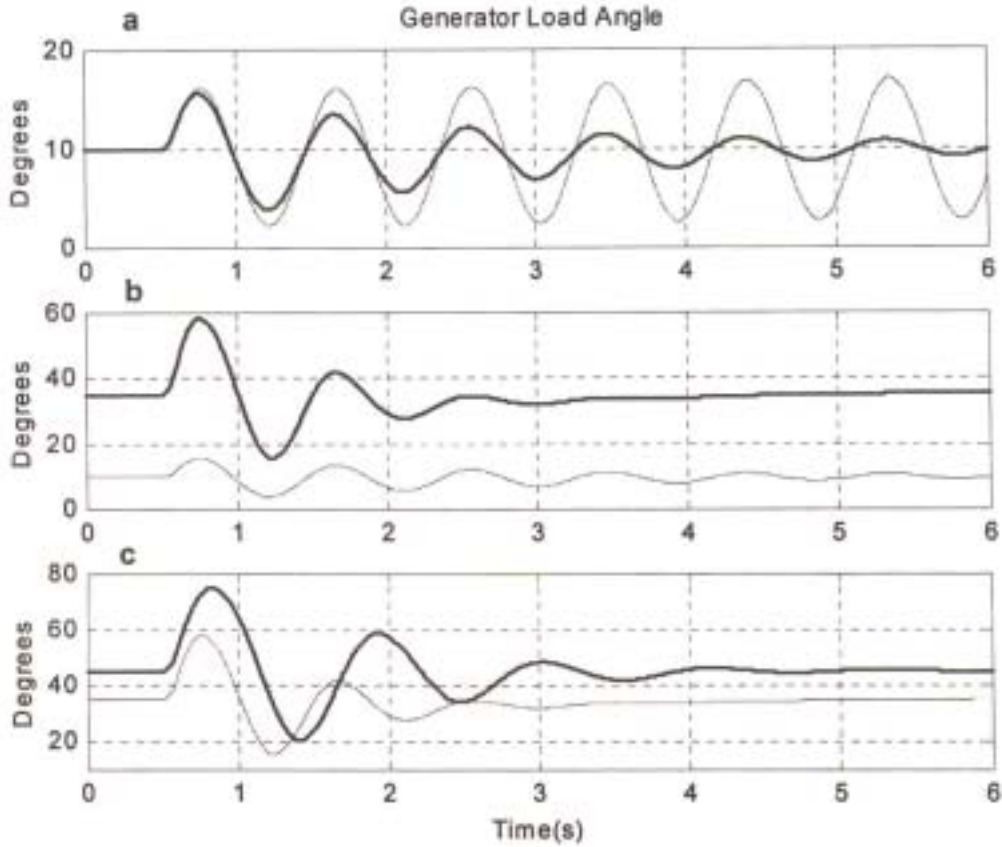


Fig. 4.4: Time-domain simulation results of the SMIB system in Fig. 3.1 using the simplified non-linear system model in eqns. (3.27) to (3.33).

Effect of CSC controller gain K_C

The time-domain results of Fig. 4.4 have confirmed the predictions of the linearised analysis in section 4.3.1 regarding the effect of system conditions on the performance of the CSC damping controls at a given controller design. However, the linearised analyses have also predicted (Figs. 4.1 and 4.3) how the performance of the CSC damping controller is related to its own controller gain K_C at any given system operating point. Moreover, the linearised analyses indicated that a very high controller gain results in the best performance of the CSC damping scheme. In practice however, it is necessary that limits are placed on the maximum allowable controlled series compensating reactance [Webster,Chen] and hence high values of the controller gain K_C would be expected simply to drive the CSC controller output into limit. The linearised model is valid only for small disturbances around the system operating point, and hence the eigenvalues of the linearised (Phillips-Heffron) model only

predict what the damping of the system oscillations will be when these oscillations have decayed to a small enough amplitude that the output of the CSC is continuous. Thus in cases where the CSC output is driven into limit, it is necessary to check the performance of the system (via simulation) using the non-linear model in order to determine whether the system can successfully come out of limit and return to steady-state following a disturbance; that is, it is necessary to ensure that the system does not get into a limit cycle (the relay chatter problem referred to in Chapter Two of the thesis).

Fig. 4.5 now shows the time-domain response of the system in Fig. 3.1 to a three-phase fault at the infinite bus (at the same system operating point in each case) but for two different values of damping controller gain K_C : the light curve shows the response for a modest value of $K_C = 0.2$ whilst the dark curve shows the response for a high value of $K_C = 2.0$. In each case the CSC has its output (capacitive reactance) limited to variations of ± 0.1 p.u. around its steady state set point value of 0.1 p.u, with the inductive reactance of the transmission line changing from $X_L = 0.8$ p.u to $X_L = 1.6$ p.u. after the clearance of the fault. The results of Fig. 4.5 confirm that, while a high value of K_C does in fact drive the output of the CSC into limit, the CSC controller is able successfully to come out of limit.

This section has successfully reconfirmed Swift and Wang's theoretical findings using an idealised controllable series compensator model. The following section now considers a more-detailed generator model and the detailed representation of the inverter-based series compensator scheme in order to access the validity of these findings in a more complete system model.

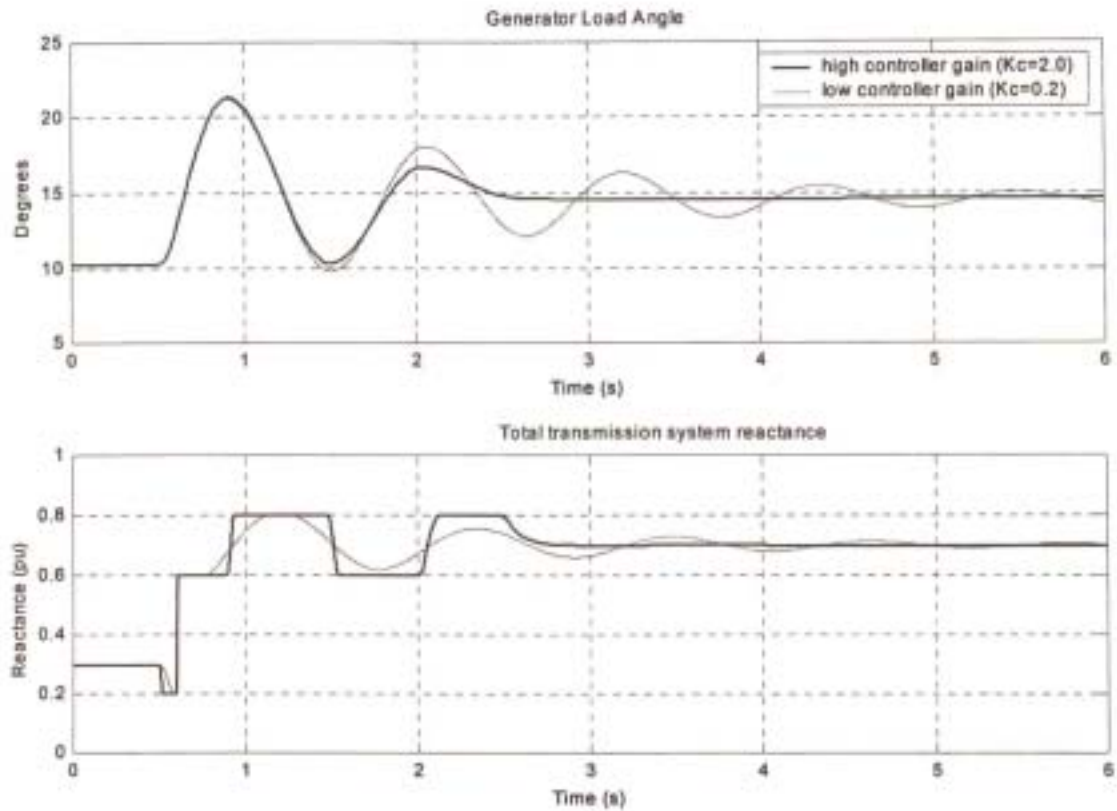


Fig. 4.5: Time-domain simulation results of the single-machine infinite bus system at two values of the controller gain.

4.4 Results and Analysis Using the Detailed Model of the Inverter-Based Series Compensator

4.4.1 Introduction

The investigations presented thus far (both linearised and non-linear) have been carried out using a simplified generator model and have assumed an idealised, generic controllable series compensator in which the compensating reactance can be varied instantaneously. This section now examines the time-domain response of the single-machine infinite bus power system using a more-detailed simulation model as shown in Fig. 3.4, in which the controllable series compensator itself is modelled in detail. The objective of this investigation is twofold: firstly, to determine whether the specific type of CSC considered in this thesis (inverter-based series compensation) is in fact suitable for damping swing mode oscillations; secondly, to determine whether the assumption made in the analytical work of Swift and Wang (repeated in section

4.3 of the thesis) of an idealised CSC is valid for the case of inverter-based compensation.

However, in order to accommodate a more detailed compensator model in the system of Fig. 3.1 it has also been necessary to employ a model of a synchronous generator in which the stator (and hence transmission line) current dynamics are represented; this change in machine model from the simplified representation of Fig. 3.1 (no generator stator transients) is in itself expected to affect the predicted response of the system to some extent. Thus, in order to isolate the various contributing factors, the investigation has been carried out, and is presented, as follows.

- (i) Non-linear time-domain simulation results obtained with the simplified MATLAB model are compared with those of a more-detailed model of a generator in PSCAD/EMTDC with no CSC damping control in each case. In this study, a fixed amount of series capacitive compensating reactance is considered for both models of the system. The objective of this study is to isolate, via time domain simulations, the extent to which the level of detail of the synchronous generator model affects the predicted response of the system;
- (ii) The time-domain response of the system in the simplified MATLAB model (once again, with a fixed amount of conventional series compensating reactance) is then compared with response predicted by the detailed PSCAD/EMTDC model; however in the detailed PSCAD/EMTDC model, the fixed amount of series compensating reactance is now provided by the inverter-based series compensator. The objective of this analysis is to determine the extent to which an inverter-based compensator affects the response of the system with no damping controls in place;
- (iii) Finally, the response of the system predicted using the simplified MATLAB model with an idealised CSC and damping controller in place is compared to the response predicted using the system model developed in PSCAD/EMTDC with a detailed representation of an inverter-based

series compensator and the same damping controller in place. This comparison, in conjunction with those described in parts (i) and (ii) above, will allow the validity of the simplified representation of a CSC to be assessed.

Appendix C shows the slightly modified transmission system parameters for the investigations of this particular section; for both the simplified and detailed non-linear simulations in this section the transmission system comprises a single rather than a double line as shown in Fig. 3.1. As explained in Chapter Three, for the purposes of this study, an inverter-based series compensator scheme in PSCAD/EMTDC has been implemented as shown in Fig. 3.4, and its internal controls have been presented in [Rigby1].

4.4.2 Simulation Results Using a Fixed Amount of Conventional Series Capacitive Reactance

Fig. 4.6 compares the time-domain response of the SMIB system to a temporary three phase fault at the infinite bus lasting 100 milliseconds as determined using the simplified model equations (3.25) to (3.31) and the detailed model implemented in PSCAD/EMTDC (Fig. 3.4). In both cases the transmission line is compensated with a fixed amount of conventional series capacitive reactance. The results show that the time-domain response predicted by two models agrees very closely: the small differences that are present between the simulation results are due to the effects of generator stator transients being ignored in the simplified model, since this is the only modelling difference in the two studies. Therefore, the significance of the non-linear simulation results in Fig. 4.6 is twofold: firstly, they confirm that neglecting the generator stator transients in the simplified model used to derive the Phillips-Heffron equations is in fact reasonable; secondly, these results indicate that the presence of generator stator transients in the detailed PSCAD/EMTDC model of the system is not responsible for any significant differences in the behaviour that may be predicted by this model and that predicted by the simplified model when controllable series compensators are subsequently introduced into the study.

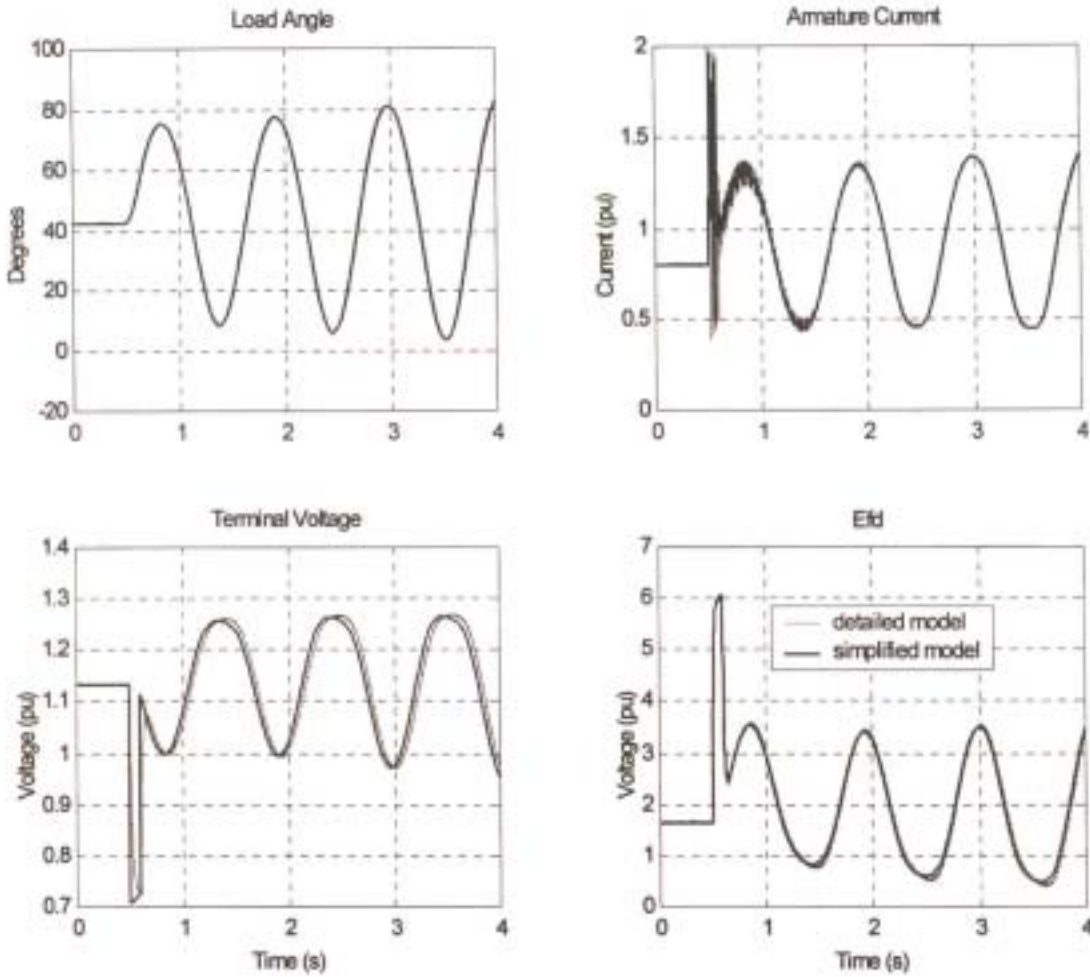


Fig. 4.6: Simplified MATLAB and detailed PSCAD/EMTDC non-linear time domain SMIB simulation models of the same system using a fixed amount of conventional capacitive series compensating reactance.

4.4.3 Simulation Results Using a Fixed Amount of Inverter-Based Series Compensation

Fig. 4.7 once again compares the time-domain response of the SMIB system predicted using both the simplified and detailed system models with a fixed amount of series compensating reactance: the light curve shows the generator rotor angle swing using a simplified generator model and a fixed amount of conventional series compensating reactance; the bold curve shows the response predicted using the detailed model of the system, but with the fixed amount of capacitive compensating reactance now provided by an inverter-based series compensator. The comparison of the responses in Fig. 4.7 shows that the amplitude of the predicted generator rotor angle oscillations is smaller in each swing when the inverter-based series compensator is modelled in detail than is

the case when the inverter-based compensator is modelled as an ideal capacitive reactance. Thus the results of Fig. 4.7 indicate that the simplified representation of an inverter-based compensator does lead to a degree of error in the predicted results. However, examining Fig. 4.7 more closely indicates firstly that this error is conservative (that is, the simplified representation of the inverter-based compensator predicts a larger amplitude of rotor oscillation than is actually the case). Secondly, Fig. 4.7 shows that despite the error in predicted amplitude of the rotor oscillations, the *damping* of the oscillations predicted by the two models is in close agreement (both models predict the oscillations to increase at the same rate).

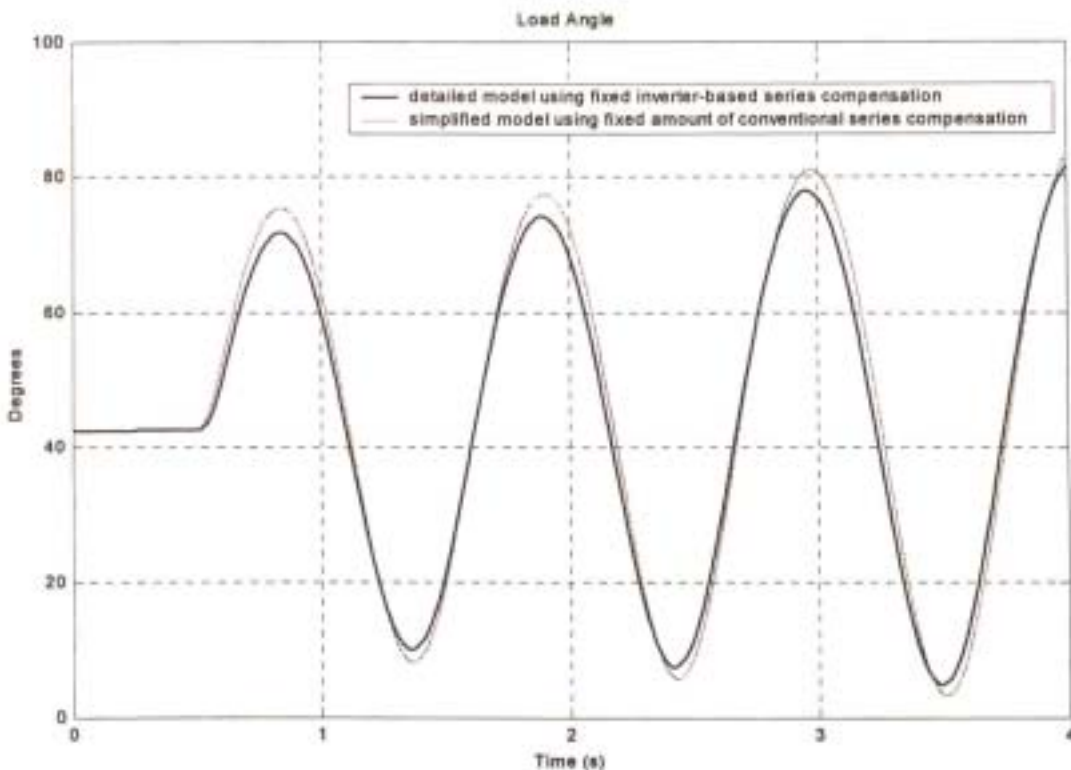


Fig. 4.7: *Simplified MATLAB and detailed PSCAD/EMTDC non-linear models showing the generator rotor swing following a temporary disturbance.*

The differences in the predicted responses of Fig. 4.7 can be isolated to the different level of modelling of the inverter-based series compensator between the two studies. Consequently, these differences indicate that the internal behaviour of the inverter-based compensator and its controls does in fact have an influence on the response of the system following a disturbance. The reasons for the influence of the compensator's internal characteristics on the response of the system as a whole have

not yet been examined in detail and lie outside the scope of this thesis. However, given the observations that (i) the simplified representation of the CSC results in a conservative error in the predicted amplitude of generator rotor oscillations and (ii) that the damping of these oscillations predicted with the simplified model agrees with that predicted by the detailed compensator model, the simplified representation of the CSC in the linearised analyses seems reasonable for power oscillation damping studies involving an inverter-based series compensator.

4.4.4 Simulation Results Using Controlled Inverter-Based Series Compensation

Fig. 4.8 now shows the time response of the SMIB system following the temporary three-phase fault when the damping controller is active and is used to modulate the series capacitive reactance provided by the CSC. The light curves in Fig. 4.8 show the response predicted with the simplified model of the CSC whilst the dark curves show the response when the inverter-based CSC is modelled in detail. In both cases the CSC damping controller is identical and has controller gain $K_C = 0.05$. Comparison of the predicted responses in Fig. 4.8 shows, once again, that the amplitude of the rotor oscillations for a system with a detailed model of an inverter-based compensator is smaller than that of a system with an idealised CSC, but that the damping of these oscillations is similar in each case.

The results in Fig. 4.8 provide confirmation that the particular type of CSC considered in this study (that is, inverter-based series compensation) is capable of being used to vary the line reactance with sufficient speed to damp out unstable generator rotor oscillations when used as the variable reactance element in a power oscillation damping scheme. (Recall that in this study, prior to the introduction of the damping controls, the oscillations are unstable at this operating point as shown in Fig. 4.6). The results also provide further confirmation that the resulting positive value of damping obtained with the inverter-based CSC and its external controls agrees closely with that predicted using the simplified representation of the CSC as an ideal variable reactance.

The results in Fig. 4.8 illustrate the performance of the inverter-based compensator at a moderate value of damping controller gain K_C for which the controlled series capacitive reactance is in limit for only a brief period following the disturbance. In

order to examine the behaviour of the detailed inverter-based compensator scheme when driven into limit for a longer period, Fig. 4.9 now shows the response of the system to the same fault when the damping controller gain is increased tenfold to $K_C = 0.5$. The transient response of the system predicted using the two models is almost identical in limit but differs in the way the CSC comes out of limit. Despite the difference in the predicted responses, with the detailed model of the CSC system, the controller is still able to maintain the stable, damped response at high controller gains when the CSC is driven into limit.

In summary, from the time-domain simulation studies presented in this section two important conclusions can be made regarding the use of inverter-based series compensation for damping of swing mode oscillations:

- (i) the inverter-based form of series compensation is suitable for damping swing mode power oscillations both for small-signal damping control as suited to inter-area mode damping applications, and for large-signal (transient) damping of local-mode type swings where the CSC is driven into limit by a high value of controller gain; and
- (ii) the use of an idealised CSC model to represent the inverter-based series compensator for the design and analysis of the damping controller is reasonable, in particular for small-signal damping control studies and hence inter-area mode damping studies.

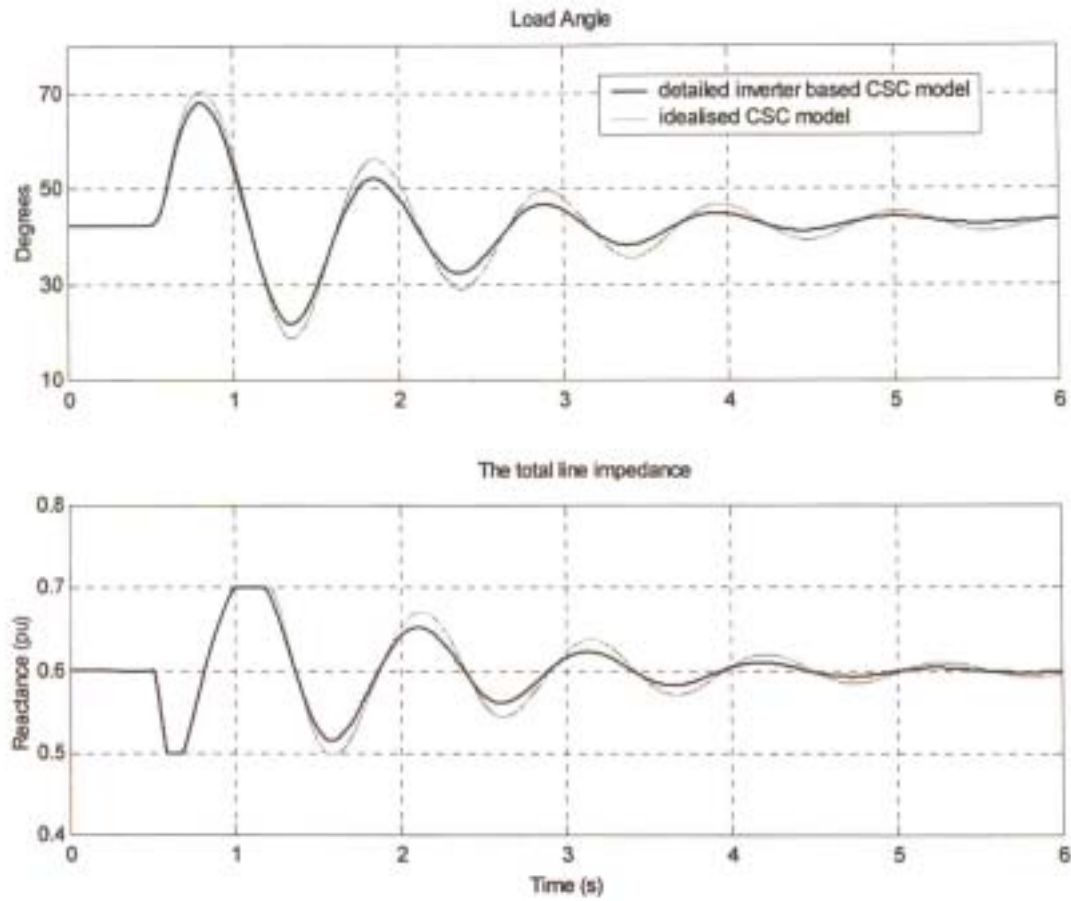


Fig. 4.8: Time-domain simulation results of the same SMIB system using an idealised CSC (light curves) and a detailed inverter-based CSC (bold curves) following a temporary disturbance with $K_C=0.05$ in each case.

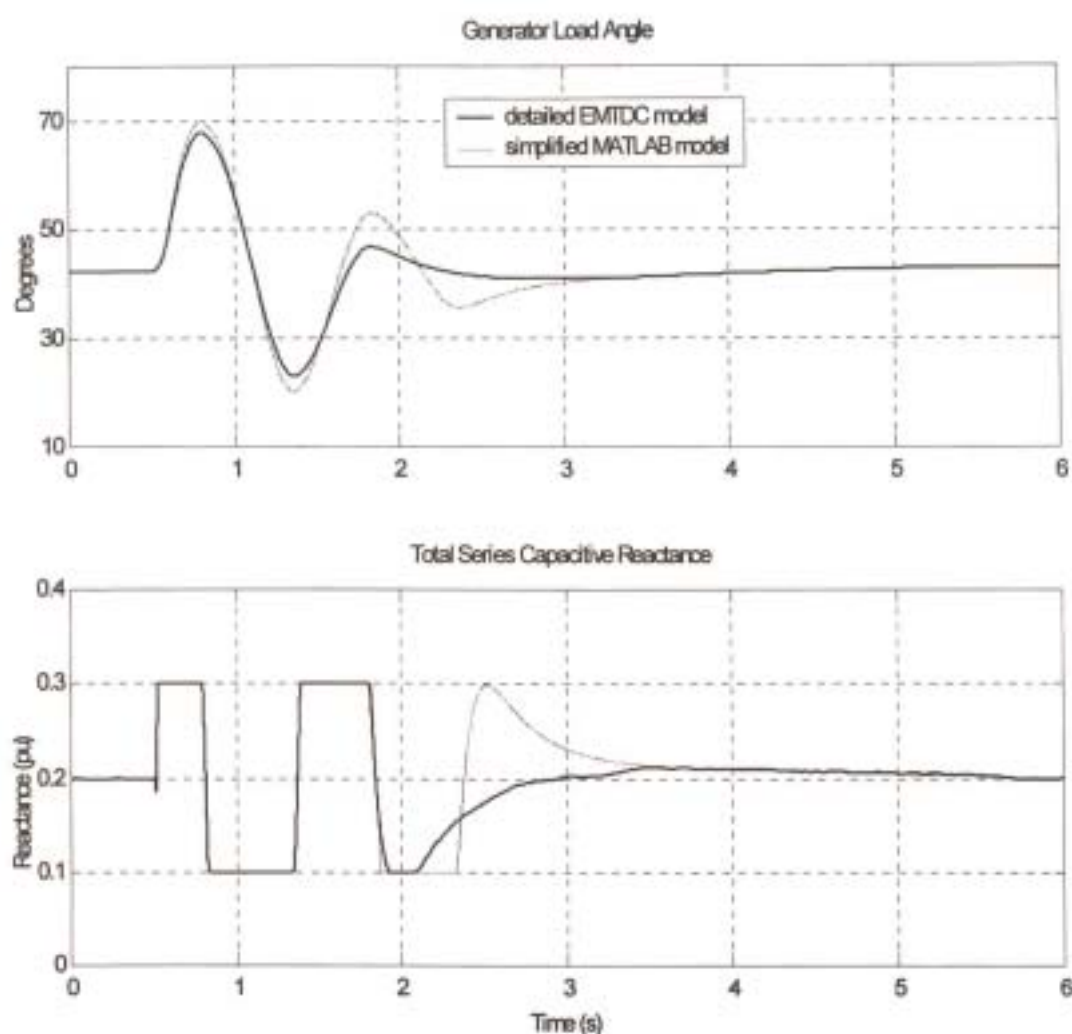


Fig. 4.9: Simplified MATLAB and detailed PSCAD/EMTDC non-linear simulation models of the SMIB system showing the predicted responses of the system following a disturbance with a high controller gain $K_C = 0.5$ in each case.

4.5 Results and Analysis Using Locally-Measured Input Signals

4.5.1 Introduction

The previous sections of this chapter have considered the single-machine infinite bus power system in Fig. 3.1, both under small signal and large signal conditions, and have considered the influence of various contributing factors to the controllable series compensator (CSC) damping controller performance and have found that the predicted responses of the system are in accordance with the findings in [Swift1,2]. In addition, subsequent studies have shown firstly that the particular inverter-based series compensator scheme considered in these analyses (as presented in [Rigby1]) can be used as another tool to damp the electromechanical system oscillations and secondly that the simplified approach employed in the analyses of Swift and Wang [Swift1,2] to represent a controllable series reactance can reasonably be applied in the case of an inverter-based series compensator. However, the analyses of the previous sections were carried out for a specific damping controller input $\Delta\omega$, since it was shown that this particular input signal is desirable in order to develop a component of torque which is in phase with the generator speed deviation $\Delta\omega$, thus maximising the CSC damping controller performance for given system operating conditions.

The particular problem being studied with the SMIB system of Fig. 3.1 is that of damping a local mode, where the oscillations of an individual generator are of direct concern and can be damped using the generator's speed deviation for the CSC controller input; however, the end-objective of this study is to re-apply the design and analysis techniques, which have been presented here for a simple case in Fig. 3.1, to investigate the inter-area mode damping problem where poorly damped oscillations occur as a result of a large group of generators in one area oscillating against a large group of generators in another area. Practically, in such an environment, the CSC controller is likely to be situated in the transmission network between the two groups of generators and is therefore likely to be physically far from the generators connected to the system; hence the speed deviations of those machines of interest are not readily available for the controller [Larsen].

Indeed, Chapter Two of this thesis reviewed a number of proposed input signals to the CSC damping controller: those suited to the inter-area mode damping problem were

identified as those that can be synthesised using variables measured locally at the site of the CSC in the system. Thus, while the generator speed deviation has been shown to be an ideal and logical input signal to the CSC damping controller, in the case of the inter-area mode damping problem this input signal must in practice be synthesised from other system variables measured locally at the controllable series compensator itself. This final section of this chapter now considers three of the proposed input signals that were reviewed in Chapter Two and compares these signals to the generator speed deviation in order to assess their suitability as locally-measured inputs to a CSC damping controller.

4.5.2 Review of Input Signals

This subsection briefly describes three types of local measurements as proposed in references [deMello1], [Larsen] and [Grongquist] that could each potentially be used to synthesise the generator speed deviation in order to act as an input to a CSC controller in the damping of an inter-area oscillation in Chapter Five of the thesis. These three approaches are presented below as follows.

Rate of change of power flow through the controllable series element

In reference [deMello1] deMello proposes that the power flowing through the CSC itself is the appropriate variable to measure for a damping controller since this signal can be calculated from local voltage and current measurements and is suited to the damping of inter-area oscillations. deMello proposed that the derivative of power flow in the series compensating element \dot{P}_{CSC} should, after proper filtering at the frequency range of interest, be fed directly to the input of a CSC damping controller.

Synthesised speed deviation

In reference [Larsen] Larsen et al. propose, for control of inter-area mode oscillations, the synthesis of angular difference between the voltages at each end of the line in which the CSC is placed; this synthesised angular difference is then differentiated in order to convert it to a synthesised speed deviation measurement $\Delta\omega_{synth}$. The remote voltages, v_{synth1} and v_{synth2} , on each side of the CSC are synthesised as functions of synthesising impedances, and the synthesised angular difference in [Larsen] as,

$$\Delta\delta_{synth} = \theta_{12} = \angle v_{synth1} - \angle v_{synth2} \quad (4.6)$$

where θ_{12} represents the angular difference between the group of machines of the two areas; the synthesised remote voltages v_{synth1} and v_{synth2} are themselves obtained from local current and voltage measurements. The proposed damping controller in [Larsen] is of the form,

$$K_{DC}(s) = K_m \frac{1}{1 + sT_{DC}} \frac{sT_{ws}}{1 + sT_{ws}} \frac{s}{1 + sT_{DC}} \quad (4.7)$$

where the terms $[s / (1 + sT_{DC})][1 / (1 + sT_{DC})]$ are the filtered derivative circuits used to convert the angle difference measurement $\Delta\delta_{synth}$ to a speed deviation measurement $\Delta\omega_{synth}$, $sT_{ws} / (1 + sT_{ws})$ is a washout circuit, and K_m is the damping controller gain. The synthesised output of this scheme $\Delta\omega_{synth}$ is then the input to the CSC damping controller. In the studies of this section, it is this synthesised speed deviation $\Delta\omega_{synth}$ that is compared to the actual speed deviation in the simplified SMIB study.

Voltage drop across the controllable series element

Grongquist et al. in reference [Grongquist] propose a control approach based on the magnitude of voltage drop across the transmission line in which the controllable reactance controller is placed; this signal is synthesised as shown in eqn. (2.7) of Chapter Two. The variables I_{LINE} and X_{LINE} are locally-measured line current and line reactance respectively, and V_{TCSC} is the voltage across the controllable element itself. The input to the CSC controller has been described as the product of the synthesised voltage V and its derivative with respect to time \dot{V} .

This subsection has provided a brief review of three locally-measured input signals to be examined for the CSC damping controller input. The following subsection now presents time-domain simulation results of the study system in Fig. 3.1 with the detailed mathematical model of the inverter-based compensator in PSCAD/EMTDC to compare the characteristics of each these synthesised signals to that of the actual

generator speed deviation $\Delta\omega$.

4.5.3 Non-Linear Simulation Results

This subsection once again considers the simulated response of the detailed single-machine infinite bus power system in Fig. 3.1 where the controlled reactance is provided by the inverter-based series compensator. The first simulation result presented compares the characteristics of each of the three input signals reviewed in the previous subsection to those of the generator speed deviation $\Delta\omega$. Initially, the synthesised signals are not actually used as inputs to the CSC damping controller. Rather, the actual generator speed deviation remains as the input signal to the CSC controller in each case but each of the three locally-synthesised candidate signals is compared in the time-domain to the actual signal $\Delta\omega$ that is being used as the input to the controller.

Characteristics of the candidate input signals

This subsection now compares the characteristics of the three locally synthesised signals to those of the measured generator speed deviation $\Delta\omega$ in order to determine which of these signals might be used as a replacement for generator speed deviation in an inter-area mode damping controller. Fig. 4.10 shows the response of the SMIB system in Fig. 3.1 when subjected to a temporary three-phase disturbance at the infinite bus terminals with $\Delta\omega$ used at the CSC input; each plot window in Fig. 4.10 compares the time response of the actual speed deviation with that of a locally-synthesised candidate input signal.

In Fig. 4.10 (a) the actual speed deviation $\Delta\omega$ (bold curve) is compared with the synthesised speed deviation signal $\Delta\omega_{synth}$ proposed by Larsen et al. [Larsen] (light curve). The magnitude of the synthesised signal $\Delta\omega_{synth}$ has been scaled such that it corresponds to the magnitude of $\Delta\omega$ in the later (small-signal) stages of the oscillation. The comparison in Fig. 4.10 (a) shows that, after appropriate magnitude scaling, the time response of the synthesised signal $\Delta\omega_{synth}$ corresponds closely to that of the actual speed deviation $\Delta\omega$, but that there is nevertheless a small phase lag in $\Delta\omega_{synth}$ with respect to $\Delta\omega$. The phase relationship between $\Delta\omega_{synth}$ and $\Delta\omega$ at the frequency of the generator oscillations is determined by the value of the time constant

T_{DC} chosen for the differentiator-filter stage that is used to convert the synthesised angle difference into a synthesised speed deviation (eqn. (4.7)). This time constant T_{DC} can be set to give a signal $\Delta\omega_{synth}$ exactly in phase with $\Delta\omega$ at a particular operating point if desired; however it is better practice [Larsen] to design the differentiator-filter block to allow a small phase lag in $\Delta\omega_{synth}$ with respect to $\Delta\omega$ thereby introducing a small positive component of synchronising torque when the signal is used as a CSC controller input. The consequence of erring on the side of *phase lead* between $\Delta\omega_{synth}$ and $\Delta\omega$ would be to introduce negative synchronising torque which is clearly undesirable. Fig. 4.10 (a) thus confirms that the small-signal behaviour of the locally-measured signal $\Delta\omega_{synth}$ is therefore a slightly conservative (and hence reasonable) approximation to the generator speed deviation $\Delta\omega$. However, Fig. 4.10 (a) also shows that there is a significant difference between the characteristics of $\Delta\omega_{synth}$ and $\Delta\omega$ during the fault and in the period shortly after the fault is cleared. Thus while the locally measured signal $\Delta\omega_{synth}$ is clearly suitable for small-signal damping in the post-fault period, it is still necessary to check its effect on the system response during, and immediately after a system fault occurs.

In Fig. 4.10 (b) the actual speed deviation $\Delta\omega$ (bold curve) is compared with the rate of change of power \dot{P}_{CSC} flowing through the CSC (light curve) (the input signal proposed by deMello [deMello1]). Once again the locally-measured signal is scaled such that its magnitude corresponds to that of generator speed deviation $\Delta\omega$ during small signal oscillations. The results of Fig. 4.10 (b) show that this input signal \dot{P}_{CSC} exhibits much the same characteristics as the synthesised speed deviation $\Delta\omega_{synth}$ of Larsen (Fig. 4.10 (a)): the signal \dot{P}_{CSC} exhibits a small phase lag with respect to $\Delta\omega$ for small-signal variations in generator speed but does not correspond to $\Delta\omega$ during the fault period and for a short period immediately following the clearance of the fault. Thus, as with the signal $\Delta\omega_{synth}$, the locally-measured signal \dot{P}_{CSC} proposed by deMello is a reasonable signal to use in place of generator speed deviation as an input to a CSC damping controller but the effect of this signal on the system response during, and immediately after a system fault needs examination.

Finally, in Fig. 4.10 (c) the speed deviation $\Delta\omega$ (bold curve) is compared with the signal $V \cdot \dot{V}$ (light curve) (the input signal proposed by Grongquist et al. [Grongquist]). Once again, the magnitude of the synthesised signal (light curve) has been scaled such that it corresponds to the magnitude of $\Delta\omega$ during small signal oscillations. Fig. 4.10 (c) shows that, unlike the signals $\Delta\omega_{synth}$ and \dot{P}_{CSC} , the locally synthesised signal $V \cdot \dot{V}$ is not in phase with $\Delta\omega$; rather, the oscillations in the signal $V \cdot \dot{V}$ are found to lag those of $\Delta\omega$ by close to 90° . The results of Fig. 4.10 (c) therefore indicate that the signal $V \cdot \dot{V}$ proposed by Grongquist in fact synthesises the deviation in generator rotor angle $\Delta\delta$ rather than the generator speed deviation $\Delta\omega$. As a result, while such a signal could be expected to provide positive synchronising torques if used as an input to the CSC, it would not be expected to result in addition of significant small-signal damping torques. Thus the signal $V \cdot \dot{V}$ is not suitable as an input for a CSC damping controller as applied to the inter-area mode damping problem.

This subsection has examined three locally-measured input signals for the CSC controller that have been proposed in the literature, and the studies have identified two of these signals that can be considered suitable for the damping of inter-area oscillations namely, the locally-synthesised speed deviation measurement of Larsen et al. in [Larsen] and the rate of change of power flowing through the controllable series reactance of deMello in [deMello1]. The following subsection now examines the performance of the CSC damping controller when each of these two signals is actually used as the input to the controller in place of the ideal signal $\Delta\omega$.

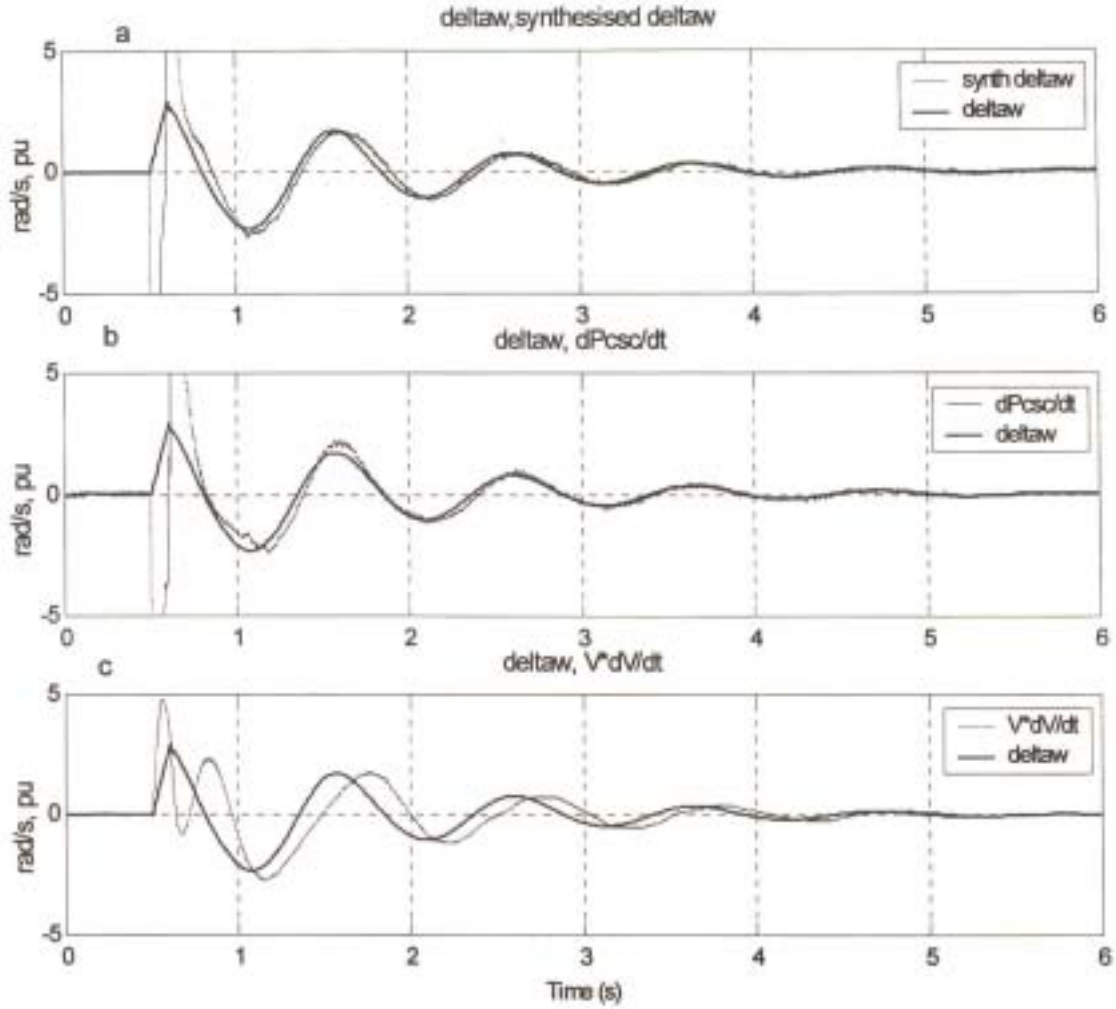


Fig. 4.10: Time-domain simulation results comparing various synthesised signals to the actual speed deviation $\Delta\omega$.

Simulation results using the synthesised signals

Fig. 4.10 has shown that the two locally-measured signals $\Delta\omega_{synth}$ and \dot{P}_{CSC} can, after suitable magnitude scaling, be used as replacements for the generator speed deviation $\Delta\omega$ at the input of the CSC damping controller for small-signal variations in $\Delta\omega$. However it has also been shown that these signals differ significantly from the signal $\Delta\omega$ during, and immediately after clearing of, a large system disturbance. It is therefore necessary to evaluate how the CSC controller responds when such signals are actually used as inputs to the damping controller. This subsection now examines the performance of the CSC damping controller when the input signal $\Delta\omega$ (for which

the controller has been designed) is replaced first by the signal \dot{P}_{CSC} and then by the signal $\Delta\omega_{synth}$. The time-domain simulation results of this subsection show, for each of these signals, the response of the system following a temporary three-phase short circuit fault lasting 100 milliseconds applied at the terminals of the infinite bus.

Fig. 4.11 compares the performance of the CSC damping controller in the detailed SMIB system of Fig. 3.4 with $\Delta\omega$ as input (bold curve) with the response of the same system with \dot{P}_{CSC} as input (light curve) to the damping controller. As in the previous subsection, the input \dot{P}_{CSC} is appropriately scaled to correspond in magnitude to $\Delta\omega$ before being used as a replacement for $\Delta\omega$; in this way the effective gain of the CSC damping controller is unchanged and its small-signal performance can be expected to remain the same for both signals. However, consider firstly the initial response of the system shown in Fig. 4.11 (b) and (c): Fig. 4.10 (b) showed a significant difference between $\Delta\omega$ and \dot{P}_{CSC} during, and immediately after a fault which is observed again in Fig. 4.11 (b) (light curve); Fig. 4.11 (c) now shows the effect that this difference has on the system when \dot{P}_{CSC} is used as input to the CSC damping controller. During the fault, when \dot{P}_{CSC} is negative and $\Delta\omega$ positive, the synthesised signal \dot{P}_{CSC} in Fig. 4.11 (c) drives the controller output into negative limit (light curve) whereas the actual speed signal $\Delta\omega$ drives the controller output into positive limit (bold curve). Immediately after clearance of the fault \dot{P}_{CSC} has the correct sign but is much greater in magnitude than the actual speed deviation $\Delta\omega$, so the locally-measured signal now drives the CSC controller output into positive limit. However even in the case when the actual speed deviation is used as the input signal, the CSC output is driven into positive limit immediately after the fault; as a result, there appears to be no significant difference in the predicted response of the system in the post-fault period for this particular disturbance. Clearly, the large signal behaviour of the system with \dot{P}_{CSC} as input to the CSC controller will depend on the type, location, and severity of a fault; however, the analyses of this section have considered a three-phase short circuit fault (a severe disturbance) and the results indicate that, despite the discrepancy between $\Delta\omega$ and \dot{P}_{CSC} under large signal conditions, the CSC controller performance during

the first swing is not significantly altered from that with $\Delta\omega$ as input to the damping controller.

Finally, Fig. 4.11 (c) confirms, as expected, that for small-signal system oscillations (when \dot{P}_{CSC} closely approximates $\Delta\omega$) the performance of the CSC damping controller with \dot{P}_{CSC} as input to the CSC controller is very close to that when $\Delta\omega$ is used as the input to the damping controller. The small-signal damping of the generator rotor oscillations is the primary focus of this study and Fig. 4.11 (a) shows that the damping is virtually identical for both \dot{P}_{CSC} and $\Delta\omega$ as inputs. The time-domain simulation results in Fig. 4.11 therefore confirm that, for the inter-area mode damping problem, \dot{P}_{CSC} is a reasonable locally-measured substitute for the generator speed deviation $\Delta\omega$.

Fig. 4.12 now compares the performance of the CSC damping controller in the single-machine infinite bus system (Fig. 3.1) with $\Delta\omega$ as input (bold curve) with the response of the same system when the synthesised speed deviation signal $\Delta\omega_{synth}$ is used as input (light curve) to the damping controller. Once again, the input $\Delta\omega_{synth}$ has been appropriately scaled to correspond in magnitude to $\Delta\omega$ before actually using it as a replacement for $\Delta\omega$ such that the effective gain of the CSC damping controller is unchanged when the signals are swapped. Fig. 4.12 (b) shows that, once again, there is a significant difference between $\Delta\omega_{synth}$ and $\Delta\omega$ during and immediately after a temporary three-phase short circuit fault. The effect of this initial difference can be observed in Fig. 4.12 (c): the synthesised signal $\Delta\omega_{synth}$ at first drives the damping controller output into negative limit whilst the actual speed deviation $\Delta\omega$ drives the controller output into the positive limit. However, immediately after the clearance of the fault $\Delta\omega_{synth}$ has the correct sign but is much greater in magnitude than $\Delta\omega$, thus correctly driving the CSC output into positive limit such that there is no significant difference in the controller performance in post-fault from when $\Delta\omega$ is used as the input. Thus, the results show that despite a large discrepancy between $\Delta\omega$ and $\Delta\omega_{synth}$ under large disturbance conditions, the controller performance during the first swing is not significantly altered from that with $\Delta\omega$ as input to the CSC.

Finally, when the controller output comes out of limit (that is, for small-signal system oscillations) the performance of the CSC damping controller is, as expected, very close with each of the signals used as inputs to the CSC controller. The small-signal damping of generator rotor swings in Fig. 4.12 (a) once again shows that the damping is virtually identical for both $\Delta\omega$ and $\Delta\omega_{synth}$ as inputs to the CSC damping controller.

As in the case of the input signal \dot{P}_{CSC} , a similar conclusion can be reached regarding the use of a synthesised speed deviation $\Delta\omega_{synth}$ signal as input to the CSC controller for the inter-area mode damping problem: the synthesised speed deviation $\Delta\omega_{synth}$ is a reasonable locally-measured substitute for the generator speed deviation $\Delta\omega$.

This section has presented the results of a simulation study using a detailed single-machine infinite bus system model in order to compare the performance of each of the proposed locally-measured signals in [Larsen] and [deMello1] when used as inputs to the CSC damping controller to that of the generator speed deviation $\Delta\omega$. The results have indicated that both these signals are reasonable candidate input signals for consideration in the damping of inter-area oscillations of the multi-machine system in [Kundur] that is to be studied in Chapter Five of this thesis.

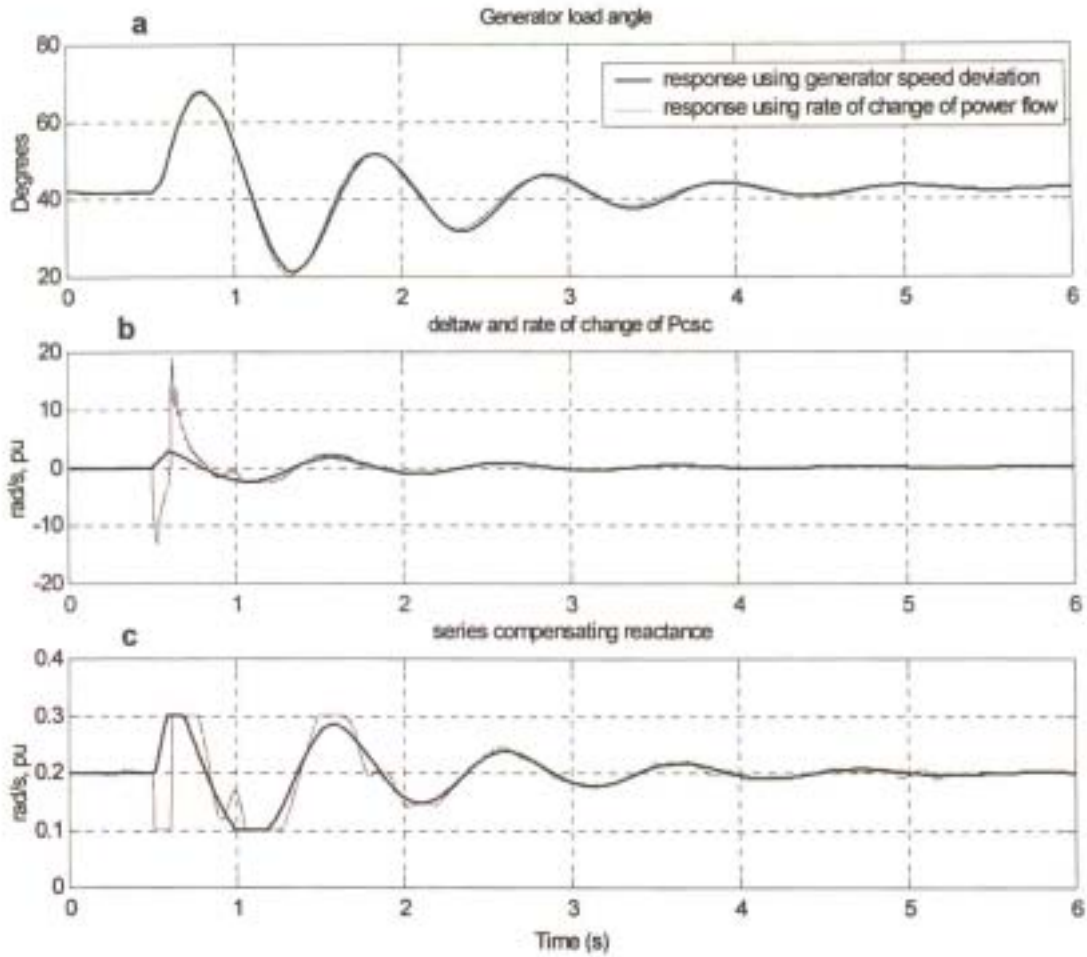


Fig. 4.11: Non-linear simulation of the system response in PSCAD/EMTDC following a temporary disturbance using, for the CSC controller input, the generator speed deviation and the synthesised rate of change of power flow.

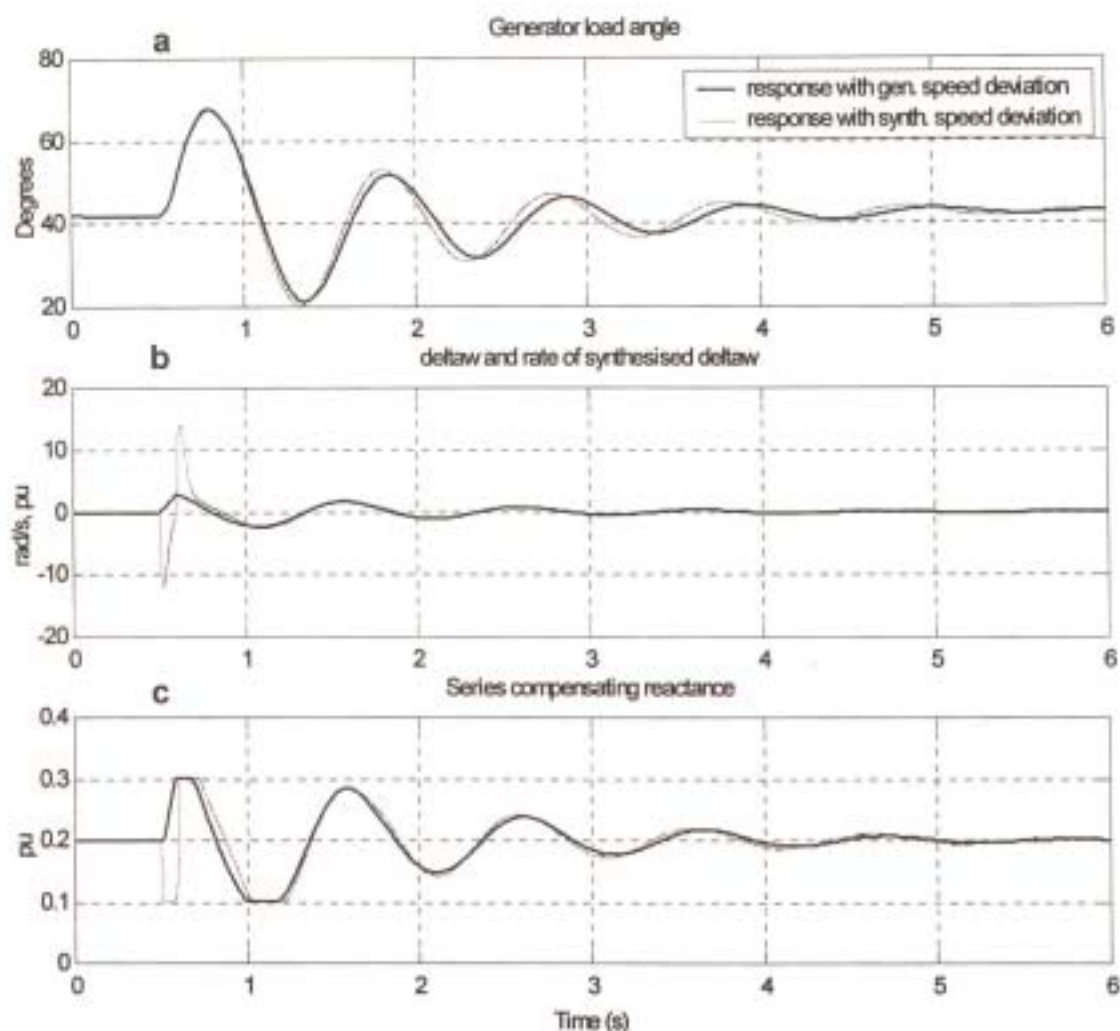


Fig. 4.12: Non-linear simulation of the system response in PSCAD/EMTDC following a temporary disturbance using, for the CSC controller input, the generator speed deviation and the synthesised speed deviation measurement.

4.6 Conclusion

This chapter has presented studies of a single-machine infinite bus power system which are similar to those of Swift and Wang in references [Swift1,2] where an idealised controllable series compensator, with an external damping controller, is used to damp electromechanical system oscillations. Initially, a linearised Phillips-Heffron model was used to analyse the damping and synchronising torques added to the system by the CSC damping controller. In this chapter, although a generalised signal was initially assumed for the CSC damping controller input (as in the analyses of Swift and Wang [Swift1,2]), it was however established that if *all* the torque contributed by the CSC controller to the system is actually desired to add to system *damping*, then the generator speed deviation is the appropriate signal to use (subject to minimal phase lag between this input and the output of the CSC controller).

This chapter subsequently demonstrated, using the generator speed deviation for the damping controller input, the factors with considerable bearing on the CSC damping controller performance in the SMIB study system namely, the generator loading, the damping controller gain, and system interconnection strength. The influence of these factors on the performance of the CSC damping controller was found to be in accordance with the findings of Swift and Wang in [Swift1,2] using the linearised Phillips-Heffron model with further confirmation provided from non-linear models of the system. The non-linear system models were also used to predict the system's response when the CSC damping controller output is driven into limit in order to determine the performance of the damping controller with very high controller gains.

This chapter further extended the scope of the analytical study carried out in [Swift1,2] where the performance of a power oscillation damping scheme was predicted using an idealised representation of the CSC; in this chapter the performance of the same damping scheme was considered but using a detailed representation of an inverter-based CSC. The significance of the findings of this extended investigation is twofold: firstly, an inverter-based series compensator is a suitable device to use particularly for small-signal damping of system oscillations; secondly, subject to a small degree of conservative error in the predicted response of the system, the use of a generic, idealised CSC model as has been proposed in

[Swift1,2] to represent the inverter-based series compensator itself for design and analysis of the damping controller is in fact reasonable.

Finally, in this chapter, alternative input signals to the CSC damping controller were considered, recognising that for the inter-area mode damping problem the speed deviations of the generators of interest are not likely to be readily available. The chapter therefore examined three of the proposed locally-synthesised input signals for the CSC controller as proposed in the literature and compared each of the signal's characteristics to those of the actual generator speed deviation. The time-domain simulation results showed that two of the locally-synthesised signals considered in the analyses in fact contain similar information to the actual generator speed deviation and can therefore be considered as reasonable substitutes for the generator speed deviation in the inter-area mode damping problem.

Since an understanding of the correct design approach for a CSC damping controller, and the factors that influence its performance have been made clear from the SMIB system studies conducted in this chapter, the following chapter now makes use of this understanding by considering a particular four-generator study system and examining the more-complex, inter-area mode damping problem that manifests itself in this system.

CHAPTER FIVE

APPLICATION OF THE CSC TO DAMPING INTER-AREA MODE OSCILLATIONS

5.1 Introduction

The previous chapter of this thesis has described in detail the design and analysis of a CSC damping controller for the relatively simple case of a single-machine infinite bus (SMIB) power system, initially using an idealised representation of the CSC; subsequent investigations considered the use of a detailed representation of an inverter-based CSC in the system model. In each case, factors with significant impact on the ability of the CSC damping scheme to provide additional damping torques in the system were examined. The analyses of Chapter Four concluded that the inverter-based series compensator considered in the thesis is in fact a suitable device to use particularly for enhancing small-signal damping.

In addition, the SMIB studies of Chapter Four showed that generator speed deviation is the logical input signal to a CSC damping controller but identified that such a signal could present practical difficulties in an inter-area mode (multi-generator) environment. Chapter Four then identified two alternative input signals to a CSC damping controller that have been proposed in the literature; each of these input signals is synthesised from variables measured locally to the CSC and has been shown in Chapter Four to be a suitable replacement for generator speed deviation, at least in the case of a SMIB system. Chapter Four thus concluded that each of these signals can be considered as reasonable substitutes for generator speed deviation when the CSC is applied to the inter-area mode damping problem. This chapter now considers the application of the inverter-based CSC to damping the inter-area mode of a particular four-generator study system, and examines the performance of the CSC damping controller with each of these proposed input signals.

This chapter begins by describing the four-generator power system to be considered in the analyses, as well as the development of the simulation model of this system in

PSCAD/EMTDC. Simulation results are then presented to demonstrate the nature of the inter-area mode oscillation problem, and to show that the inverter-based series compensator can be used to mitigate the problem. The following section begins by describing the four-generator power system that is considered in the analyses of this chapter.

5.2 System Description

5.2.1 The Two-Area Power System

An eleven-bus, four-generator, two-area power system that is considered in the analyses of this chapter is shown in Fig. 5.1; this study system has been considered in references [Kundur,Klein1,2] for the study of inter-area mode oscillations. While inter-area oscillations in large interconnected power systems are actually more complex, the system in Fig. 5.1 is chosen because it has the advantage of being simple and hypothetical, and thus allows the characteristics of inter-area oscillations that are present in the system to be seen readily. Despite the size of the system of Fig. 5.1 being small, the system parameters (in Appendix D) and its structure are realistic, and hence the general conclusions drawn using this system will also apply to large systems [Klein1]. The researchers [Kundur,Klein1,2] who have previously considered this system have examined the mitigation of its inter-area mode damping problem via power system stabiliser design. This chapter considers the mitigation of the problem with an inverter-based CSC; therefore, the CSC shown in the diagram of Fig. 5.1 is not part of the original study system.

The system in Fig. 5.1 consists of four synchronous generators: generators G1 and G2 in Area 1 and generators G3 and G4 in Area 2; each generator is directly connected to a three-phase step-up transformer. The generating units, in this study system, are each represented by a detailed two-axis model; each generator is considered to have an automatic voltage regulator and a high-gain thyristor exciter with transient gain reduction: a particular combination of the factors that is known (as discussed already) to adversely affect the small-signal damping of power systems.

The effects of the governor-dynamics in these investigations are once again neglected such that the mechanical input torque to the synchronous generators is assumed to be

constant over the time frame of the investigation. Each synchronous generator is considered to have a single lumped inertia shaft representing the combined inertia of all the turbine stages. The transmission line system in this study is assumed to have negligible shunt capacitance, and as such is represented simply by its series lumped impedance.

The inverter-based controllable series compensator is inserted into the system of Fig. 5.1 in the main inter-tie between buses 7 and 9 as shown by the dotted box; for the purposes of these analyses, the inter-tie between buses 7 and 9 is modelled as a single transmission line whose reactance is half that of the two lines connecting buses 7 and 9 in the original system model.

As mentioned before, this chapter investigates the inter-area mode damping problem using the two-area power system of Fig. 5.1. This system is characterised by both inter-area and local mode oscillations as will be seen in the linearised results that are presented later in the chapter. In this study system, the Areas 1 and 2 are identical and are connected by a relatively weak tie-line. The constant impedance loads L_7 and L_9 assumed in this study are connected as shown at buses 7 and 9 in Fig. 5.1. In order to ensure a satisfactory voltage profile in this four-machine system, additional reactive power is supplied by shunt capacitors C_7 and C_9 connected at buses 7 and 9, respectively.

This subsection has described the constituents and layout of the study system of Fig. 5.1. The following subsection now describes the development of a detailed, time-domain simulation model of this system in PSCAD/EMTDC.

5.2.2 Two-Area Power System in PSCAD/EMTDC

The previous subsection has briefly described the two-area power system (in Fig. 5.1) which is considered in the studies of this chapter. Fig. D.1 in Appendix D shows the graphical representation of this four-generator power system in PSCAD/EMTDC, excluding the inverter-based series compensator. In the PSCAD/EMTDC graphical representation of the system in Fig. D.1, the synchronous generators are represented by their detailed two-axis model: generator stator transients and damper windings are now represented, the automatic voltage regulator and thyristor exciter with transient

gain reduction are also represented as shown in a single block labelled (exciter (SCRX)). In this PSCAD/EMTDC representation, the loads L_7 and L_9 are represented simply as constant impedances. Each area consists of two coupled generating units, and each unit has a rating of 900 MVA base power and 20 kV base voltage. The active power transfer from Area 1 to Area 2, over the single tie-line reactance, is 400 MW, and it is created by an uneven distribution of the system load amongst the generators; the generating units are loaded as shown in Appendix D.

Fig. D.2 in Appendix D now shows the same system in PSCAD/EMTDC as in Fig. D.1, but the system in Fig. D.2 now includes the detailed representation of the inverter-based controllable series compensator (and its damping controls), including its power-electronic switching and internal controls, which ensure that the device behaves as a capacitive reactance of the desired magnitude as has been described in Chapter Three (Fig. 3.4) of this thesis. The parameters of the inverter-based series compensator and its internal controls have been adjusted from those in previous chapters in order to suit the characteristics of the study system in Fig. 5.1; these parameters, and how they have been obtained, can be seen in Appendix D.

Once again, the power oscillation damping controller external to the compensator in Fig. D.2 is identical to that of Chapter Three: the input signal to the damping controller is in each case passed through a first-order filter, the output of which forms the commanded value of variable compensating reactance X_{CSCV} at the input to the inverter controls; however, the input to the damping controller used in these studies is now synthesised from measurements local to the CSC itself. The variable component X_{CSCV} of series compensating reactance is once again added to the fixed component X_{CSC0} to yield the overall commanded value X_{CSC} that is supplied to the inverter controls.

This section has described the four-generator study system to be considered in this chapter, and the development of a detailed model for time-domain simulation of this system in PSCAD/EMTDC. The following section now discusses the various oscillatory modes that characterise this system.

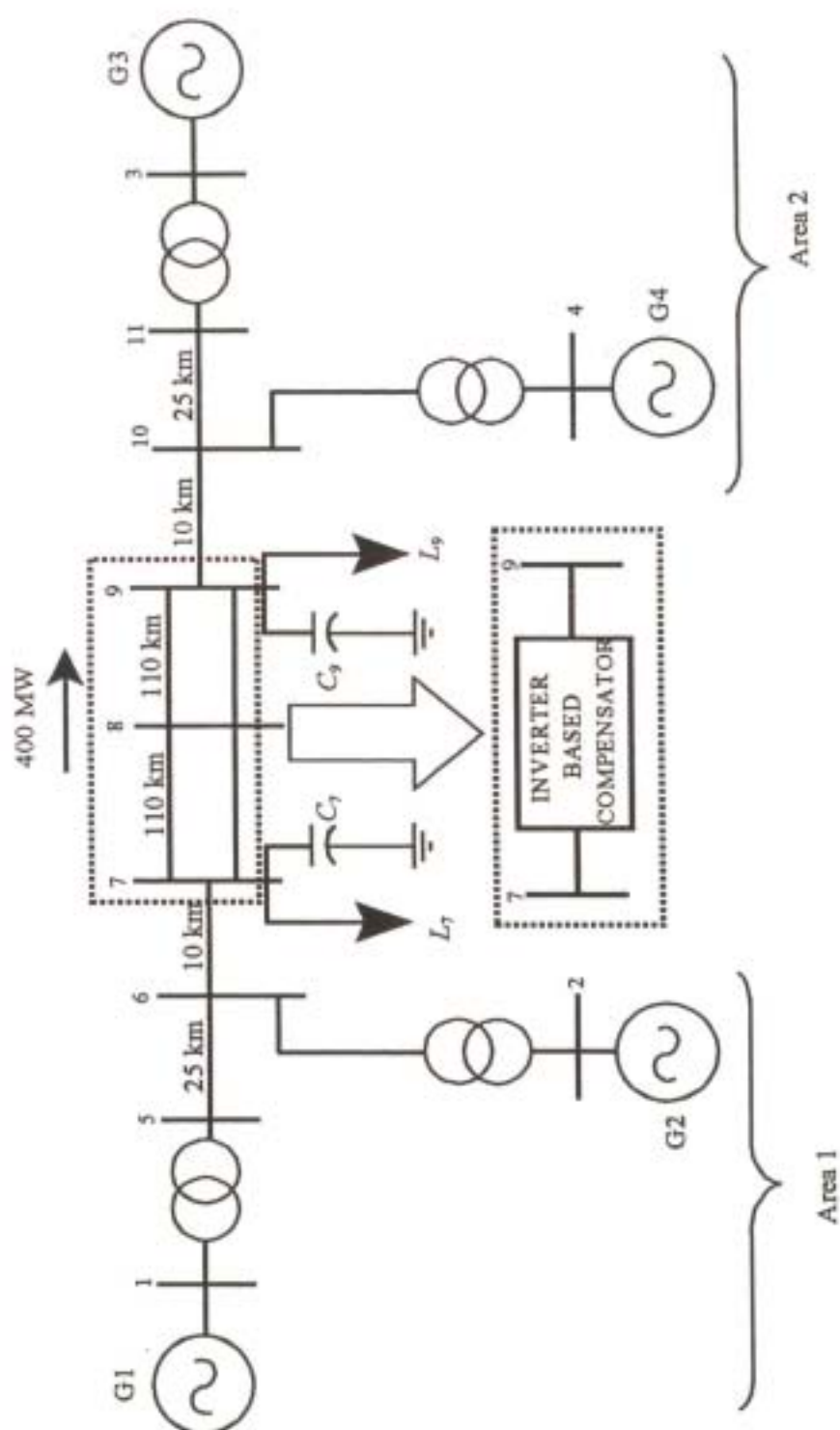


Fig. 5.1: An eleven-bus, four-generator, two-area power system.

5.3 Small-Signal Characteristics of the Study System

5.3.1 Eigenvalues of the System

It was pointed out in section 3.2.3 of Chapter Three that one of the drawbacks of the PSCAD/EMTDC simulation program is that powerful control analysis and design features (that is, the ability to calculate eigenvalues, eigenvectors and participation factors) are not available. However, the linearised eigenvalues and mode shapes of the four-generator power system under consideration (Fig. 5.1) which illustrate the system's small-signal behaviour, have been examined previously in reference [Kundur]. Hence this section reviews the linearised results of the system as presented in [Kundur] in order to form the basis for understanding the time-domain response of the system that is to be presented in later sections of this chapter.

The parameters of the four-generator power system in Fig. 5.1 are shown in Appendix D. The linearised eigenvalues of the system at this operating point, reproduced from [Kundur], are shown in Table 5.1 below.

Table 5.1: Eigenvalues of the system in Fig.5.1 with high-gain exciter and transient gain reduction and AVR, reproduced from [Kundur].

Rotor Oscillation Mode	Eigenvalues	Frequency, Damping Ratio
Area 1 local mode	$-0.450 \pm j6.86$	$\omega_d = 1.09 \text{ Hz}, \zeta = 0.06$
Area 2 local mode	$-0.462 \pm j7.05$	$\omega_d = 1.12 \text{ Hz}, \zeta = 0.06$
Inter-area mode	$+0.123 \pm j3.46$	$\omega_d = 0.55 \text{ Hz}, \zeta = -0.036$

The small-signal stability characteristics of the four-generator power system may be explained from these eigenvalues in Table 5.1 as follows.

Table 5.1 shows that there are three complex conjugate eigenvalues associated with different oscillatory modes of the system: there are two inter-machine (local) modes of oscillation (one in Area 1 and one in Area 2) which have the same degree of positive damping ($\zeta = 0.06$) and one inter-area mode of oscillation which is *negatively damped* ($\zeta = -0.036$) and therefore unstable. The frequencies of oscillation of the two inter-machine modes (which are stable for this set of operating conditions) are 1.09

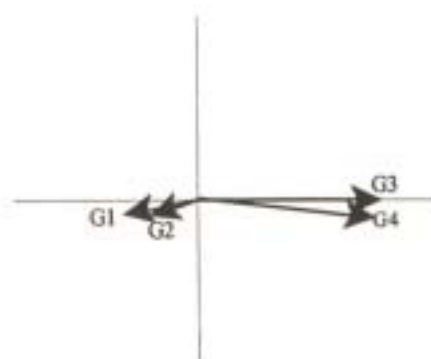
Hz and 1.12 Hz in Areas 1 and 2, respectively, whilst the frequency of the inter-area mode oscillation is 0.55 Hz. In the time-domain simulation studies that follow, it would be clearly desirable to improve the damping of the inter-area mode oscillations of this system using the inverter-based CSC and its damping controls.

This subsection has discussed the small-signal behaviour of the four-machine system via eigenvalue analysis. The following subsection now discusses the mode shapes of this system.

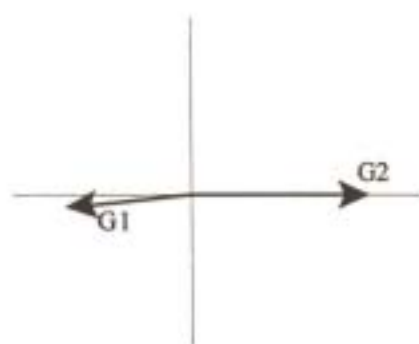
5.3.2 Mode Shapes of the System

Fig. 5.3 now shows the mode shapes of the system, that is, the normalised eigenvector components corresponding to the rotor speed deviations of each of the four synchronous generators of the system in Fig. 5.1 (as presented in [Kundur]). From the mode shapes in Fig. 5.3 (a) three observations can be made with regard to the inter-area mode: firstly, from the relative phase of the eigenvectors, in the inter-area mode the synchronous generators G1 and G2 of Area 1 swing against the synchronous generators G3 and G4 of Area 2; secondly, again from the phase of the eigenvectors, the generators of each area swing almost in-phase with each other in the inter-area mode; thirdly, from the relative sizes of the eigenvectors, the amplitude of the oscillations of the Area 2 generators (G3 and G4) is larger than the amplitude of the oscillations of the Area 1 generators (G1 and G2) in the inter-area mode. Fig. 5.3 (b) shows that in the inter-machine oscillation local to Area 1, generator G1 swings in anti-phase with generator G2. Similarly, Fig. 5.3 (c) shows that in the inter-machine oscillation mode local to Area 2, generator G3 swings in anti-phase with generator G4.

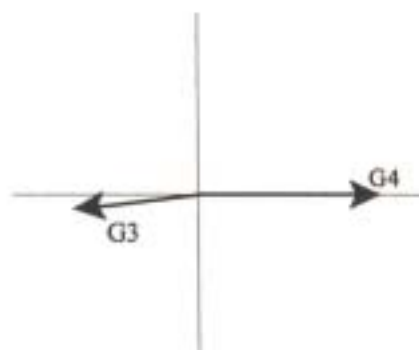
In summary, this section has described the small-signal characteristics of the four-machine system under consideration (Fig. 5.1) and has shown the nature of all the various modes present in the system by means of eigenvalue analysis and mode shapes. The following section now presents time-domain simulation results of the system in Fig. 5.1, using the detailed system model developed in PSCAD/EMTDC, in order to confirm the small-signal behaviour predicted thus far, and subsequently investigates the use of the inverter-based series compensator to damp the inter-area mode oscillations.



(a) Inter-area mode



(b) Area 1 local mode



(c) Area 2 local mode

Fig. 5.2: Mode shapes of the oscillatory modes of the system in Fig. 5.1, as presented in [Kundur].

5.4 Simulation Results

5.4.1 Introduction

The previous section has described the linearised eigenvalues of the system in Fig. 5.1 that were presented in reference [Kundur]. This section now presents time-domain simulation results of this system, using the detailed model developed in PSCAD/EMTDC, in order to determine whether the inverter-based series compensator and its damping controls are able to mitigate the inter-area mode problem. The investigations carried out in this final part of the thesis are structured as follows.

- (i) The time-domain response of the four-generator power system is initially considered for the case when there is no inverter-based compensator in the inter-tie. The purpose of this study is to confirm (by comparison with the linearised results of [Kundur]) the correctness of the small-signal behaviour of this system (and hence the model developed in PSCAD/EMTDC), particularly the characteristics of its inter-area mode oscillations, prior to the introduction of the inverter-based compensator.
- (ii) The time-domain response of the four-generator power system is then considered for the case when the inverter-based compensator is used to provide a fixed amount of series compensating reactance in the inter-tie. The purpose of this study is to examine the impact of the inverter-based compensator on the system when its damping controller is inactive as well as to observe the characteristics of the locally-synthesised controller inputs before they are each used as inputs to the damping scheme.
- (iii) Finally, the time-domain response of the system is considered for the case when the inverter-based compensator is included in the inter-tie and its damping controls are activated. This study is repeated for each of the two controller input signals identified in Chapter Four in order to demonstrate the performance of the damping controller for both of these input signals.

These simulation studies will therefore serve as a basis to assess the ability of a damping controller based on an inverter-based series compensator to mitigate the problem of poorly damped inter-area modes in power systems.

5.4.2 Simulation Results with No Series Compensation

As described before, a detailed model of the system of Fig 5.1 has been developed in PSCAD/EMTDC, both with and without an inverter-based compensator in series with the main inter-tie. This section now presents time-domain simulation results of the system in Fig. 5.1 for the case where there is no compensator in the main inter-tie. The detailed PSCAD/EMTDC model for this study is shown in Fig. D.1 of Appendix D, and the parameters and operating conditions of the four-generator system are also shown in appendix D.

Fig. 5.3 now shows the time-domain response of the system following a disturbance caused by reducing the mechanical power input to generator G2 from its initial steady-state value of 700 MW to 540 MW and back to 700 MW after one second. The predicted response shown in Fig. 5.3 shows the active power outputs of all the generating units in the system as well as the active power transfer over the inter-tie between buses 7 and 9. Fig. 5.3 (a) shows the active power outputs of generators G1 to G4 during the first ten seconds of the simulation whilst Fig. 5.3 (c) shows these same variables during the last six seconds of the simulation study.

In Fig. 5.3 (a), it is seen that during, and immediately after the disturbance the generating units in Area 1 (generators G1 and G2) oscillate in anti-phase with each other with a frequency of 1 Hz; these oscillations are associated with the local mode of Area 1 and remain positively damped as expected. Comparison of Figs. 5.3 (a) and (c) however shows that, in the later stages of the simulation, there is no longer any anti-phase oscillation between generators G1 and G2. In fact, in the later stages of the post-disturbance response (Fig. 5.3 (c)) when the positively damped local mode oscillations have died out, the generators in Area 1 (G1 and G2) are seen to oscillate in phase with each other, as are the generators in Area 2 (G3 and G4). However, in the later stage of the response, the oscillations of generators G1 and G2 in Area 1 are *out of phase* with those of generators G3 and G4 in Area 2; furthermore these oscillations are seen to have a frequency of approximately 0.5 Hz and to be slightly negatively

damped. Finally, the generators in Area 2 (G3 and G4) are seen to oscillate with a higher amplitude than the generators in Area 1 as noted in [Klein1]. Each of these characteristics of the oscillations in generators G1 to G4 is consistent with the small-signal characteristics of the inter-area mode of this system as predicted by the inter-area mode eigenvalue in Table 5.1 and by the inter-area mode shape in Fig. 5.2 (a). The simulation results of Fig. 5.3 thus confirm that the detailed model of the four-generator system developed in PSCAD/EMTDC faithfully reproduces the known characteristics of the inter-area mode oscillation problem associated with this system.

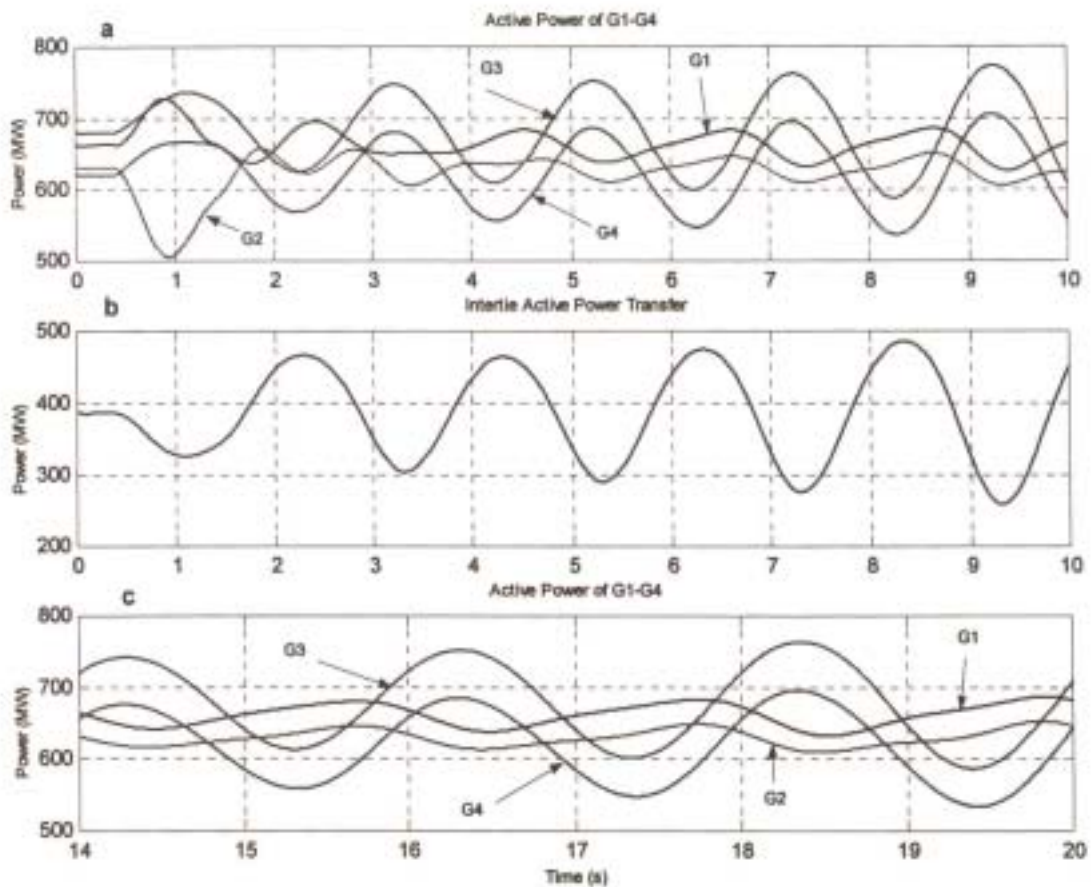


Fig. 5.3: Time-domain simulation results of the four-machine system showing various oscillatory modes of the system following a disturbance to the input power of generator G2.

Fig. 5.3 (b) shows how the inter-tie active power transfer between the two areas is affected by the negatively damped inter-area mode oscillations. Superimposed on the desired power transfer of 400 MW from Area 1 to Area 2 is a slowly increasing power oscillation of significant amplitude at approximately 0.5 Hz. This section has thus

both illustrated how the inter-area mode damping problem manifests itself in this study system as well as confirming the validity of the PSCAD/EMTDC simulation model of that system. A later section of this chapter will consider the use of the inverter-based compensator and its damping controls in order to improve the inter-area mode damping situation in this study system.

5.4.3 Simulation Results with CSC and No Damping Controls Active

The previous subsection has presented simulation results from the four-generator study system in Fig. 5.1 from which the nature of the various oscillatory modes of the system has been observed. This subsection now presents the time-domain response of the same system but with a fixed amount of compensating reactance in the main system inter-tie provided by the inverter-based series compensator. The time-domain simulation model used in this subsection (and the remainder of this chapter) is shown in Fig. D.2 in appendix D. The steady-state inter-tie active power transfer with the inverter-based series compensator included is once again approximately 400 MW. Fig. 5.4 shows the predicted time-domain response of the system when the mechanical power input to generator G2 is reduced from a value of 700 MW to 585 MW and back to 700 MW after one second.

The curves shown in Fig. 5.4 illustrate the behaviour of the active power output from each generating unit, the inter-tie active power transfer, as well as the characteristics of the two locally-measured signals that are to be used as inputs to the CSC damping controller in the next subsection. The behaviour of the system variables indicates that with a fixed amount of inverter-based series compensation, the inter-area oscillations in the system are once again negatively damped. Thus, the results in Fig. 5.4 show that, as was the case in the SMIB system in Chapter Four, the introduction of an inverter-based series compensator with no damping controls (that is, with a fixed magnitude of series compensating reactance), does not improve the inter-area mode damping situation.

Finally, the results in Fig. 5.4 show the characteristics of the locally-measured signals that are to be considered as inputs to the damping controller, namely the rate of change of power flow through the controlled series element \dot{P}_{CSC} of deMello

[deMello1] and the synthesised speed deviation $\Delta\omega_{synth}$ of Larsen [Larsen]. The synthesis of these two signals was discussed in Chapter Four. As was the case in Chapter Four, these signals have been scaled to have equal amplitudes in the small-signal region prior to their being used as inputs to the CSC damping scheme. This magnitude scaling has been carried out to ensure that the effective gain of the CSC controller remains unchanged with either signal in use; in this way, the small-signal performance with each signal would be expected to be similar for the same value of damping controller gain K_C . However, the small phase lag that is seen between these two signals means that the small-signal performance will nevertheless be expected to differ slightly when each of these signals is in use. The following subsection will examine the performance of the CSC and its damping controls with each of these signals used as the input to the damping controller.

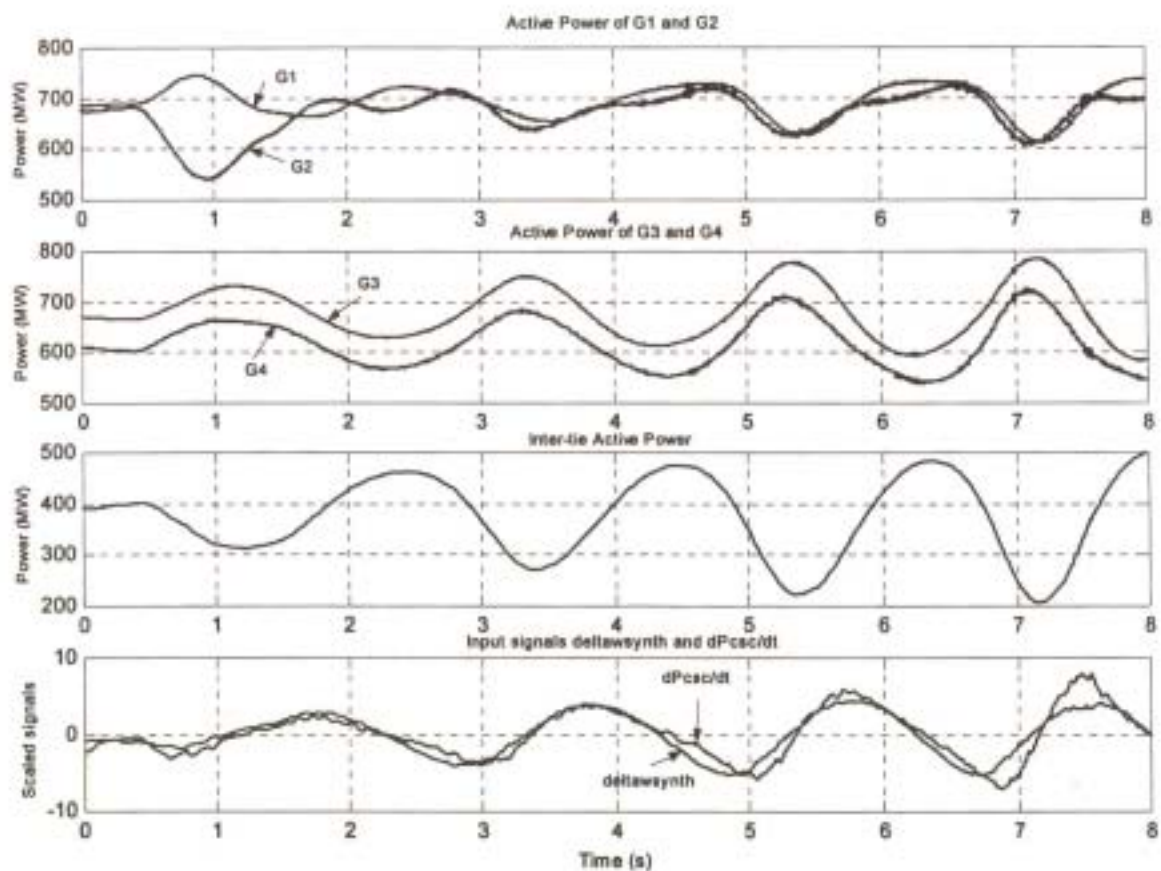


Fig 5.4: Time-domain simulation results of the four-machine system with a fixed amount of inverter-based series compensation and the damping controls inactive.

5.4.4 Simulation Results with CSC and Damping Controls Active

Rate of change of power flowing through the controllable element used as input to the damping controller

Fig 5.5 now shows the predicted time-domain response of the four-generator system of Fig. 5.1 with the inverter-based series compensator in the main inter-tie and with the damping controls now activated. In the case of the results shown in Fig. 5.5, the rate of change of power flowing through the controllable series element \dot{P}_{CSC} is used as the input to the CSC damping controller, and the controller gain is set at $K_C = 0.0025$. The time-domain response predicted in the results of Fig. 5.5 was considered for the same disturbance as in Fig. 5.4, where the mechanical power input to generator G2 was reduced from its steady-state value of 700 MW to 585 MW and back to 700 MW after one second.

The results in Fig. 5.5 show the predicted behaviour of the active power output in all the generating units, the active power transfer over the main inter-tie between buses 7 and 9, as well as the CSC damping controller output (that is, the total series compensating reactance X_{CSC}). Firstly, in contrast with the response predicted in Fig. 5.4 where the amplitude of the inter-area oscillations increases with time, the predicted response in Fig. 5.5 now shows that with the inverter-based compensator's damping controls activated, the amplitude of these oscillations decreases with time. Furthermore, while the frequency of the inter-area oscillations is once again approximately 0.5 Hz with the damping controls activated, it is seen that after only three cycles of these oscillations, they have now decayed to a small amplitude relative to that of the steady-state inter-tie power transfer.

Secondly, the damping controller output X_{CSC} in Fig. 5.5 is not driven into limit at any stage during the post-disturbance transient such that the controller output remains continuous. (In this study the upper and lower limits on the variations in X_{CSC} were set at $\pm 5.29 \Omega$ around the steady-state value of $X_{CSC0} = 29.6 \Omega$). Indeed, it was pointed out in the literature review of Chapter Two that a continuous control approach is suited to the requirements of damping inter-area type oscillations since these oscillations are a small-signal stability problem.

These results therefore demonstrate that, with the signal \dot{P}_{CSC} used as input to the CSC damping controller, the series compensating reactance provided by the inverter-based compensator is modulated in such a way that sufficient damping torques are introduced into the synchronous generators of the system to successfully overcome the inter-area mode oscillation problem that manifests itself in the original study system.

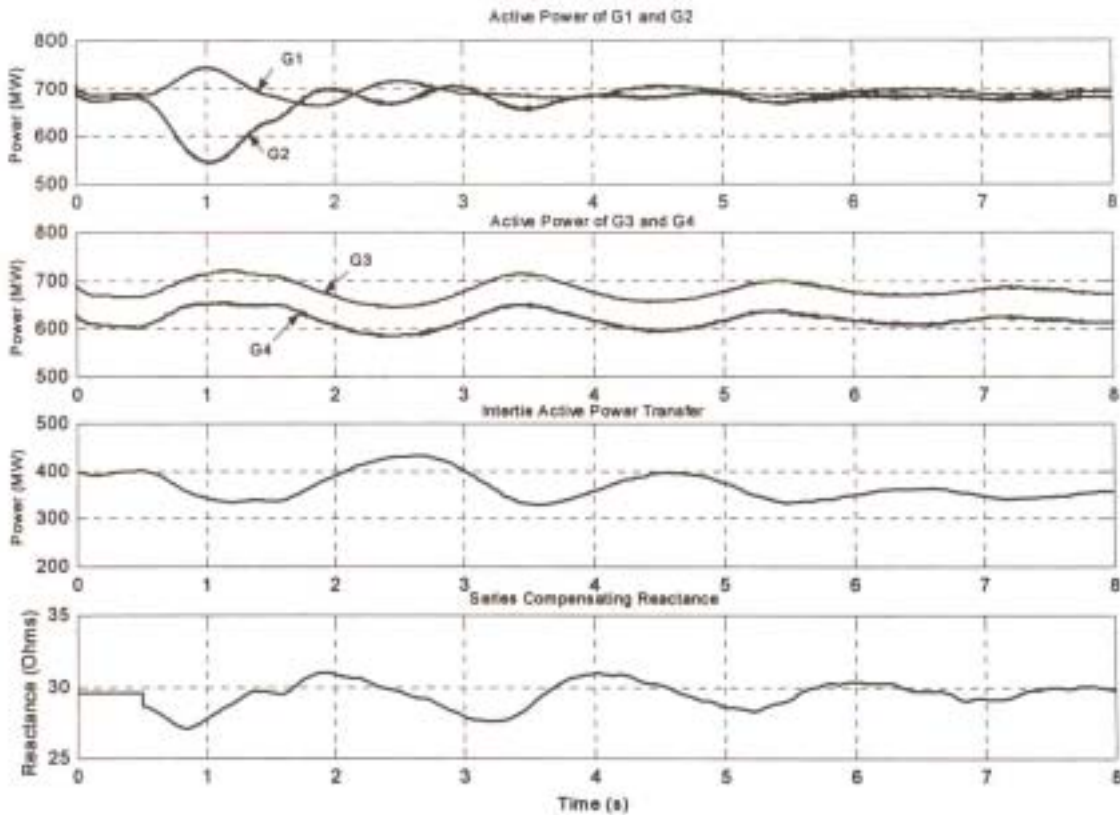


Fig. 5.5: Time-domain simulation results showing the damping effect of the inverter-based series compensator using dP_{CSC}/dt as input to the damping controller for inter-area mode oscillations.

Synthesised speed deviation used as input to the damping controller

Fig 5.6 now shows the predicted time-domain response of the four-generator system of Fig. 5.1 with the inverter-based series compensator in the main inter-tie and with the damping controls once again activated. In the case of the results shown in Fig. 5.6, the synthesised speed deviation measurement $\Delta\omega_{synth}$ is used as the input to the CSC damping controller, and the controller gain is set at $K_C = 0.0025$. The time-domain

response predicted in the results of Fig. 5.6 was also considered for the same disturbance as in the previous studies, where the mechanical power input to generator G2 was reduced from its steady-state value of 700 MW to 585 MW and back to 700 MW after one second.

The results in Fig. 5.6 show the predicted behaviour of the active power output in all the generating units, the active power transfer over the main inter-tie between buses 7 and 9, as well as the CSC damping controller output (that is, the total series compensating reactance X_{CSC}). Firstly, once again in contrast with the response predicted in Fig. 5.4 (where the amplitude of the inter-area oscillations increases with time), the predicted response in Fig. 5.6 shows that with the inverter-based compensator's damping controls activated, the amplitude of these oscillations now decreases with time. Furthermore, while the frequency of the inter-area oscillations is once again approximately 0.5 Hz, it is seen that after only three cycles of these oscillations, they have decayed to a small amplitude relative to the steady-state inter-tie power transfer.

Secondly, the damping controller output X_{CSC} in Fig. 5.6 is not driven into limit at any stage during the post-disturbance transient such that the controller output remains continuous. (As in the previous study the upper and lower limits on the variations in X_{CSC} are set at $\pm 5.29 \Omega$ around the steady-state value of $X_{CSC0} = 29.6 \Omega$). These results therefore demonstrate that, with the signal $\Delta\omega_{synth}$ used as input to the CSC damping controller, the series compensating reactance provided by the inverter-based compensator is modulated in such a way that sufficient damping torques are introduced into the synchronous generators of the system to successfully overcome the inter-area mode oscillation problem that manifests itself in the original study system.

The results of Figs. 5.5 and 5.6 show that both the locally-measured signals considered (\dot{P}_{CSC} and $\Delta\omega_{synth}$) can successfully be used as inputs to an inverter-based compensator damping control scheme to mitigate the inter-area mode damping problem in the four-generator study system. In the results presented in Figs. 5.5 and 5.6, the damping controller gain is in each case set at $K_C = 0.0025$. However, the

results of the investigations into the local-mode damping problem in Chapter Four showed that the extent of the positive damping added to an oscillatory mode by the CSC's damping controls depends on the controller gain K_C (as well as on the operating point of the system). The following subsection therefore briefly examines how the performance of the CSC's damping controller is influenced by its controller gain in the multi-machine (inter-area mode) environment.

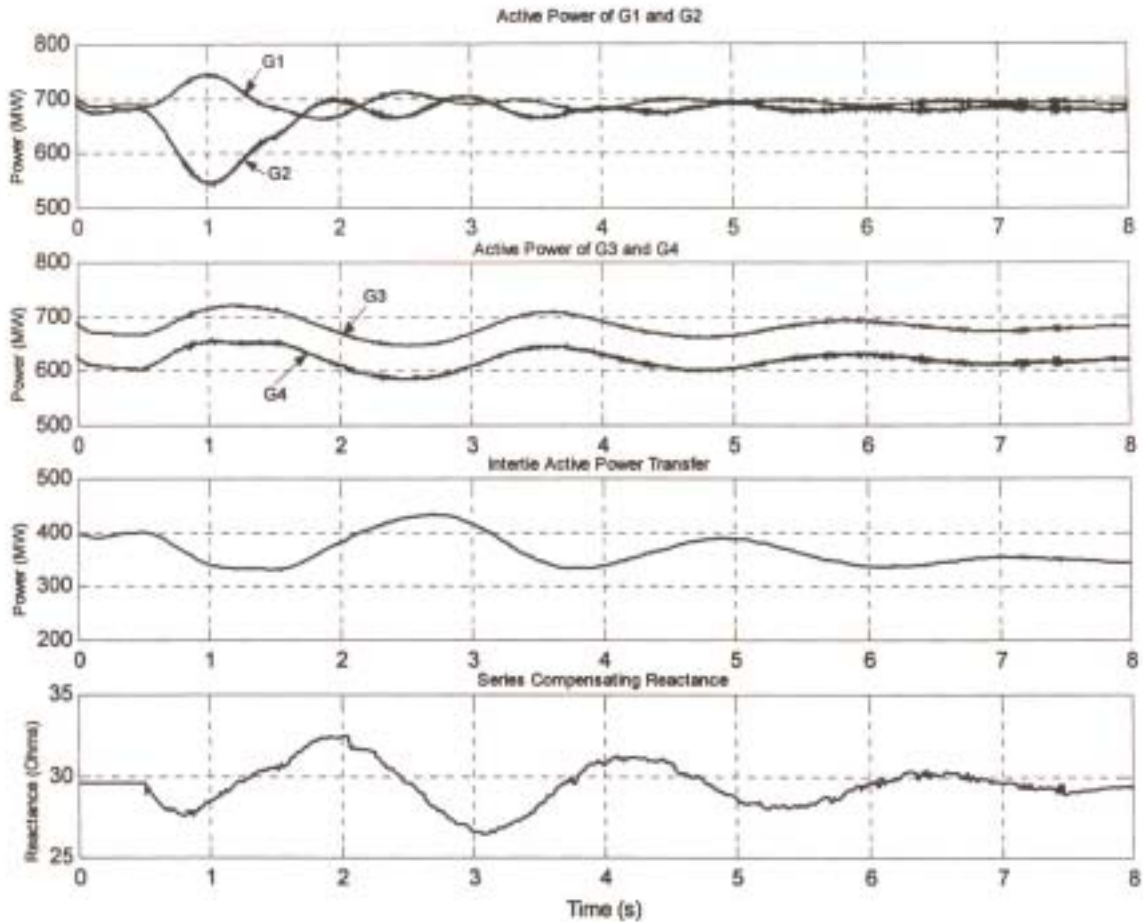


Fig. 5.6: Time-domain simulation results showing the damping effect of the inverter-based series compensator using the synthesised speed deviation as input to the damping controller for inter-area mode oscillations.

Effect of the CSC controller gain K_C on the inter-area mode damping

Various factors with significant influence on the performance of a CSC damping control scheme were examined in the SMIB system studies of Chapter Four; in particular the influence of system interconnection, generator loading, and the damping controller gain were examined. In the case of the inter-area mode damping problem in the four-machine study system, these factors could also be expected to contribute significantly to the CSC damping controller's performance. In order to illustrate this point with one example, Fig 5.7 now shows the time-domain response of the four-generator study system for three different values of the damping controller gain K_C , for the particular case of the synthesised speed deviation measurement $\Delta\omega_{synth}$ used as input to the damping controller. The same initial disturbance to the system as in previous studies is once again considered in Fig. 5.7.

The predicted time-domain response of the system in Fig. 5.7 firstly shows that, for three different values of controller gain K_C , as the damping controller gain is increased, the damping added to the inter-area mode oscillations of the system also increases. This is in accordance with the local-mode damping studies conducted in Chapter Four, where the damping added to the oscillatory mode by the CSC was shown to increase with the damping controller gain K_C ; in fact, a linear relationship in the SMIB system (in Chapter Four) was established between the damping torque added by the damping control scheme and the controller gain K_C . However, although in the time-domain simulation in Fig. 5.7 the same trend is shown to exist for the inter-area mode oscillation problem (that is, damping increases with the controller gain), it would be difficult to assess whether a fairly *linear* relationship exists in this case due to difficulties in determining the damping ratios from time-domain results (particularly in cases of well-damped responses that decay rapidly as in Fig. 5.7).

In the case of all three values of the controller gain that have been considered in the time-domain study in Fig. 5.7, the damping controller output has not been driven into limit, and hence the controller action remains continuous in each case. Thus, at least for moderate values of gain K_C at the operating point considered, the results indicate that not only is the CSC's damping controller able to damp out the inter-area mode oscillations of this system, but that the extent of the positive damping added to the

inter-area mode can be chosen by an appropriate choice of damping controller gain K_C .

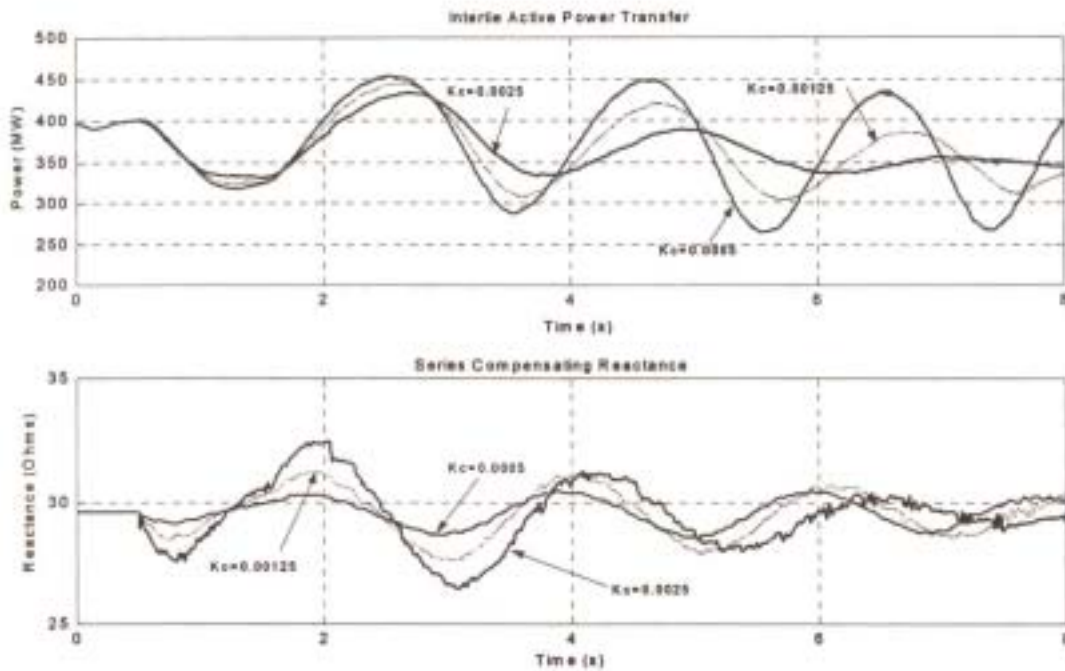


Fig. 5.7: Time-domain simulation results of the four-generator power system at various damping controller gains K_C using the synthesised speed deviation measurement as input to the damping controller in each case.

5.5 Conclusion

This chapter has examined the issue of inter-area mode damping in a well-known four-generator power system that has been considered by others [Kundur, Klein1,2]. For the time-domain simulations considered in this chapter, a detailed model of the four-generator power system was developed in PSCAD/EMTDC. Initially, linearised eigenvalue results of the study system (as presented in reference [Kundur]) were reviewed; the system was shown to have two stable inter-machine (local) modes and an unstable inter-area mode. Time-domain simulation studies, using the detailed model developed in PSCAD/EMTDC, were conducted firstly to confirm that simulation model correctly predicts the nature of the inter-area mode damping problem of the four-generator power system and secondly, to examine whether the inverter-based CSC and its damping controls is able to mitigate the inter-area mode oscillation problem.

The time-domain simulation studies presented in the chapter have confirmed the nature of various oscillatory modes in the study system, particularly the characteristics of the negatively-damped inter-area mode that manifests itself in the system. The results of the simulation studies have also shown that the introduction of an inverter-based series compensator in the main inter-tie between the two areas participating in this inter-area mode, together with appropriate damping controls to dynamically vary the reactance of this compensator, is able to mitigate the inter-area mode oscillation problem. Two candidate input signals to the inverter-based compensator's damping controls have been considered, each signal being synthesised from measurements made locally to the compensator itself, and the CSC controller with each of these signals has been shown to result in successful addition of positive damping to the inter-area mode.

In the simulation studies presented in the chapter, the performance of the damping control scheme has been considered for different values of damping controller gain, but the influence of other factors on damping performance (in particular operating point changes and system interconnection changes) have not been examined. As such, the study presented here constitutes a preliminary investigation into the use of an inverter-based CSC to damp inter-area modes. Nevertheless, the results of this preliminary study have clearly demonstrated that an inverter-based series compensator can, in principle, be used to damp the inter-area modes of a power system. Furthermore, the investigation has shown how, once a detailed insight into the nature of the power oscillation damping problem has been gained from a single-machine case, the selection and evaluation of appropriate input signals to a damping controller for the inter-area mode problem is made conceptually straightforward.

While the results of this chapter have shown how an inverter-based compensator can be used to mitigate the inter-area mode damping problem in power systems, it was recognised in the literature review of Chapter Two that other, more traditional approaches to solving this problem already exist, in particular the use of the power system stabiliser (PSS). While it is not the aim of this thesis to judge the relative merits of the two approaches, some discussion of this issue is appropriate.

As indicated before, reference [Klein2] has examined the damping of the electromechanical system oscillations of the same four-generator power system using power system stabilisers. The findings of that study showed that a PSS provides additional damping to the system by modulating the system loads, and therefore that the stabiliser's performance depends on the characteristics of the loads; in addition the PSS location was shown to influence its performance with respect to the inter-area mode damping phenomenon. By contrast, as identified in the literature review of Chapter Two, the exact location of a CSC in a transmission line connecting two groups of generators that are involved in an inter-area oscillation has no significant bearing on its performance as a damping controller, provided that the CSC is located somewhere in between the two areas. Similarly, the literature suggests that the performance of the CSC's damping controls are not likely to be significantly affected by load characteristics. Neither of these issues has been examined in the preliminary study considered here, but they are issues that must be considered in detail if a meaningful comparison of the damping performance of power system stabilisers and controllable series compensators is to be made. However, at the very least, the results of the preliminary study presented here demonstrate the relative ease (in terms of damping controller design, placement and choice of input signal) with which the inter-area mode damping problem can be overcome using a CSC in comparison with the design challenge presented by the siting and tuning of a single, or multiple power system stabilisers for inter-area mode damping.

In the design of power system stabilisers, particularly in multi-generator environments, residue techniques and participation factors are commonly used in order to decide where the stabilising device could be placed to effectively control the oscillations of the mode of interest. However, at times, residues have led to erroneous results when used to determine PSS location as discussed in [Klein2]. Reference [Klein2] works out the eigenvalues of the four-generator study system considered in this chapter for various stabiliser gains with a stabiliser located at each one of the four generating units in turn, so as to understand the influence of a PSS on the modes of interest; subsequently, [Klein2] examines the case where stabilisers have been placed on all four of the generating units. This analysis procedure illustrates that, even in such a small study system, the correct placement and tuning of power system stabilisers in order to achieve better damping is often difficult to achieve.

On the other hand, a strong argument in favour of the power system stabiliser is that it requires little capital expenditure (a supplementary signal to an existing excitation control system) whereas a controllable series compensator (either inverter-based or TCSC-based) requires a more significant capital outlay. An appraisal of the cost-benefit of installing a controllable series compensator for damping control will by its very nature be different for each application, and lies outside the scope of this thesis. However, any such assessment will still require a comparison of the *performance* of a CSC-based damping controller relative to that of PSS-based damping controls, and in this area there is certainly scope for further work as will be discussed in the concluding chapter of the thesis which now follows.

CHAPTER SIX

CONCLUSION

6.1 Introduction

This thesis has examined the specific issue of *damping* the electromechanical oscillations in power systems using a particular form of FACTS controllable series compensation, namely inverter-based series compensation. The investigations have shown that such a FACTS device is capable of being used as another tool to damp power system oscillations in general and, in particular, the inter-area mode oscillation phenomenon. This chapter summarises and reviews the principal findings and conclusions of the thesis before suggesting further research work that could be undertaken in this area.

6.2 Salient Points of the Literature Review

Chapter Two presented a thorough review of the technical literature on the subject of controlling power system oscillations by variable series compensating reactance. This review highlighted that while the idea of enhancing system damping using variable series compensating reactance has been around for some time, this technique did not find serious application for many years owing to the impracticality of repeated high-speed switching of series capacitors using mechanical circuit breakers. However, with the emergence of modern FACTS series compensators, dynamic control of series compensation to damp power system oscillations has become practically feasible.

The literature review in Chapter Two also considered a number of control signals that could potentially be used as inputs to a power oscillation damping scheme. The review indicated that particularly where a CSC is to be used to damp inter-area mode oscillations, the CSC itself is likely to be physically far from the generators in the system. In this case, input signals to the damping controller such as generator speed deviations or generator accelerating powers would not, in practice, be easily obtainable. The review therefore concluded that, particularly for the inter-area mode

damping phenomenon, it would be desirable to use an input signal to the CSC damping scheme that is synthesised from local measurements; a selection of promising input signals that meet this criterion was outlined in Chapter Two.

The review in Chapter Two discussed the two different control strategies that have been considered for damping electromechanical system oscillations, bang-bang control and continuous control of the series compensating reactance. It was shown that while continuous control is more suited to the inter-area mode-damping problem, the bang-bang method is most suited for use in the short time period following a severe system disturbance. Finally, the review in Chapter Two identified an insightful approach for simplified modelling and analysis of a CSC-based power oscillation damping scheme due to Swift and Wang.

6.3 Mathematical Models Developed for Analysis of a SMIB System

Chapter Three described the development of the mathematical models of a single-machine infinite bus power system required for the design and analysis of a CSC damping controller using the approach of Swift and Wang. Three different models of a SMIB system were presented, namely a simplified non-linear model of the system with an idealised representation of the CSC, a linearised Phillips-Heffron model of the system again with an idealised representation of the CSC, and a more-detailed non-linear model of the system including a detailed representation of the inverter-based CSC. The validity of the simplified analysis models was assessed both by comparison with a detailed model of the system and by examining the characteristics of the SMIB system model against the known characteristics of such a system for various operating conditions and parameter changes.

The investigations subsequently carried out in the thesis made use of the models developed in Chapter Three and led to the findings and conclusions outlined in the following section.

6.4 Findings and Conclusions of the Thesis

6.4.1 Local Mode Damping Studies Using CSC

As mentioned before, the literature review identified an insightful approach to the analysis of a controllable series compensator (CSC) damping controller due to Swift and Wang [Swift1,2] for a simple case of a single-generator infinite bus power system using Phillips-Heffron linear design equations; this approach was considered in detail in the analyses of Chapter Four of the thesis. Chapter Four presented the results of an investigation where a controllable series compensator was used to damp the electromechanical system oscillations of a single-machine infinite bus system, the aim of the investigation being to properly understand the damping controller design issues and the factors that affect the CSC damping controller performance in a relatively simple system (local mode damping), before tackling the more complex issue of inter-area mode damping in Chapter Five. In order to isolate the various factors that contribute to system damping, a base-case of a poorly damped system was chosen with no damping controls in place so that any damping observed when the CSC is introduced is due only to the effect of the CSC and its damping controls.

The linearised Phillips-Heffron model of Swift and Wang has been used to examine the influence of the CSC damping controller on the stabilising torques of the single-machine infinite bus system. Initially, the linearised analysis considered the case of a generalised signal as the input to the CSC's damping controller (as in the analyses of Swift and Wang); however, Chapter Four established that if *all* the torque contributed by the CSC controller is actually desired to add to system *damping* (as in the case in the investigations of this thesis), then the generator speed deviation is the appropriate signal to use as input to the CSC's damping controller. Subsequently, Chapter Four repeated the linear analysis of Swift and Wang for this special case where the damping controller input is the generator speed deviation. The findings of this linear analysis were similar to those reached by Swift and Wang, in particular that:

- (i) the damping torque added to the system by the CSC and its damping controls is always positive for positive values of damping controller gain K_C when the input to the controller is generator speed deviation;

- (ii) at a given damping controller gain K_C an increase in generator loading causes an increase in the damping torque contributed by the CSC's damping controls;
- (iii) with a weak system inter-connection the CSC damping controller performance is degraded; and
- (iv) at a given system operating point the damping torque provided by the CSC controller is a fairly linear function of the controller gain K_C .

As in the original work of Swift and Wang, the above findings, reached from linearised analysis, were then confirmed by means non-linear time-domain simulation studies using an idealised representation of the CSC. However, Chapter Four then extended the work of Swift and Wang by carrying out further non-linear time-domain simulation studies in which the system was modelled in detail, including a detailed representation of the inverter-based CSC's power electronics and internal controls. The results from these simulation studies showed that while the level of detail in the generator model (that is, neglecting the generator stator transients in the simplified model used to derive Phillips-Heffron linear equations) is reasonable for damping studies, the use of a simplified representation of the inverter-based series compensator does lead to a degree of conservative error in the predicted time-domain response of the system; however, the results showed that the *damping* of system oscillations, which is the particular focus of this thesis, is not significantly affected by the level of detail in the compensator model.

The conclusions drawn from the extended investigations into the use of an inverter-based CSC to damp local mode oscillations are twofold: firstly, an inverter-based series compensator is a suitable device to use for this application, particularly for small-signal damping of power system oscillations; secondly, the use of a generic, idealised CSC model, as has been proposed by Swift and Wang, to represent the inverter-based series compensator itself for design and analysis of the damping controller is in fact reasonable for studies where damping is the particular focus – however, if accurate prediction of the *amplitude* of the oscillations is of concern, then a more detailed representation of the inverter-based compensator is required.

Chapter Four used the linearised Phillips-Heffron model of Swift and Wang to provide analytical justification for the type of input signal that is required for the specific CSC control objective considered in this thesis, namely enhancement of small-signal damping of the electromechanical oscillations in the system. It was shown that in such a case, where the modulation of the CSC reactance is intended to add a component of positive *damping* torque to the system, the input to the CSC controller should be a signal in phase with generator speed deviation. However, the ultimate objective of this thesis has been to apply the CSC to the *inter-area mode* damping problem, in which the intent is to damp oscillations between two *groups* of generators. In such cases, where the CSC is likely to be situated between the two groups of generators (and is therefore likely to be physically far from the generators) the speed deviations of the generators are not readily available.

Thus, for the inter-area mode damping problem, it was necessary to consider alternative input signals to generator speed deviation that could in practice be synthesised from locally-measured variables at the CSC installation in the transmission system. To this end, Chapter Four then examined three locally-synthesised candidate input signals for the CSC's damping controller (as identified in the literature review of Chapter Two) and compared each of these signal's characteristics to those of the actual generator speed deviation. The results showed that two of the locally-synthesised candidate signals considered in the analyses were directly suitable for inter-area mode damping; each of these two signals was tested as an input to the damping control scheme in the SMIB system, and each signal's performance was compared against that of the damping controls with the actual generator speed deviation as input. The results of these comparisons confirmed that each of these signals could be considered as a CSC damping controller input for the inter-area mode damping studies that were to be considered in the final part of the thesis.

6.4.2 Inter-Area Mode Damping Problem Using Inverter-Based CSC

Finally, Chapter Five of the thesis considered a well-known four-generator study system (considered previously in references [Kundur, Klein1,2]) in which to investigate the application of the CSC to the inter-area mode-damping problem. A detailed simulation model of the four-generator, two-area power system was

developed in PSCAD/EMTDC; however, owing to the unavailability of any linearisation and linear analysis tools in PSCAD/EMTDC, the eigenvalues and mode shapes of this study system were reviewed from a previous study in [Kundur]. Comparison of the small-signal characteristics of the study system as predicted by the eigenvalues and mode shapes in [Kundur] with the time-domain simulation results obtained from the PSCAD/EMTDC model of the system developed in this thesis was used to establish the validity of this latter model. Hence the time-domain simulation model was used to confirm the characteristics of the poorly damped inter-area mode oscillations in the study system before being used to examine the mitigation of the inter-area mode problem by means of an inverter-based CSC and its damping controls.

Chapter Five then considered the introduction the inverter-based series compensator into the four-generator study system in the main inter-tie between the two areas that participate in its inter-area mode. The two locally-synthesised candidate input signals that were identified in the local mode damping studies of Chapter Four, namely the rate of change of power flowing through the controllable series element and the synthesised speed deviation measurement, were then each considered as inputs to the inverter-based compensator's damping controller. The analysis of the four-generator study system then confirmed that the CSC damping controller, with either of these signals in use, does in fact modulate the series compensating reactance in a manner that yields additional damping torques in the system, and as such is able to successfully mitigate the inter-area mode oscillation problem of this system. Furthermore, Chapter Five examined the performance of the CSC damping control scheme for various damping controller gains, and the trend was shown to be similar to that found in the local mode damping study of Chapter Four, in that the positive damping added to the inter-area mode also increases with increasing damping controller gain. Thus the conclusion drawn from the study conducted in Chapter Five is that an inverter-based CSC can successfully be used to mitigate inter-area mode damping problems in power systems.

6.5 Suggestions for Further Work

It has not been possible to cover every aspect of the research problem considered in this thesis. As it stands, while some important issues have been addressed on the particular subject of damping electromechanical system oscillations using an inverter-based form of series compensation, the thesis has uncovered further areas of concern. Therefore the scope that exists in this area for further research work is outlined below.

- (i) The results presented in this thesis have shown that although an idealised model of an inverter-based controllable series compensator is suitable for damping studies, it does nevertheless lead to a degree of conservative error in the *amplitude* of the power and generator rotor oscillations predicted in simulations of interconnected power systems. A more detailed examination of this finding, and an assessment of the level of detail required in an inverter-based compensator for studies other than damping investigations, should be considered.
- (ii) This thesis has focused exclusively on input signals to a controllable series compensator that are suitable for damping power system oscillations and has identified two suitable substitutes for the generator speed deviation. However, one of the input signals evaluated was found to synthesise the generator load angle deviation rather than the generator speed deviation. A CSC controller using this type of input signal might be expected to provide additional synchronising torque to the power system and thus improve its transient stability characteristics. The influence of a CSC that uses such an input signal (or that uses an input signal partially in phase with both generator speed deviation and generator load angle) could be examined.
- (iii) The investigation could be extended to examine the factors that influence the performance of the CSC's damping controls in the four-generator system in the same way as has been done for the SMIB studies of this thesis, in particular by developing a suitable linearised model of this multi-machine system. The influence on the damping controller performance of system load

characteristics and the location of the CSC within the system also needs examination.

- (iv) The issue of whether FACTS controllable series compensators are a more effective means than power system stabilisers for mitigating the inter-area mode damping problem requires a thorough theoretical treatment; the evaluation of the two devices' relative performance with respect to the inter-area mode damping problem is essential.
- (v) Finally, practical confirmation of the findings of this thesis could be considered by implementing a laboratory-scale test system of a small power system, including an inverter-based series compensator equipped with damping controls.

APPENDIX A

PER-UNIT SYSTEM

A.1 Introduction

In power systems it is convenient to normalise system variables by using per-unit systems. The per-unit system offers computational facility since it eliminates units and expresses system quantities as dimensionless ratios. While various per-unit systems exist for analysis of electrical power systems, each with its own inherent advantages and disadvantages, one of the significant distinctions between per-unit systems is the choice of the time base. The time base is normally chosen as either one second or the reciprocal of the nominal speed. The per-unit system used in this thesis has a time base of one second; the advantage of this approach is that the per-unit values of power and torque are then numerically equal at nominal speed.

In order for the machine equations to be independent of the number of pole pairs in a per-unit system, a multi-pole machine is converted to an equivalent two-pole machine of the same power. This effectively requires a separate set of base values for the electrical parameters and mechanical parameters of the machine.

A.2 Derivation of the Per-Unit System

Four base values are chosen independently for this per-unit system, namely the base armature power P_a^b , the base armature voltage V_a^b , the base time t^b , and the base electrical angle θ_e^b . The remaining quantities' base values are calculated from these four. The base field power is fixed by the particular Park's transform used while the base field current is chosen in order for X_{ad} and X_{fd} to be equal in per-unit.

Electrical base values

Base armature power P_a^b = total three phase rating in Watts (W)

Base armature voltage	$V_a^b = \text{rated rms voltage per phase in ac Volts (V)}$
Base armature current	$I_a^b = P_a^b / (3 V_a^b)$ in rms ac Amps (A)
Base armature impedance	$Z_a^b = V_a^b / I_a^b$ in Ohms (Ω)
Base field power	$P_f^b = 1.5 (P_a^b / 3)$ in Watts
Base field current	$I_f^b = I_a^b X_{md} / X_{fd}$ in dc Amps
Base field voltage	$V_f^b = P_f^b / I_f^b$ in dc Volts
Base field impedance	$V_f^b = V_f^b / I_f^b$ in Ohms
Base time	$t^b = 1 \text{ second}$
Base electrical angle	$\theta_e^b = 1 \text{ electrical radian (rad}^\circ\text{)}$
Base electrical speed	$\omega_e^b = \theta_e^b / t^b \text{ (rad}^\circ\text{/s)}$
Base electrical acceleration	$\alpha_e^b = \omega_e^b / t^b \text{ (rad}^\circ\text{/s}^2\text{)}$

Base electrical torque is defined as that torque which produces base power at nominal electrical speed ω_{en} .

$$\text{Base electrical torque} \quad T_e^b = P_a^b / \omega_{en} = P_a^b / \omega_o$$

where ω_o is the system electrical speed expressed in electrical rad/s.

The per-unit value of torque in the two-axis theory is calculated from the per-unit values of d and q axis currents and flux linkages as follows:

In physical units

$$T_e = \psi_d i_q - \psi_q i_d$$

Normalising this equation (and using the subscript 'u' to denote the per-unit value of a parameter) yields

$$\begin{aligned} T^u &= T_e / T_e^b = (\psi_d i_q - \psi_q i_d) / T_e^b \\ &= \omega_o (\psi_d i_q - \psi_q i_d) / (P_a^b) \end{aligned}$$

Since $P_a^b = 3 V_a^b I_a^b = 1.5 I_a^b$ and $V_d^b = V_a^b$

$$\begin{aligned} T^u &= \omega_o (\psi_d i_q - \psi_q i_d) / (2 V_d^b I_d^b) \\ &= \omega_o (\psi_d^u i_q^u - \psi_q^u i_d^u) / 2 \end{aligned}$$

In order for the mechanical angles, speeds, acceleration and torques to be equal to the corresponding electrical quantities when expressed as per-unit values (for an equivalent two-pole machine) the following base values are chosen with 'n' as the number of pole pairs and ω_{mn} as the mechanical nominal speed:

Mechanical base values

Base mechanical angle	$\theta_m^b = \theta_e^b / n$ in mechanical radians (rad^m)
Base mechanical speed	$\omega_m^b = \omega_e^b$ (rad^m / s)
Base mechanical acceleration	$\alpha_m^b = \alpha_e^b / n$ ($\text{rad}^m / \text{s}^2$)
Base mechanical torque	$T_m^b = P_a^b / \omega_{mn} = n P_a^b / \omega_o$

Thus $T_m^b = n T_e^b$

In physical units the mechanical and electrical parameters are related as follows:

$$\theta_e = n \theta_m, \omega_e = n \omega_m, \alpha_e = n \alpha_m$$

and since the mechanical power P_m and the electrical power P_e must be equal at steady state:

$$T_e \omega_e = T_m \omega_m$$

and thus

$$n T_e = T_m$$

The mechanical parameters of inertia J_m and shaft stiffness K_m in physical units are normalised into per-unit values by considering the second order differential equation of motion in physical units as follows:

$$T_m = J_m \alpha_m + K_m \theta_m$$

or

$$n T_e = J_m \alpha_e / n + K_m \theta_e / n$$

and normalising it yields (in per-unit)

$$\begin{aligned} T^U &= \frac{T_e}{T_e^b} = \frac{J_m \alpha_e}{n^2 T_e^b} + \frac{K_m \theta_e}{n^2 T_e^b} = \frac{J_m}{n^2 T_e^b / \alpha_e^b} \frac{\alpha_e}{\alpha_e^b} + \frac{K_m}{n^2 T_e^b / \theta_e^b} \frac{\theta_e}{\theta_e^b} \\ &= J^U \alpha^U + K^U \theta^U \end{aligned}$$

where

Base inertia $J_b = n^2 T_e^b / \alpha_e^b = T_m^b + \alpha_m^b$

Base stiffness $K_b = n^2 T_e^b / \theta_e^b = T_m^b + \theta_m^b$

Physical inertias can also be expressed in terms of the inertia constant H in seconds where

$$H = \frac{\text{Stored kinetic energy at synchronous speed [W-sec]}}{\text{Turbo-generator rated power [VA]}}$$

$$= J_m \omega_{mn}^2 / (2P_a^b)$$

Now $J_b = n^2 T_e^b / \alpha_e^b = n^2 P_a^b / (\alpha_e^b \omega_o)$

Thus

$$H = \frac{J_m (\omega_o / n^2)^2 n^2 \alpha_e^b}{2P_a^b n^2 \alpha_e^b} = J_m \frac{\alpha_e^b \omega_o}{n^2 P_a^b} \frac{\omega_o}{2\alpha_e^b} = \frac{J^U \omega_o}{2\alpha_e^b}$$

Thus $J^U = 2 H \alpha_e^b / \omega_o$

$$= 2 H / \omega_o$$

where H and ω_o are in per-unit (or in seconds and electrical rad/s respectively since the base time and base electrical speed are both numerically equal to one). The equation of motion in per-unit is then given by

$$T^U = (2 H / \omega_o) \alpha^U + K^U \theta^U$$

APPENDIX B

LINEARISATION OF THE PHILLIPS-HEFFRON MODEL

B.1 Introduction

Chapter Three of this thesis has shown the linearised Phillips-Heffron model equations together with a block diagram (Fig. 3.5) representation of these linear equations. This Appendix shows the linearisation procedure of the simplified non-linear model described in Chapter Three in order to arrive at a model which is suitable for small-signal stability studies.

B.2 Linearisation of the Simplified Non-Linear Model

The non-linear equations of a SMIB system in Chapter Three describe the synchronous generator with no damper windings, stator transient ($p\psi$) terms neglected, and connected to an infinite busbar with voltage E_b . Consider now a SMIB system with an external impedance jX_e ; with this external impedance, the stator voltage equations in eqns. (3.1) and (3.2) in Chapter Three become

$$v_d = -\psi_q p\theta \quad (\text{B.1})$$

$$v_q = \psi_d p\theta \quad (\text{B.2})$$

The transmission line equations are

$$v_d = pX_e i_d - X_e i_q p\theta + e_b \sin \delta \quad (\text{B.3})$$

$$v_q = pX_e i_q + X_e i_d p\theta + e_b \cos \delta \quad (\text{B.4})$$

where $\omega = p\theta$. Furthermore, the simplified non-linear equations of Chapter Three are re-written as follows.

$$\omega_o \psi_d = -X_d i_d + E_{fd} \quad (\text{B.5})$$

$$\omega_o \psi_q = -X_q i_q \quad (\text{B.6})$$

$$E_q' = E_{fd} - (X_d - X_d') i_d \quad (\text{B.7})$$

$$E_{fd} = E_{fd} + T_{do}' p E_q' \quad (\text{B.8})$$

$$2Hp^2\theta = T_m - \psi_d i_q + \psi_q i_d - Bp\Delta\theta \quad (\text{B.9})$$

$$E_t^2 = v_d^2 + v_q^2 \quad (\text{B.10})$$

where eqn. (B.10) is the terminal voltage equation. Now considering small variations of these variables around a particular operating point, and noting that

$$p\theta = 1 + p(\Delta\theta) = 1 + p(\Delta\delta)$$

equations (B.1) to (B.10) reduce to:

$$\Delta v_d = -\Delta\psi_q - [\psi_{qo} p\Delta\delta] \quad (\text{B.11})$$

$$\Delta v_q = \Delta\psi_d + [\psi_{do} p\Delta\delta] \quad (\text{B.12})$$

$$\Delta v_d = [X_e p\Delta i_d] - X_e \Delta i_q + (e_{bo} \cos \delta_o) \Delta\delta - [i_{qo} X_e p\Delta\delta] \quad (\text{B.13})$$

$$\Delta v_q = [X_e p\Delta i_q] + X_e \Delta i_d - (e_{bo} \sin \delta_o) \Delta\delta + [i_{do} X_e p\Delta\delta] \quad (\text{B.14})$$

$$\omega_o \Delta\psi_d = -X_d \Delta i_d + \Delta E_{fd} \quad (\text{B.15})$$

$$\omega_o \Delta\psi_q = -X_q \Delta i_q \quad (\text{B.16})$$

$$\Delta E_q' = \Delta E_{fd} - (X_d - X_d') \Delta i_d \quad (\text{B.17})$$

$$\Delta E_{fd} = \Delta E_{fd} + T_{do}' p \Delta E_q' \quad (\text{B.18})$$

$$(2Hp^2 + Bp)\Delta\delta = \Delta T_m - \psi_{do} \Delta i_q - i_{qo} \Delta\psi_d + \psi_{qo} \Delta i_d + i_{do} \Delta\psi_q \quad (\text{B.19})$$

$$\Delta E_t = \frac{v_{do}}{v_{to}} \Delta v_d + \frac{v_{qo}}{v_{to}} \Delta v_q \quad (\text{B.20})$$

The square bracketed terms in the above equations are now neglected. The next step is to eliminate all the variables in the above expressions except ΔE_t , $\Delta\delta$, $\Delta E_q'$, ΔT_m and ΔE_{fd} using the following additional equations:

$$E_{bo} \sin \delta_o = v_{do} + X_e i_{qo} \quad (\text{B.21})$$

$$E_{bo} \cos \delta_o = v_{qo} - X_e i_{do} \quad (\text{B.22})$$

$$E_{qo} = v_{qo} + X_q i_{do} \quad (\text{B.23})$$

$$T_{dt}' = \frac{X_d' + X_e}{X_d + X_e} T_{do}' \quad (\text{B.24})$$

Now consider first re-writing the torque equation (eqn. B.19) in terms of the variables mentioned above. Initially, Δi_q and Δi_d are determined using the relationships in eqns. (B.11) and (B.13) in conjunction with eqn (B.16) to write Δi_q as follows.

$$\Delta i_q = \frac{E_{bo} \Delta \delta \cos \delta_o}{X_e + X_q} \quad (\text{B.25})$$

Using eqns. (B.12) and (B.14) in conjunction with eqn. (B.18) to write Δi_d yields

$$\Delta i_d = \frac{\Delta E_q' + E_{bo} \Delta \delta \sin \delta_o}{X_e + X_d'} \quad (\text{B.26})$$

Substituting eqns. (B.25) and (B.26) into the torque expression in eqn. (B.19), using the relationships in eqns. (B.21-B.23) gives

$$(2Hp^2 + Bp)\Delta\delta = \Delta T_m - \frac{E_{bo} \sin \delta_o}{X_e + X_d'} \Delta E_q' - \left[\frac{E_{bo} E_{qo} \cos \delta_o}{X_e + X_q} + \frac{E_{bo} v_{do} \sin \delta_o}{X_e + X_d'} \left(1 - \frac{X_d'}{X_q} \right) \right] \Delta\delta \quad (\text{B.27})$$

Now, consider eqn. (B.17) and use eqns. (B.18), (B.26) and (B.24) to obtain:

$$\Delta E_q' = \frac{X_e + X_d'}{X_e + X_d} \frac{1}{1 + pT_{dt}'} \Delta E_{fd} - \frac{X_d - X_d'}{X_e + X_d} E_{bo} \sin \delta_o \frac{1}{1 + pT_{dt}'} \Delta\delta \quad (\text{B.28})$$

Finally, expressing ΔE_f (eqn. B.20) in terms of these variables using eqns. (B.11) to (B.14) gives

$$\Delta E_t = \frac{v_{q0}}{v_{\omega}} \frac{X_e}{X_e + X_d'} \Delta E_q' + \left[\frac{v_{q0}}{v_{\omega}} \frac{X_q}{X_e + X_q} E_{b0} \cos \delta_0 - \frac{v_{q0}}{v_{\omega}} \frac{X_d'}{X_e + X_d'} E_{b0} \sin \delta_0 \right] \quad (\text{B.29})$$

In order to draw a block diagram for the system described by eqns. (B.27) to (B.29), these equations are now shortened by defining constants K_1 to K_6 as shown below.

From the linearised torque expression in eqn. (B.27), this equation can be written as

$$(2Hp^2 + Bp)\Delta\delta = \Delta T_m - \Delta T_e \quad (\text{B.30})$$

where the linearised electrical torque expression from eqn. (B.27) is

$$\Delta T_e = \left[\frac{E_{b0} E_{q0} \cos \delta_0}{X_e + X_q} + \frac{E_{b0} e_{d0} \sin \delta_0}{X_e + X_d'} \left(1 - \frac{X_d'}{X_q} \right) \right] \Delta\delta + \frac{E_{b0} \sin \delta_0}{X_e + X_d'} \Delta E_q' \quad (\text{B.31})$$

In terms of coefficients K_1 to K_6 the linearised electric torque equation (eqn. B.31), the field voltage equation (eqn. B.28) and the generator terminal voltage equation (eqn. B.29) are:

$$\Delta T_e = K_1 \Delta\delta + K_2 \Delta E_q' \quad (\text{B.32})$$

$$\Delta E_q' = \frac{1}{1 + pT_{d0}} (K_3 \Delta E_{fd} - K_4 \Delta\delta) \quad (\text{B.33})$$

$$\Delta E_t = K_5 \Delta\delta + K_6 \Delta E_q' \quad (\text{B.34})$$

and these eqns. (B.30), (B.32) to (B.34) are thus used to construct the block diagram of a single-machine infinite bus system in Fig. B.1 for small-signal stability studies, where the coefficients K_1 to K_6 are defined as:

$$K_1 = \frac{E_0 E_{q0} \cos \delta_0}{X_e + X_d} + \frac{E_0 e_{d0} \sin \delta_0}{X_e + X_d'} \left(1 - \frac{X_d'}{X_q} \right) \quad (\text{B.35})$$

$$K_2 = \frac{E_0 \sin \delta_0}{X_e + X_d'} \quad (\text{B.36})$$

$$K_3 = \frac{X_e + X_d'}{X_e + X_d} \quad (\text{B.37})$$

$$K_4 = \frac{X_d - X_d'}{X_e + X_d} E_0 \sin \delta_0 \quad (\text{B.38})$$

$$K_5 = \frac{e_{d0}}{e_{q0}} E_0 \cos \delta_0 \frac{X_q}{X_e + X_q} - \frac{e_{q0}}{e_{d0}} \sin \delta_0 \frac{X_d'}{X_e + X_d'} \quad (\text{B.39})$$

$$K_6 = \frac{e_{q0}}{e_{d0}} \frac{X_e}{X_e + X_d'} \quad (\text{B.40})$$

Using the above expressions, the linearised Phillips-Heffron model block diagram representation is now shown in Fig. B.1.

In order to extend the block diagram in Fig. B.1 to include the influence of the exciter with transient gain reduction and AVR, consider the thyristor-type exciter and AVR shown in Fig. 3.3 of Chapter Three. For small variations around a particular operating point, the following expressions can be written (by inspection of Fig. 3.3):

$$p\Delta E_m = (\Delta E_f - \Delta E_m) \quad (\text{B.41})$$

$$p\Delta v_f = \frac{1}{T_B} [K_A(-\Delta E_m) - \Delta v_f] \quad (\text{B.42})$$

$$\Delta E_f = \frac{T_A}{T_B} K_A(-\Delta E_m) + \left(1 - \frac{T_A}{T_B} \right) \Delta v_f \quad (\text{B.43})$$

The block diagram representation of the system with the exciter and AVR equations above (eqns. (B.41) to (B.43)) is shown in Fig. B.2.

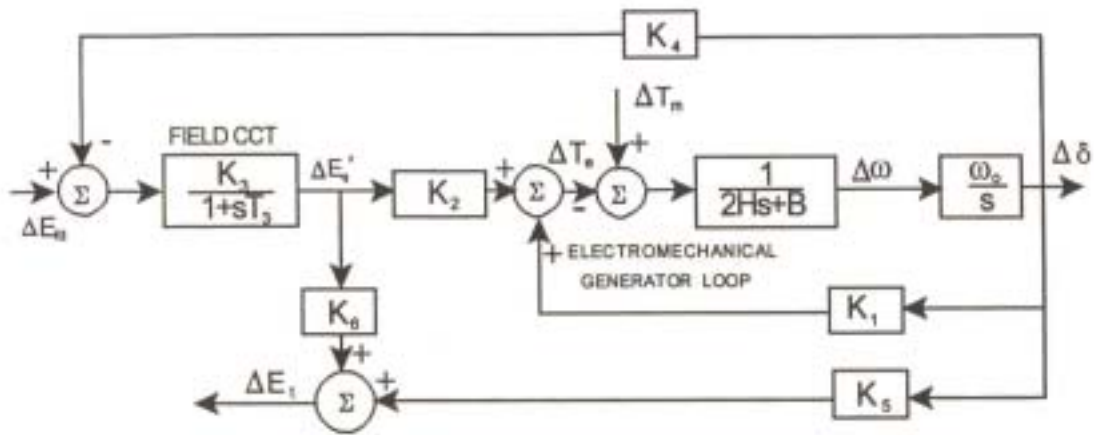


Fig. B.1 Linearised Phillips-Heffron model of a single-machine infinite bus system.

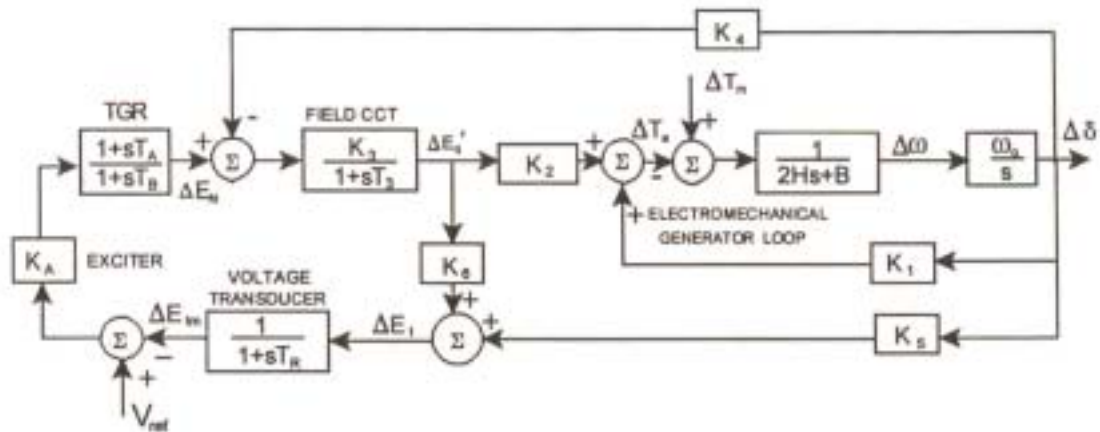


Fig. B.2: Linearised Phillips-Heffron model of a single-generator equipped with the AVR and exciter and transient gain reduction, connected to an infinite bus.

Finally, the extension of the block diagram in Fig. B.2 to include an idealised CSC and its damping controls is the work of Swift and Wang [Swift1,2] and is now shown in Fig. B.3 in the dotted box labelled (3).

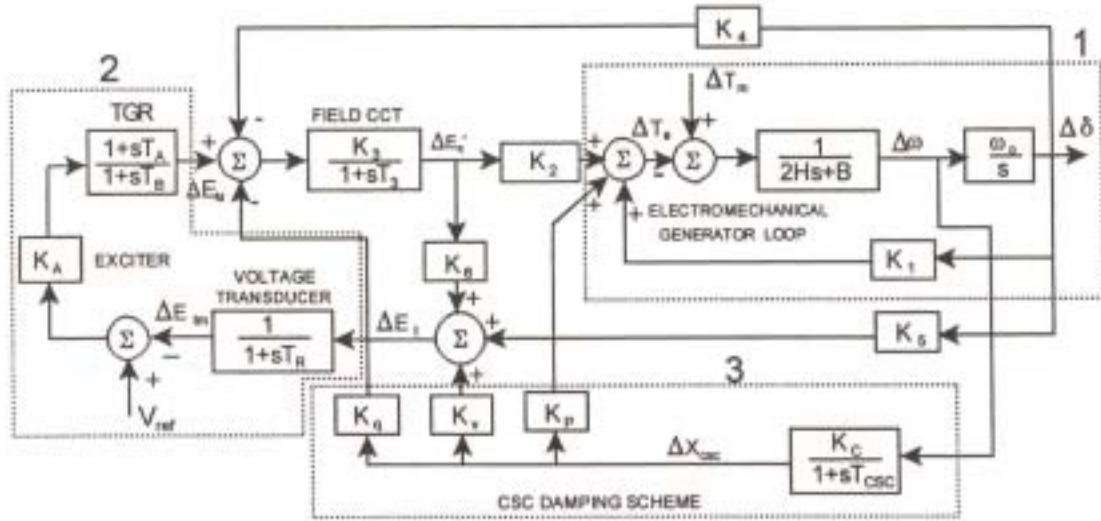


Fig. B.3: Linearised Phillips-Heffron model of a single-machine infinite bus system with the AVR and exciter with transient gain reduction and CSC damping scheme.

where,

$$\begin{aligned}
 K_p &= \frac{\partial P_e}{\partial \Delta X_{CSC}} = \frac{1}{X_{dT}} \left[\frac{E_0 E_{q0}' \sin \delta_0}{X_{dT}'} - \frac{E_0^2 (X_q - X_d') \sin(2\delta_0)}{2X_{dT}' X_{qT}} \right] - \frac{1}{X_{qT}} \frac{E_0^2 (X_q - X_d') \sin(2\delta_0)}{2X_{dT}' X_{qT}} \\
 &= \frac{1}{X_{dT}'} P_{e0} - \frac{1}{X_{qT}} P_{e02}
 \end{aligned} \tag{B.44}$$

and

$$X_{dT} = X_d + X_e - (X_{CSC0} + X_{CSCV}) \tag{B.45}$$

$$X_{dT}' = X_d' + X_e - (X_{CSC0} + X_{CSCV}) \tag{B.46}$$

$$X_{qT} = X_q + X_e - (X_{CSC0} + X_{CSCV}) \tag{B.47}$$

APPENDIX C

PARAMETERS OF THE SMIB SYSTEM

This appendix lists the parameters used in the studies of the single-machine infinite bus system in Chapters Three and Four.

C.1 Parameters of the Single-Machine Infinite Bus System in Per-Unit

C.1.1 Generator

R_a	= 0.005
X_{ad}	= 0.85
X_l	= 0.15
X_{aq}	= 0.45
X_{fd}	= 1.03
R_{fd}	= 0.00065
B	= 0.0
H	= 4.0 s

C.1.2 Thyristor Exciter with TGR and Automatic Voltage Regulator

K_A	= 100.0
T_A	= 1.0 s
T_B	= 10.0 s
T_R	= 0.01 s

C.1.3 Transmission Line System Parameters

For simplified studies

R_L	= 0.0
X_L	= 0.8
X_{CSC0}	= 0.1
$\Delta X_{CSC MAX}$	= 0.1
$\Delta X_{CSC MIN}$	= -0.1

For detailed PSCAD/EMTDC studies

R_L	= 0.01
X_L	= 0.8
X_{CSC0}	= 0.2
$\Delta X_{CSCV MAX}$	= 0.1
$\Delta X_{CSCV MIN}$	= -0.1

C.1.4 Controllable Series Compensator Damping Controller

$$T_{CSC} = 0.01 \text{ s}$$

$$K_C = 0.1$$

C.1.5 Initial Operating Conditions

$$P_{eo} = 0.2 \text{ (low loading)}$$

$$P_{eo} = 0.8 \text{ (high loading)}$$

$$Q_b = 0.03$$

$$E_b = 1.0$$

C.1.6 Base-values

Base time	1	s
Base armature power	3	kVA
Base armature voltage (phase)	127	V
Base armature current	7.87	A
Base armature impedance	16.133	Ω
Base electrical angle	1	rad ^e
Base electrical speed	1	rad ^e / s

APPENDIX D

PARAMETERS OF THE FOUR-GENERATOR SYSTEM AND ITS PSCAD/EMTDC MODELLING

This Appendix lists the parameters used in the four-machine study system in Chapter Four and further shows the PSCAD/EMTDC models of the system.

D.1 Parameters of the Four-Machine System in Per-Unit

D.1.1 Generators

$R_a = 0.0025$	
$X_\ell = 0.2$	
$X_d = 1.8$	$X_q = 1.7$
$X_d' = 0.3$	$X_q' = 0.5$
$X_d'' = 0.25$	
$T_{d0}' = 8.0 \text{ s}$	$T_{q0}' = 0.4 \text{ s}$
$T_{d0}'' = 0.03 \text{ s}$	$T_{q0}'' = 0.05 \text{ s}$
$A_{Sat} = 0.015$	$B_{Sat} = 9.6$
$\psi_T = 0.9$	$B = 0$
$H = 6.5 \text{ s}$ (for G1 and G2)	
$H = 6.175 \text{ s}$ (for G3 and G4)	

Base power = 900 MVA

Base voltage = 20 kV

D.1.2 Transmission Line System

r	= 0.0001 p.u. / km
x_L	= 0.001 p.u. / km
b_C	= 0.00175 p.u. / km
Base power	= 100 MVA
Base voltage	= 230 kV

Transformers

R_T	= 0.0
X_T	= 0.15
Base power	= 900 MVA
Base voltage	= 20 / 230 kV

D.1.3 Initial Conditions

G1:	$P = 700 \text{ MW},$	$Q = 185 \text{ MVar},$	$E_t = 1.03 \angle 20.2^\circ$
G2:	$P = 700 \text{ MW},$	$Q = 235 \text{ MVar},$	$E_t = 1.01 \angle 10.5^\circ$
G3:	$P = 719 \text{ MW},$	$Q = 176 \text{ MVar},$	$E_t = 1.03 \angle -6.8^\circ$
G4:	$P = 700 \text{ MW},$	$Q = 202 \text{ MVar},$	$E_t = 1.01 \angle -17.0^\circ$

D.1.4 Loads

Bus 7:	$P_L = 967 \text{ MW},$	$Q_L = 100 \text{ MVar},$	$Q_C = 200 \text{ MVar}$
Bus 9:	$P_L = 1767 \text{ MW},$	$Q_L = 100 \text{ MVar},$	$Q_C = 350 \text{ MVar}$

D.1.5 Thyristor Exciter with TGR and Automatic Voltage Regulator

K_A	$= 200.0$
T_A	$= 1.0 \text{ s}$
T_B	$= 10.0 \text{ s}$
T_R	$= 0.01 \text{ s}$

D.2 PSCAD/EMTDC Representation With and Without Inverter-Based Series Compensator

Fig D.1 shows the graphical representation of the four-generator power system that excludes the inverter-based series compensator in PSCAD/EMTDC as outlined in Chapter Five. Fig. D.2 shows the graphical representation of the same four-generator power system that includes the inverter-based series compensator in PSCAD/EMTDC. The parameters and gains of the inverter-based series compensator used in Fig. D.2 were determined by converting those of the SMIB system (Fig. 3.17) into per-unit using the per-unit system described in Appendix A as follows.

$C = 0.0075 \text{ pu.}$	(across V_{dcap} label in Fig. 3.17)
$H_V = 0.1 \text{ pu.}$	(gain block of 0.1 in Fig. 3.17 in the control scheme)
$H_P = 0.3 \text{ pu.}$	(gain block of 0.3 in Fig. 3.17 in the control scheme)
$V_{dco} = 1.18 \text{ pu.}$	(gain input of 150 in desired voltages in Fig 3.17)
$K_{AI} = 3.4 * \omega_0 \text{ pu.}$	(gain block of 1068.14 in Fig 3.17 in the control scheme)
$K_{VP} = 12.7 \text{ pu.}$	(gain block of 100 in Fig. 3.17 in the control scheme)

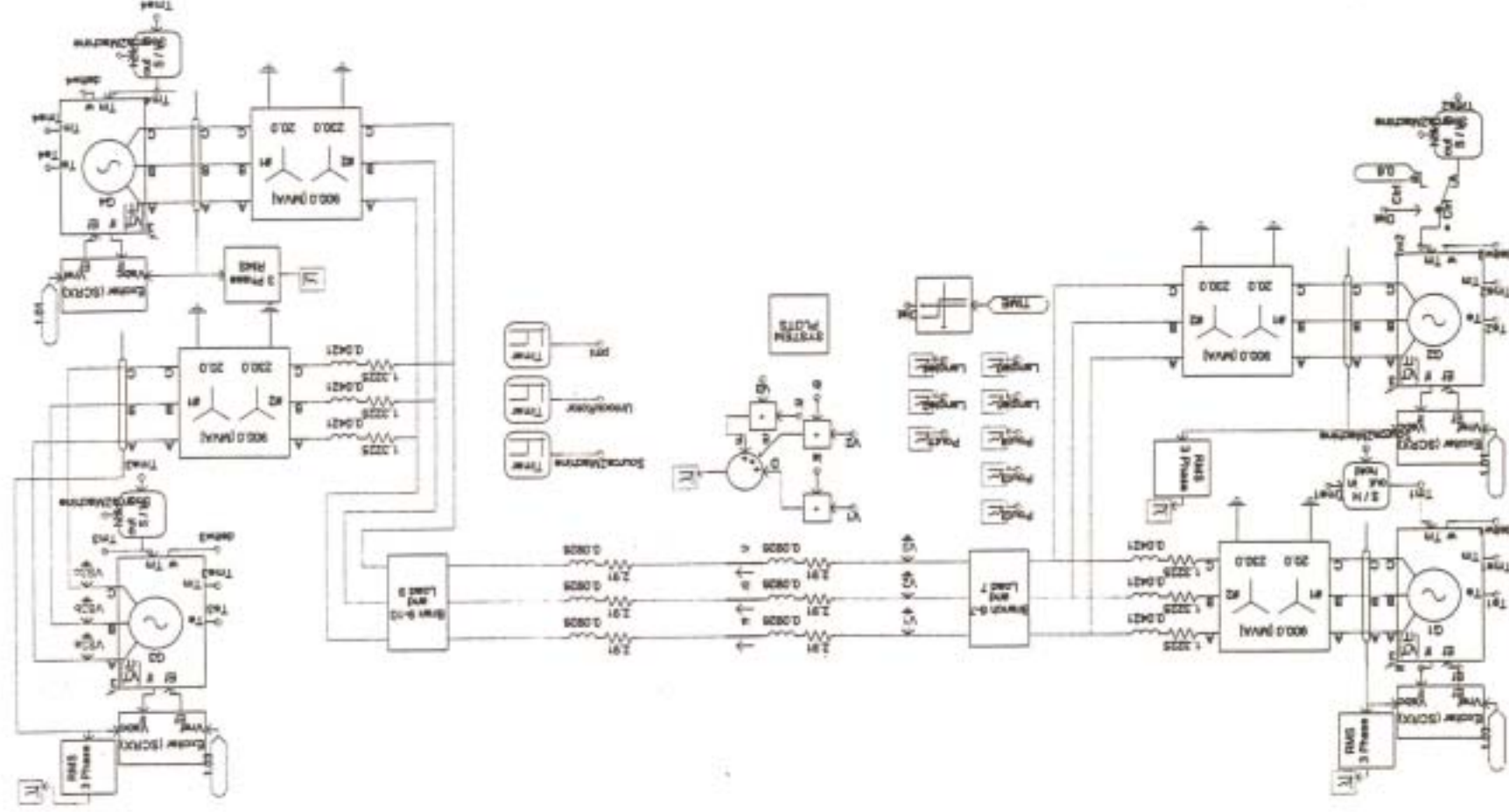


Fig. D.1: A detailed PSCAD/EMTDC representation of the four-machine system.

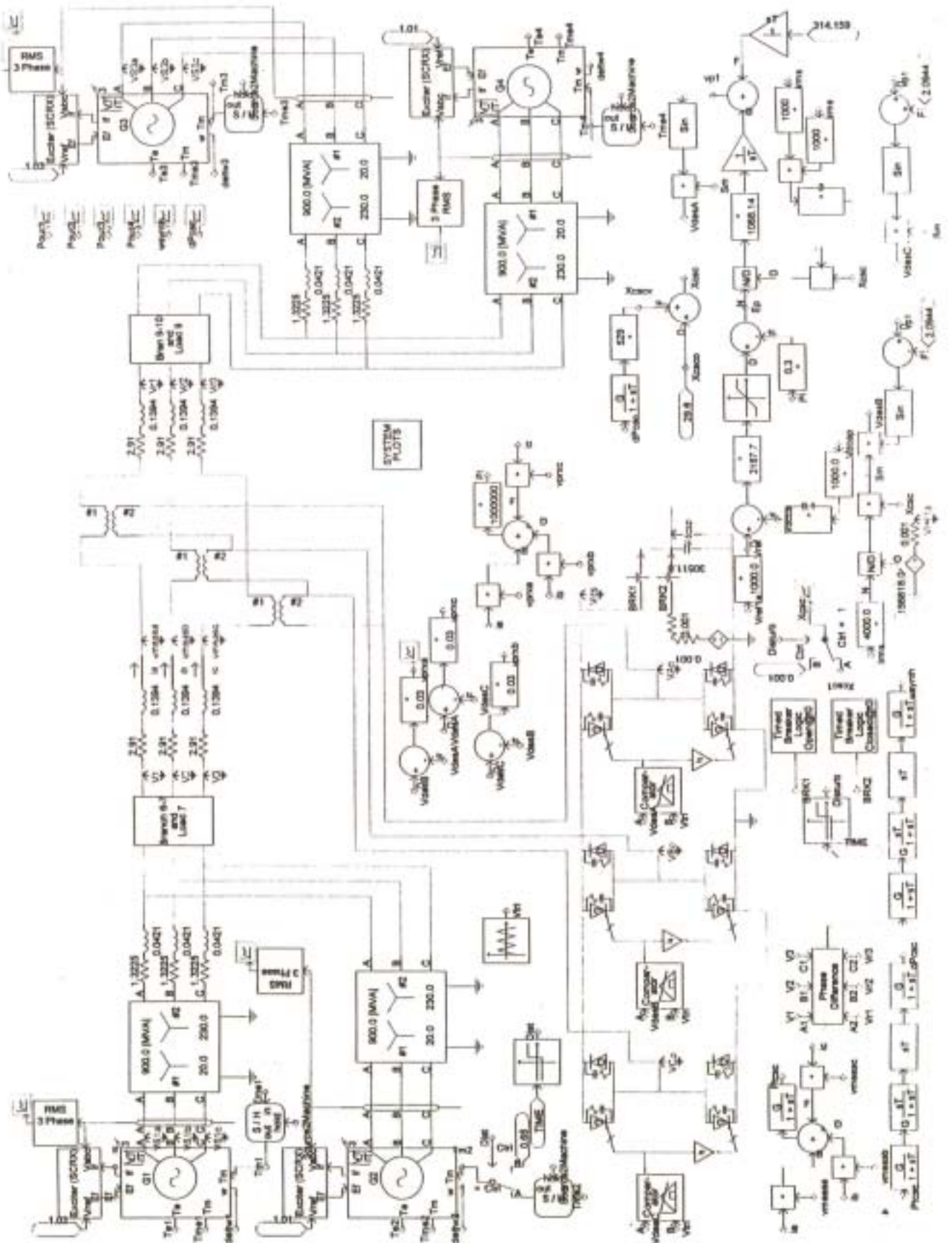


Fig. D.2: A detailed PSCAD/EMTDC representation of the four-machine system, including the inverter-based series compensator.

APPENDIX E

SIMPLIFIED SMIB SYSTEM MATLAB CODE

E.1 General

In Chapter Three the non-linear time-domain simulation model (in eqns. 3.27 to 3.33) and the linearised model of the single-machine infinite bus system were derived. Non-linear simulation studies and linearised eigenvalue analyses were presented in Chapter Four using the simplified models which have been programmed in the MATLAB software package. The linearised model of the simplified SMIB system has been obtained by numerical linearisation of the non-linear model, using the linearisation functions provided in the MATLAB programming environment [MathWorks]. The abbreviated MATLAB M-files which follow show the programmed non-linear model equations, and the accompanying numerical linearisation procedure; sections of the code, where necessary, have been omitted in the interest of conciseness.

E.2 Non-Linear SMIB System Code

```
% Non-linear model of the single-machine infinite bus with the
% AVR and high-gain exciter and idealised CSC and the damping
% controls - generator damper windings and stator transient are
% not represented.
clc
clf
clear

% ----Initial conditions at the generator terminals in p.u.----%
Pb    = 0.8;
Vinf  = 1.0;
Qb    = 0.03;

% ----- System Parameters in p.u.-----%

% Generator
Xad    = 0.85;
Xaq    = 0.45;
Xl     = 0.15;
Xfd    = 1.03;
Xd     = Xad + Xl;
Xq     = Xaq + Xl;
Xffd   = Xad + Xfd;
Xdpr   = Xl + Xad* Xfd/(Xad + Xfd);
Ra     = 0.005;
Rfd    = 0.00065;
```

```

H      = 4.0;
Wo     = 100 * pi;
Jm     = 2*H / Wo;
B      = 0.0;
Tdopr  = Xffd/(Wo * Rfd);

% Transmission line parameters
Rline  = 0.0;
Xline  = 0.4;
Xcsc0  = 0.1;
Zline  = Rline + j*(Xline-Xcsc0);

Ra     = Ra + Rline;
Xd     = Xd + Xline-Xcsc0;
Xq     = Xq + Xline-Xcsc0;
Xdpr   = Xdpr + Xline-Xcsc0;

% AVR and Exciter initialisation data
Ka     = 100;
Ta     = 1.0;
Tb     = 10.0;
Tr     = 0.01;

% Variable impedance parameters
Tcsc   = 0.01;
Kc     = 0.1;
Xcscv  = 0;

%-----Simulation Time Settings-----%
deltat = 0.002;
T0     = 0.5;
Tfinal = 6;
Tflt   = 0.1;

%-----
disp('Calculations in progress...');
%-----

% Calculate the machine terminal current
It = (Pb-j*Qb) / Vinf;
pfAng = -angle (It);

% Calculate the load angle
Eq = Vinf+(Ra + j*Xq)*It;
Langle = angle(Eq);

Id = abs(It)*sin(Langle+pfAng);
Iq = abs(It)*cos(Langle+pfAng);
Ia = Id + j*Iq;

vq = Vinf * cos(Langle);
vd = Vinf * sin(Langle);

Eqpr = vq + Ra*Iq + Xdpr*Id;
Eo = Eqpr + (Xd - Xdpr)*Id;
Fi = sqrt(2)*Eo/Xad;
Te = Eqpr*Iq + Id*Iq*(Xq - Xdpr);
Pm = Te;

Vto = abs(vd+j*vq+Ia*Zline);
Vtm = Vto;

```

```

Vref = Vto + Eo/Ka;
Vy = Ka * (Vref - Vto);

% States initialisation
t=0;
x(1) = 0;
x(2) = Langle;
x(3) = Eqpr;
x(4) = Vtm;
x(5) = Vy;
x(6) = Xcscv;

% Non-linear differential equations are in subroutine swiftplt.m
% Given the parameters and initial operating conditions the
% subroutine calculates and returns the state variables.

[xdot, Id, Iq, Ia, Vt, Te, Efd] =
swiftplt(x, Zline, Vinf, Ra, Xd, Xdpr, Xq, Jm, B, Pm, Tdopr, Ka, Ta, Tb, Tr, Vref, Kc,
Tcsc);

% Integration loop
for h = 0:deltat:(Tfinal-deltat),

% Applying a 3-phase disturbance at the generator terminals.
if (t>=T0),
    Vinf = 0;
end

% Clearing the fault.
if (t>= T0+Tflt),
    Vinf = 1.0;
end

%Integrate differential equations
y = x+xdot*deltat;
[ydot, Id, Iq, Ia, Vt, Te, Efd] =
swiftplt(y, Zline, Vinf, Ra, Xd, Xdpr, Xq, Jm, B, Pm, Tdopr, Ka, Ta, Tb, Tr, Vref, Kc,
Tcsc);

x = x+deltat*(xdot+ydot)/2;
[xdot, Id, Iq, Ia, Vt, Te, Efd] =
swiftplt(x, Zline, Vinf, Ra, Xd, Xdpr, Xq, Jm, B, Pm, Tdopr, Ka, Ta, Tb, Tr, Vref, Kc,
Tcsc);

t = t+deltat;

%Field current
Fi = sqrt(2)/Xad*(x(3) + Id*(Xd-Xdpr-2*x(6)));

%Setting Xcscv limits
if (x(6) >= 0.1),
    x(6) = 0.1;
end
if(x(6) <= -0.1),
    x(6) = -0.1;
end
z = [z;t];
xo = [xo; x(2) abs(Ia) abs(Vt) Te Efd x(6) Fi x(1)];
end;

```



```
% Subroutine swiftplt.m
% Solves the differential equations and returns the state variables

function [xdot, Id, Iq, Ia, Vt, Te, Efd] =
swiftplt(x, Zline, Vinf, Ra, Xd, Xdpr, Xq, Jm, B, Pm, Tdopr, Ka, Ta, Tb, Tr, Vref, Kc,
, Tcsc)

Vinfid = (Vinf)*sin(x(2));
Vinfq = (Vinf)*cos(x(2));

Xq = Xq - x(6);
Xd = Xd - x(6);
Xdpr = Xdpr - x(6);

Id = (x(3) - Vinfq - Ra*Vinfid/Xq) / (Xdpr + Ra*Ra/Xq);
Iq = (Vinfid + Id*Ra) / Xq;
Te = x(3) * Iq + Id*Iq*(Xq - Xdpr);
EfdI = x(3) + Id*(Xd - Xdpr);

Ia = Id + j*Iq;
Vt = abs(Vinfid+j*Vinfq+Ia*(Zline-j*x(6)));
Efd = Ta*Ka*(Vref - x(4))/Tb + (1 - Ta/Tb)*x(5);

% State variables
xdot(1) = (Pm - Te - B * x(1)) / Jm;
xdot(2) = x(1);
xdot(3) = (Efd - EfdI) / Tdopr;
xdot(4) = (Vt - x(4)) / Tr;
xdot(5) = (Ka*(Vref - x(4)) - x(5))/ Tb;
xdot(6) = (Kc*x(1) - x(6)) / Tcsc;
```

E.3 Linearised SMIB System Code

```
% Linearisation of the single-machine infinite bus
% non-linear model with the AVR and high-gain exciter
% and idealised CSC and the damping controls.
% Generator damper windings and stator transients are
% not represented.

global Ra Xd Xdpr Xq Jm B Pm Tdopr Ka Ta Tb Tr Kc Tws Zline Vref

% Initial conditions at the generator terminals

Pb = 0.8;
Vinf = 1.0;
Qb = 0.03;

% Generator Parameters

Xad = 0.85;
Xaq = 0.45;
Xl = 0.15;
Xfd = 1.03;
Xd = Xad + Xl;
Xq = Xaq + Xl;
Xffd = Xad + Xfd;
Xdpr = Xl + Xad* Xfd/(Xad + Xfd);
```

```

Ra      = 0.005;
Rfd     = 0.00065;
H       = 4.0;
Wo      = 100 * pi;
Jm      = 2*H / Wo;
B       = 0.0;
Tdopr   = Xffd/(Wo * Rfd);

% Transmission line parameters

Rline = 0;
Xline = 0.6;
Zline = Rline + j*Xline;

Ra = Ra + Rline;
Xd = Xd + Xline;
Xq = Xq + Xline;
Xdpr = Xdpr + Xline;

% Calculate the machine terminal current
It = (Pb-j*Qb) / Vinf;
pfAng = -angle (It);

% Solving for the internal angle
Eq = Vinf+(Ra + j*Xq)*It;
Langle = angle(Eq);

Id = abs(It)*sin(Langle+pfAng);
Iq = abs(It)*cos(Langle+pfAng);
Ia = Id + j*Iq;

vq = Vinf * cos(Langle);
vd = Vinf * sin(Langle);

Eqpr = vq + Ra*Iq + Xdpr*Id;
Eo = Eqpr + (Xd - Xdpr)*Id;
Fi = sqrt(2)*Eo/Xad;
Te = Eqpr*Iq + Id*Iq*(Xq - Xdpr);
Pm = Te;

% AVR and Exciter initialisation data
Ka      = 200;
Ta      = 1.0;
Tb      = 10.0;
Tr      = 0.01;
Vto     = abs(vd+j*vq+Ia*Zline);
Vtm     = Vto;
Vref    = Vto + Eo/Ka;
Vy      = Ka * (Vref - Vto);

% Variable impedance parameters
Kc      = 0.1;
Tcsc    = 0.01;
Xcscv   = 0;

% Input vector at the steady state operating point about
% which to linearise numerically
u = [Vinf; Eo; Pm; Vto];
XX0 = [0; Langle; Eqpr; Vtm; Vy; Xcscv];

% Test this steady-state vector for correctness if necessary

```

```

[xdots] = avrpltsmiblin(0,XX0,u,1);

% Form linearised state space matrices using function linmod
% non-linear model equations for the SMIB
% are in subroutine avrsmiblin.m; steady-state operating
% point in state vector XX0
[AA,BB,CC,DD] = linmod('avrsmiblinblk',XX0,u,1e-8);

eval = eig(AA);

x = real(eval);
y = imag(eval);

% Subroutine avrsmiblin.m
% Contains the non-linear, differential equations
% describing the SMIB

function [sys,x0,str,ts] = avrpltsmiblin(t,x,u,flag)
%AVRPLTSMIBLIN General M-file S-function template
global Ra Xd Xdpr Xq Jm B Pm Tdopr Ka Ta Tb Tr Kc Tcsc Zline Vref
switch flag,

% Initialization %
    case 0,
        [sys,x0,str,ts] = mdlInitializeSizes;

        % Derivatives %
        case 1,
            sys=mdlDerivatives(t,x,u);

        % Outputs %
        case 3,
            sys=mdlOutputs(t,x,u);

        % Unused Flags%
        case { 2, 4, 9 }
            sys=[];

        % Unexpected flags %
        otherwise
            error(['Unhandled flag = ',num2str(flag)]);

end

% end avrpltsmiblin
%=====
% mdlInitializeSizes
% Return the sizes, initial conditions, and sample times for the
% S-function.
%=====

function [sys,x0,str,ts] = mdlInitializeSizes

sizes = simsizes;

sizes.NumContStates = 6;
sizes.NumDiscStates = 0;
sizes.NumOutputs = 2;
sizes.NumInputs = 4;
sizes.DirFeedthrough = 0;

```

```

sizes.NumSampleTimes = 1; % at least one sample time is needed

sys = simsizes(sizes);

% initialize the initial conditions
x0 = zeros(6,1);

% str is always an empty matrix
str = [];

% initialize the array of sample times
ts = [0 0];

% end mdlInitializeSizes
%=====
% mdlDerivatives
% Return the derivatives for the continuous states.
%=====

function sys = mdlDerivatives(t,x,u)
global Ra Xd Xdpr Xq Jm B Pm Tdopr Ka Ta Tb Tr Kc Tcsc Zline Vref

Vinf = u(1,1);
Eo = u(2,1);
Pm = u(3,1);
Vto = u(4,1);

Vinfq = (Vinf)*sin(x(2));
Vinfj = (Vinf)*cos(x(2));

% Equations to be linearised
Xq = Xq - x(6);
Xd = Xd - x(6);
Xdpr = Xdpr - x(6);

Id = (x(3) - Vinfj - Ra*Vinfq/Xq) / (Xdpr + Ra*Ra/Xq);
Iq = (Vinfq + Id*Ra) / Xq;
Te = x(3) * Iq + Id*Iq*(Xq - Xdpr);
EfdI = x(3) + Id*(Xd - Xdpr);

Ia = Id + j*Iq;
Vt = abs(Vinfq+j*Vinfj+Ia*(Zline-j*x(6)));
Efd = Ta*Ka*(Vref - x(4))/Tb + (1 - Ta/Tb)*x(5);

sys(1,1) = (Pm - Te - B * x(1)) / Jm;
sys(2,1) = x(1);
sys(3,1) = (Efd - EfdI) / Tdopr;
sys(4,1) = (Vt - x(4)) / Tr;
sys(5,1) = (Ka*(Vref - x(4)) - x(5))/ Tb;
sys(6,1) = (Kc*1*x(1) - x(6)) /Tcsc;

% end mdlDerivatives
%=====
% mdlOutputs
% Return the block outputs.
%=====

function sys=mdlOutputs(t,x,u)

sys(1,1)= x(1,1);

```

```
sys(2,1) = x(2,1);  
% end mdlOutputs
```

REFERENCES

- [Angquist] Angquist L., Lundin B., Samuelsson J.: "Power Oscillation Damping Using Controlled Reactive Power Compensation – A Comparison Between Series and Shunt Approaches", *IEEE Transactions on Power Systems*, Vol. 8, No. 2, May 1993, pp. 687-695.
- [Breuer] Breuer G. D., Rustebakke H. M., Gibley R. A., and Simmons H. O. Jr: "The Use of Series Capacitors to Obtain Maximum EHV Transmission Capability", *IEEE Transactions on Power Apparatus and Systems*, Vol. 83, November 1964, pp. 1090-1102.
- [Chen1] Chen X. R., Pahalawaththa N. C., Annakkage U. D., Kumble C. S.: "Controlled Series Compensation for Improving the Stability of Multi-Machine Power Systems", *IEE Proceedings – Generation, Transmission and Distribution*, Vol. 142, No. 4, July 1995, pp. 361-366.
- [Chen2] Chen X. R., Pahalawaththa N. C., Annakkage U. D., Kumble C. S.: "Output Feedback TCSC Controllers to Improve Damping of Meshed Multi-Machine Power Systems", *IEE Proceedings – Generation, Transmission and Distribution*, Vol. 144, No. 3, May 1997, pp. 243-248.
- [Choi] Choi S. S., Jiang F., Shrestha G.: "Suppression of Transmission System Oscillations by Thyristor-Controlled Series Compensation", *IEE Proceedings – Generation, Transmission and Distribution*, Vol. 143, No. 1, January 1996, pp. 7-12.
- [Chonco1] Chonco N. S., Rigby B. S., Harley R. G.: "Strategies for Damping Power Oscillations Using Controllable Series Compensators",

Proceedings of the Eighth Southern African Universities Power Engineering Conference, Potchefstroom, January 1999, pp. 131-134.

- [Chonco2] Chonco N. S., Rigby B. S., Harley R. G.: "Damping of Power System Oscillations Using An Inverter-Based Controllable Series Compensator", *Proceedings of the Ninth Southern African Universities Power Engineering Conference*, Durban, January 2000, pp. 192-196.
- [Chonco3] Chonco N. S.: "An EMTDC Implementation of An Advanced Series Compensation Scheme", *Fourth Year Design Project*, University of Natal, Durban, 1997.
- [deMello1] de Mello F. P.: "Exploratory Concepts on Control of Variable Series Compensation in Transmission Systems to Improve Damping of Intermachine/System Oscillations", *IEEE Transactions on Power Systems*, Vol. 9, No. 1, February 1994, pp. 102-108.
- [deMello2] deMello F. P., Concordia C.: "Concepts of Synchronous Machine Stability as Affected by Excitation Control", *IEEE Trans. on Power Apparatus and Systems*, Vol. PAS-88, No. 4, April 1969, pp. 316-329.
- [deOliveira] de Oliveira S.E.M., Gardos I., Fonseca E.P.: "Representation of Series Capacitors in Electric Power System Stability Studies", 1991, *IEEE Transaction on Power Systems*, Vol. 6, No. 3, pp. 1119-1125.
- [Dolan] Dolan P. S., Smith J. R., Mittelstadt W. A.: "A Study of TCSC Optimal Control Parameters for Different Operating Conditions", *IEEE Transactions on Power Systems*, Vol. 10, No. 4, November 1995, pp. 1972-1977.
- [Ewart] Ewart D. N., Koessler R. J., Mountford J. D., and Maratukulam D.: "FACTS Options Permit the Utilization of the Full Thermal Capacity of AC Transmission", *IEE Conference Publication No. 345*, Published by IEE, Michael Faraday House, Steverage, 1991, pp. 13-18.

-
- [Gronquist] Gronquist J. F., Setares W. A., Alvarado F. L., Lasseter R. H.: "Power Oscillation Damping Control Strategies for FACTS Devices Using Locally Measurable Quantities", *IEEE Transactions on Power Systems*, Vol. 10, No. 3, August 1995, pp. 1598 - 1605.
- [Gyugyi1] Gyugyi L.: "Dynamic Compensation of AC Transmission Lines by Solid-State Synchronous Voltage Sources", *IEEE Transactions on Power Delivery*, Vol. 9, No. 2, April 1994, pp. 904-911.
- [Gyugyi2] Gyugyi L., Schauder C. D., Sen K. K.: "Static Synchronous Series Compensator: A Solid-State Approach to the Series Compensation of Transmission Lines", *IEEE Transactions on Power Delivery*, Vol. 12, No. 1, January 1997, pp. 406-413.
- [Gyugyi3] Gyugyi L.: "Solid-State Control of AC Power Transmission", *Proceedings EPRI FACTS Conference 1*, Cincinnati, USA, 1990, pp. (1.7-1)-(1.7-44).
- [Hedin] Hedin R., Jalali S., Weiss S.: "Improving System Stability Using An Advanced Series Compensation Scheme to Damp Power Swings", *Sixth International Conference, AC and DC Power Transmission*, 29 April-3 May 1996, Conference Publication No. 423, ©IEE, pp. 311-314.
- [Heffron] Heffron W.G., Phillips R. A.: "Effect of Modern Amplidyne Voltage Regulators on Underexcited Operation of Large Turbine Generators", *AIEE Transactions (Power Apparatus and Systems)*, Vol. 71, August 1952, pp. 692-697.
- [Kimbark1] Kimbark E.W.: "Improvement of System Stability by Switched Series Capacitors", *IEEE Transactions on Power Apparatus and Systems*, Vol. PAS-85, No. 2, February 1966, pp. 180-188.
-

-
- [Kimbark2] Kimbark E. W.: "How to Improve Stability Without Risking Subsynchronous Resonance", *IEEE Transactions on Power Apparatus and Systems*, Vol. PAS-96, No. 5, September/October 1977, pp. 1608-1619.
- [Kimbark3] Kimbark E. W.: "Improvement of Power System Stability by Changes in the Network", *IEEE Transactions on Power Apparatus and Systems*, Vol. PAS-88, No. 5, May 1969, pp. 773-778.
- [Klein1] Klein M., Rogers G. J., Kundur P.: "A Fundamental Study of Inter-Area Oscillations in Power Systems", *IEEE Transactions on Power Systems*, Vol. 6, No. 3, August 1991, pp. 914-921.
- [Klein2] Klein M., Rogers G. J., Moorty S., Kundur P.: "Analytical Investigation of Factors Influencing Power System Stabilizers Performance", *IEEE Transactions on Energy Conversion*, Vol. 7, No. 3, September 1992, pp. 382-390.
- [Kundur] Kundur P.: "Power System Stability and Control", *McGraw-Hill*, New York, 1993.
- [Larsen] Larsen E. V., Sanchez-Gasca J.J., Chow J.H.: "Concepts for Design of FACTS Controllers to Damp Power Swings", *IEEE Transactions on Power Systems*, Vol. 10, No. 2, May 1995, pp. 948-955.
- [Lerch] Lerch E., Povd D., Xu L.: "Advanced SVC Control for Damping Power System Oscillations", *IEEE Transactions on Power Systems*, Vol. 6, No. 2, May 1991, pp. 524-531.
- [Manitoba] Manitoba HVDC Research Centre: "EMTDC V3 User's Manual", *The Manitoba HVDC Research Centre*, © 1986 1988.
- [MathWorks] MathWorks: "MATLAB for Windows User's Guide", *The MathWorks, Inc.*, 1991.
-

-
- [Mihalic1] Mihalic R., Papic I.: "Power Flow Control Using Static Synchronous Series Compensator", *Proceedings of the Universities Power Engineering Conference*, Vol. 1, 1997, pp. 174-177.
- [Mihalic2] Mihalic R., Papic I.: "Static Synchronous Series Compensator – A Means for Dynamic Power Flow Control in Electric Power Systems", *Electric Power Systems Research*, Vol. 45, 1998, pp. 65-72.
- [Mittelstadt] Mittelstadt W.A.: "Four Methods of Power System Damping", *IEEE Transactions on Power Apparatus and Systems*, Vol. PAS-87, May 1968, pp. 1323-1327.
- [Nelson] Nelson R. J., Bian J., Ramey D. G., Lemak T. A., Rietman T. R., Hill J. E.: "Transient Stability Enhancement with FACTS Controllers", *Sixth International Conference, AC and CD Power Transmission*, Conference Publication No. 423, © IEE, 29 April-3 May 1996, pp. 269-274.
- [Noroozian1] Noroozian M., Andersson G.: "Damping of Power System Oscillations by Use of Controllable Components", *IEEE Transactions on Power Delivery*, Vol. 9, No. 4, October 1994, pp. 2046-2053.
- [Noroozian2] Noroozian M., Angquist L., Ghandhari M., Andersson G.: "Improving Power System Dynamics by Series-Connected FACTS Devices", *IEEE Transactions on Power Delivery*, Vol. 12, No. 4, October 1997, pp. 1635-1641.
- [Nyati] Nyati S., Wegner C. A., Delmerico R. W., Piwko R. J., Baker D. H., Edris A.: "Effectiveness of Thyristor Controlled Series Capacitor in Enhancing Power System Dynamics: An Analog Simulator Study", *IEEE Transactions on Power Delivery*, Vol. 9, No.2, April 1994, pp. 1018-1027.
-

- [Olwegard] Olwegard A., Walve K., Waglund G., Frank H., Torsen S.: "Improvement of Transmission Capacity by Thyristor Controlled Reactive Power", *IEEE Transactions on Power Apparatus and Systems*, Vol. PAS-100, No. 8, August 1981, pp. 3930-3939.
- [RamaRao] RamaRao N., Reitan D. K.: "Improvement of Power System Transient Stability Using Optimal Control: Bang-Bang Control of Reactance", *IEEE Transactions on Power Apparatus and Systems*, Vol. PAS-89, May/June 1970, pp. 975-984.
- [Ramey] Ramey D.G., Nelson R. J., Bian J.: "Use of FACTS Power Flow Controllers to Enhance Transmission Transfer Limits", *Proceedings of the 56th Annual American Power Conference*, USA, Published by Illinois Institute of Technology, 1994, Chicago, pp. 712-718.
- [Reitan] Reitan D.K., RamaRao N.: "A Method of Improving Transient Stability by Bang-Bang Control of Tie-Line Reactance", *IEEE Transactions on Power Apparatus and Systems*, Vol. PAS-93, Jan/Feb. 1974, pp. 303-311.
- [Rigby1] Rigby B. S., Harley R. G.: "An Improved Control Scheme for a Series Capacitive Reactance Based On A Voltage Source Inverter", *IEEE Transactions on Industry Applications*, Vol. 34, No.2, March/April 1998, pp. 355-363.
- [Rigby2] Rigby B. S., Harley R. G.: "A Solid-State Controllable Series Capacitive Reactance for Improved Utilisation of High-Power Transmission Lines", *Proceedings of the Cigre Third Southern Africa Regional Conference*, Midrand, Johannesburg, South Africa, 1998.
- [Rigby3] Harley R.G., Rigby B. S., Jennings G. D.: "Design of a Controlled Converter which Emulates a Series Capacitive Compensator for Long Power Lines", *Proceedings of the International Conference on Power*

Electronics and Motion Control PEMC'94, Warsaw, Poland, September 1994, pp. 213-218.

- [Sen] Sen K.K.: "SSSC – Static Synchronous Series Compensator: Theory, Modeling, and Applications", *IEEE Transactions on Power Delivery*, Vol. 13, No. 1, January 1998, pp. 241-246.
- [Smith] Smith O.J.M.: "Power System Transient Control by Capacitor Switching", *IEEE Transactions on Power Apparatus and Systems*, Vol. PAS-88, No. 1, January 1969, pp. 28-35.
- [Swift1] Swift F.J., Wang H. F., Li M.: "Analysis of Controllable Series Compensator to Suppress Power System Oscillations", *Sixth International Conference, AC and DC Power Transmission*, Conference Publication No. 423, © IEE, 29 April-3 May 1996, pp. 202-207.
- [Swift2] Swift F. J., Wang H. F.: "Application of the Controllable Series Compensator in Damping Power System Oscillations", *IEE Proceedings - Generation, Transmission and Distribution*, Vol. 143, No. 4, July 1996, pp. 359-364.
- [Terms] Task Force on Terms & Definitions – Power System Engineering Committee: "Proposed Terms & Definitions for Power System Stability", *IEEE Transactions on Power Apparatus and Systems*, Vol. PAS-101, No. 7, July 1982, pp. 1894-1897.
- [Toufan] Toufan M., Annakkage U. D.: "Simulation of the Unified Power Flow Controller Performance Using PSCAD/EMTDC", *Electric Power Systems Research*, Vol. 46, 1998, pp. 67- 75.
- [Wang1] Wang H. F., Swift F. J., Li M.: "Oscillation Stabilisation of Multi-Machine Power Systems by Controllable Series Compensator", *Sixth International Conference, AC and CD Power Transmission*,

Conference Publication No. 423, ©IEEE, 29 April-3 May 1996, pp. 315-320.

- [Wang2] Wang H. F., Swift F. J., "A Unified Model for the Analysis of FACTS Devices in Damping Power System Oscillations Part I: Single-Machine Infinite-Bus Power Systems", *IEEE Transactions on Power Delivery*, 1996, pp. 1-6.
- [Wang3] Wang H. F., Swift F.J.: "Capability of the Static VAR Compensator in Damping Power System Oscillations", *IEE Proceedings - Generation, Transmission and Distribution*, Vol. 143, No. 4, July 1996, pp. 353-358.
- [Webster] Webster R.H., Smith O.J.M.: "Series Capacitor Switching to Quench Electromechanical Transients in Power Systems", *IEEE Transactions on Power Apparatus and Systems*, Vol. PAS-90, No. 2, March/April 1971, pp. 427-433.
- [Yang] Yang N., Liu Q., McCalley J. D.: "TCSC Controller Design for Damping Interarea Oscillations", *IEEE Transactions on Power Systems*, Vol. 43, No. 4, November 1998, pp. 1304-1310.